AN ABSTRACT OF THE THESIS OF

Jennifer J. Simeon for the degree of Master of Science in Oceanography presented on November 20, 2000. Title: Decomposition of Absorption Coefficients and Decorrelation Lengthscales of Hydrographic and Inherent Optical Properties in the Middle Atlantic Bight.

Abstract approved: Redacted for privacy

John A. Barth

This investigation is an exploration of the use of inherent optical properties towards further elucidation of coastal circulation processes occurring on the continental shelf and slope in the Middle Atlantic Bight, south of Cape Cod Massachusetts, during 14-Aug to 1-Sep 1996 and 25-Apr to 15-May 1997. Assessing the possibility of augmenting observations in temperature and salinity space with the use of naturally occurring tracers is a primary motivation. A decomposition method for the total (minus water) absorption coefficients into major light-absorbing components (phytoplankton, gelbstoff and tripton) was developed to examine distributions of potentially, independently behaving naturally occurring tracers. The goal is to quantify the spatial dependence between the hydrographic and optical properties and how that dependence might vary with seasons.

The decomposition of the total (minus water) absorption coefficient showed the contrast between the turbid shelf and clearer slope waters. The individual components enabled the visualization of the frontal dynamics. The distributions of the total (minus water) absorption components demonstrate evidence of the

relative insulation of the shelf waters from slope waters and the strong horizontal gradient imposed by the shelfbreak front. The decorrelation lengthscales, L, calculated for the summer data indicate the summer spatial dependence of the hydrographic and optical properties. The magnitude of L for the cross-shelf mean series of both hydrographic and optical properties at fixed depths is $O(10$ km) above the pycnocline, then decreases to 2 km near the bottom. The mean cross-shelf L magnitudes and vertical structure are likely caused by meanders (horizontal scale $\approx$ 30 km) of the shelfbreak front at the surface, while the decrease near the bottom is influenced by the stability of the foot of the shelfbreak front as well as the turbulent mixing in the bottom boundary layer. The L's over the individual shelf and slope series are coincident with the observed internal deformation radius ($L_R = 5$ km). Summer anomaly series both in depth and density coordinates show the influence of internal solitary wave packets in perturbing the mean field.

Decomposition of Absorption Coefficients and Decorrelation Lengthscales of Hydrographic and Inherent Optical Properties in the Middle Atlantic Bight

by

Jennifer J. Simeon

A THESIS

submitted to

Oregon State University

in partial fulfillment of
the requirements for the
degree of

Master of Science

Presented November 20, 2000
Commencement June 2001

Master of Science thesis of Jennifer J. Simeon presented on November 20, 2000

APPROVED:

Redacted for privacy

Major Professor, representing Oceanography

Redacted for privacy

Dean of the College of Oceanic and Atmospheric Sciences

Redacted for privacy

Dean of the Graduate School

I understand that my thesis will become part of the permanent collection of Oregon State University libraries. My signature below authorizes release of my thesis to any reader upon request.

Redacted for privacy

Jennifer J. Simeon, Author

ACKNOWLEDGMENTS

I thank my advisor, Jack A. Barth, for allowing me the privelege of working with him, giving me free reign of my creative-scientific thought processes and helping me to grow as a scientist. Thanks to Scott Pegau for his enthusiasm, generosity and honesty both personally and professionally. Thanks to Ron Zaneveld, Tim Cowles and Emmanuel Boss for their wonderful support and constructive scientific interactions. Thanks to Terry Brown for being my GCR. Thanks to Irma Delson for mitigating the fear and insecurities I experienced during graduate school. Thanks to Cindy Withrow for rescuing me on occassion. Thanks to Linda LaFleur for letting BK, R and I be her roommates in Ocean Admin. Thanks to John Allen, Dudley Chelton and Roger Samelson for patiently teaching me physical oceanography. Thanks to Steve Ackleson and Tom Kinder at ONR. Thanks to ONR (Grant #'s N00014-95-1-0382 and N00014-99-1-0225) for funding this work.

I thank my family for their selfless love and support throughout my life. I also thank terrific friends: Renellys Perez, Brandy Kuebel, James Wheeler, Claudia Mengelt, Claudius Freiherr Von Schwerin, Carrie Mock, Bertrand Dano and Guillaume Vernieres whose friendships are invaluable. Thanks awesome officemates, Stephen Pierce and Kipp Shearman, for answering my pesky questions and being terrific role models. Special thanks to Nicolai Thum, for imbuing me with a love for the mountains (and for being our home system administrator). Thanks to Louise, for keeping me company for many days of writing. Special thanks to Collin Roesler-Culbertson for being forever the first and last inspiration of my professional career. Infinite thanks to François Baratange, my best friend and confidant, for being the most beautiful person.

CONTRIBUTION OF AUTHORS

For Chapter 1 (Simeon *et al.*, in prep), co-author Collin S. Roesler provided the theoretical ground-work for the decomposition method, which I then developed and refined. Co-authors John A. Barth and W. Scott Pegau offered helpful guidance towards the refinement of the decomposition method, helpful discussions upon the application of the decomposition method and editing of the text.

For Chapter 2 (Simeon *et al.*, in prep), co-author John A. Barth provided the data, guidance in the implementation of the method, discussions as well as critical examination of every step in the course of this study. Co-author John A. Barth also provided suggestions on the structure of the text and careful editing of the text.

TABLE OF CONTENTS

Page

TABLE OF CONTENTS (Continued)

Page

LIST OF FIGURES

Figure | Page

LIST OF FIGURES (Continued)

Figure | Page

LIST OF FIGURES (Continued)

Figure | Page

LIST OF FIGURES (Continued)

Figure | Page

DECOMPOSITION OF ABSORPTION COEFFICIENTS AND DECORRELATION LENGTHSCALES OF HYDROGRAPHIC AND INHERENT OPTICAL PROPERTIES IN THE MIDDLE ATLANTIC BIGHT

1 INTRODUCTION

The mean coastal circulation on the continental shelf and slope south of Cape Cod, Massachusetts, is driven by an alongshore pressure gradient (Stommel and Leetma, 1972; Csanady, 1976) and forced by a northern originating inflow (Chapman et al., 1986). The water masses on the shelf are hypothesized to originate from the Labrador Sea, hence are cooler and fresher, and flow southwestward through the Middle Atlantic Bight (MAB) (Fairbanks, 1982; Chapman et al., 1986). Seaward of the shelf, shelf waters become entrained with warm Gulf Stream Water forming the Upper Slope Water mass (Lee, 1970; Loder et al., 1998). Below the Upper Slope Water mass rests the Labrador Slope Water and Warm/Western Slope Water, which is collectively called the Deep Slope Water (Wright, 1977).

The conservation of potential vorticity in the shelf waters enables the steep continental slope to reduce the net offshore flux of shelf water, thereby maintaining a relatively insulated shelf (Shaw and Csanady, 1983).

Evidence of the separation of the shelf waters from the slope waters is shown by the presence of a shelfbreak front (Bigelow, 1933; Ketchum and Corwin, 1964; Cresswell, 1967; Boicourt and Hacker, 1976; Beardsley et al., 1985) and this frontal boundary is known to be highly convoluted (Mooers et al., 1979).

The continuity of the mean flow in the MAB permits the characteristic alongshore lengthscales to be much longer than cross-shelf lengthscales (Chapman et al. 1986). The characteristic cross-shelf lengthscales are expected to be strongly a function of the topography of the shelf and slope that causes the insulative effects of the shelfbreak and slope (Chapman et al. 1986). Boundary effects between the shelf and slope waters have been previously observed from remotely sensed observations of sea surface temperature.

Typical internal deformation radii ($L_R = (g'h)^{1/2}/f$) for observed shelf/slope eddies are of O(5 km) (Csanady and Magnell, 1987) which indicates a meander wavelength of $2\pi\ L_R = 30$ km and an eddy diameter of 15 km. Seaward of the slope, the frontal boundary of the slope waters and Gulf Stream exhibits internal deformation radii for eddies of O(50-100 km) (Halliwell and Mooers, 1979; Garvine et al. 1988).

The shelfbreak front starkly delineates the cool, fresher, more turbid waters of the shelf from the warm, salty, optically clearer slope waters. The contrasting differences in the hydrographic and optical properties indicate distinctly different physical processes act on the shelf and slope.

The topography also plays a role in the steepening of the internal tide and the formation of tidally forced solitons. Soliton wave packets in the MAB south of Cape Cod are approximately 5-10 km wide. Distances between packets are approximately 30 km, which suggests propagation speeds of 50 cm s^{-1} (using the M_2 tidal period).

The characteristic vertical lengthscales of physical properties are influenced by surface and bottom boundary effects around a calm, inviscid core. In the vertical, solitons can strongly perturb isopycnal surface by as much as 5-30 meters.

Until the last several years, high spatial resolution observations were lacking for the validation of previous modeling efforts of the shelfbreak front (Gawarkiewicz and Chapman, 1992; Chapman and Lentz, 1994). The examination of the behavior of the decomposed total (minus water) light absorption coefficient, yields information beyond temperature-salinity space, such as the age, degree of mixing, and origin of a particular water parcel. Developing oceanic sampling strategies for future mesoscale circulation observations requires documentation of the correlation dependence of the spatial structure.

This study quantifies the spatial small-mesoscale correlation lengthscales to determine the predictablity and reliability of unmeasured estimates, the measurement resolution required to resolve prominent features, and to provide additional statistical criteria for validation of general circulation models for this region. Further, the usefulness of inherent optical properties towards elucidation of physical processes is assessed through these statistical analyses. This results of the correlation analyses will be used to determine the degree of control of physical processes on tracer spatial structures.

2 DISTRIBUTIONS OF MODELED LIGHT-ABSORBING COMPONENTS IN THE MIDDLE ATLANTIC BIGHT

2.1 ABSTRACT

This study presents a description of the distribution of major light absorbing components during summer 1996 and spring 1997 in the Middle Atlantic Bight, south of Cape Cod, Massachusetts. High spatial resolution hydrographic and inherent optical properties (IOPs) were measured with a SeaBird conductivity, temperature and depth (CTD) instrument and WET Labs nine-wavelength absorption and attenuation meter (ac-9) mounted onto a towed, undulating platform. Total (minus water) absorption coefficients were then decomposed into major light-absorbing components (phytoplankton, gelbstoff and tripton) using an iterative, least squares formulation that minimizes residuals of the matrix formulation, subject to the constraint that the solution is non-negative.

Summer distributions of modeled major light absorbing components demonstrate a subsurface phytoplankton layer following isopycnals. Associated with the subsurface phytoplankton layer was strong tripton absorption. Strong gelbstoff absorption was found above the bottom. Spring distributions of modeled component absorption coefficients were characterized by patchy blooms of phytoplankton in the surface mixed layer. Distributions of gelbstoff absorption exhibited strong absorption associated with the resuspension of bottom sediments. Tripton absorption was found in the surface mixed layer and above the bottom. The distributions of the total (minus water) absorption components demonstrate evidence of the relative insulation of the shelf waters from slope waters and the strong horizontal gradient imposed by the shelfbreak front.

2.2 INTRODUCTION

The mean coastal circulation on the continental shelf and slope south of Cape Cod, Massachusetts, is driven by an alongshore pressure gradient (Stommel and Leetma, 1972; Csanady, 1976) and forced by a northern originating inflow (Chapman et al., 1986). The water masses on the shelf are hypothesized to originate from the Labrador Sea, hence are cooler and fresher, and flow southwestward through the Middle Atlantic Bight (Fairbanks, 1982; Chapman et al., 1986). Seaward of the shelf, shelf waters become entrained with warm Gulf Stream Water forms the Upper Slope Water mass (Lee, 1970; Loder, 1998). Below the Upper Slope Water mass, rests the Labrador Slope Water and Warm/Western Slope Water, which is collectively called the Deep Slope Water (Wright, 1977). The conservation of potential vorticity in the shelf waters enables the steep continental slope to reduce the net offshore flux of shelf water and maintain a relatively insulated shelf (Shaw and Csanady, 1983). Evidence of a boundary between the shelf and slope waters is shown by the presence of a shelfbreak front (Bigelow, 1933; Ketchum and Corwin, 1964; Cresswell, 1967; Boicourt and Hacker, 1976; Beardsley et al., 1985) and this frontal boundary is known be highly convoluted (Mooers et al., 1979).

While the hydrographic properties of the Middle Atlantic Bight have been very well documented (Beardsley and Boicourt, 1981), observations of inherent optical properties (IOPs) in the Middle Atlantic Bight on the continental shelf and slope south of Cape Cod are much more rare in the literature. At best, observations of chlorophyll fluorescence (e.g. Houghton and Marra, 1983) provide an indication of the phytoplankton distributions on the continental shelf and slope. Observations of the distribution of gelbstoff absorption is limited to other regions of the Middle Atlantic Bight (DeGranpre et al., 1996; Vodacek et al., 1997) and distributions of

tripton absorption have not been systematically surveyed. In the summer 1996 and spring 1997, during the Coastal Mixing and Optics (CMO) Experiment, measurements were recorded on the continental shelf and slope (Fig. 2.1) and for the first time, direct, high spatial resolution observations of the inherent optical properties were made available (Barth et al. 1998; Barth and Bogucki, 1999). Direct observations of component absorption were independently recorded at this time through the use of conventional profiling measurement methods (Boss et al. submitted).

A description of the inherent optical properties of the various water masses in the Middle Atlantic Bight adds another characterizing property with which an investigator can understand more about the ecology, chemistry, source and motion of the water masses in the region. The total absorption coefficient of a parcel of water is due to four major absorbing components: (1) pure water, (2) gelbstoff, (3) phytoplankton and (4) tripton (Kirk, 1994). Each component has their own notational expressions, $a_w(\lambda)$, $a_g(\lambda)$, $a_\varphi(\lambda)$ and $a_t(\lambda)$. Hence, the total absorption coefficient, expressed notationally, is a linear combination of each component's absorption,

$$a_{Total} = a_w + a_g + a_\varphi + a_t. \tag{2.1}$$

The nature of the first component is self-explanatory. The second component constitutes chromophoric dissolved organic materials (CDOM). Here, "dissolved" is operationally defined as materials smaller than the pore size of the pre-filter used to prepare the water sample (typically < 2 μm). The phytoplankton absorption coefficient is determined by the algal pigment composition, while the tripton component is composed of chromophoric, non-phytoplanktonous particulate matter (e.g. detritus, bacteria, viruses, organic and inorganic sediments).

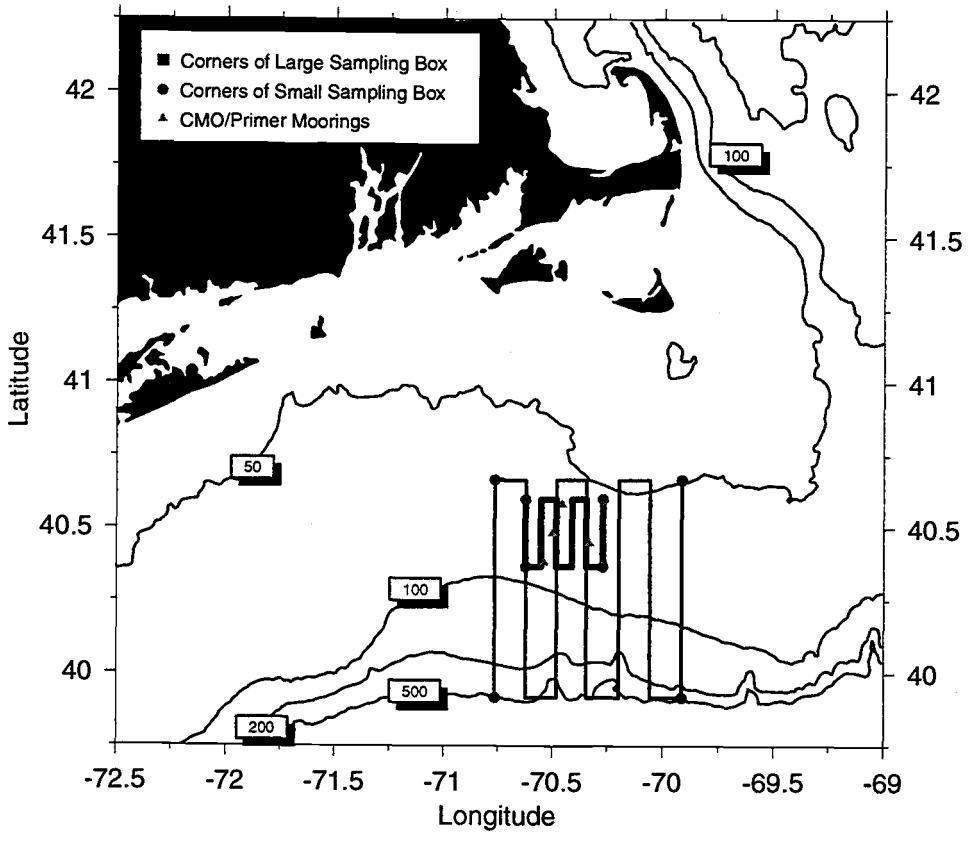

FIGURE 2.1 Map of the Coastal Mixing and Optics study region in the Middle Atlantic Bight south of Cape Cod, Massachusetts. Bottom topography in meters.

The goals for this study are (1) to present the three-dimensional structure of the hydrographic and inherent optical properties during summer and spring, (2) to present a method for the decomposition of total absorption spectrum, (3) to present the results of the application of the decomposition method, and (4) to briefly interpret the IOP signals of the coastal water masses. A companion paper presents a detailed evaluation of the relationship between IOPs and physical processes (Simeon and Barth, in prep.).

2.3 MODEL DEVELOPMENT

The collection, data processing and editing of *in situ* hydrographic and IOP measurements presented in this study has been previously documented (Barth et al. 1998; Barth and Bogucki, 1999; Simeon et al. 2000). A Western Environmental Technology Laboratories (WET Labs) nine-wavelength absorption and attenuation meter (ac-9) was used to measure the total (minus water) absorption coefficients and attenution coefficients from a towed, undulating vehicle, SeaSoar. The ac-9 absorption measurements were then mathematically decomposed into major light absorbing components as follows.

The decomposition method is a constrained multiple regression problem, similar in form to regression models presented by Candela et al. (1992) and Mackas et al. (1987). The decomposition of the total absorption signal is formalized by 2.1, where one can consider 2.1 as the Normal Equations of a regression model,

$$A \cdot \vec{x} = \vec{y}. \tag{2.2}$$

The matrix, A, is the set of basis vectors that describe the spectral shape of the component light-absorption spectra. The vector, $\vec{y}$, contains the observations of the total (minus water) absorption spectrum, as measured by the ac-9. Imposing

a least squares requirement, subject to the constraint that the solution, $\vec{x}$, remains non-negative, retrieves the regression coefficients that ascribe the magnitudes of the modeled component absorption spectra.

This decomposition method is a departure from previous absorption decomposition methods (Roesler et al. 1989; Morrow et al. 1989; Bricaud and Stramski 1990; Cleveland and Perry 1994; Cleveland 1995; Sosik and Mitchell 1995) in that it simultaneously solves for the three component spectra and relies on the characteristic properties of the individual component spectra, not empirically derived relationships between one or more of the components, nor does the decomposition require additional fluorometric measurements of chlorophyll or time-consuming high pressure liquid chromotography (HPLC) pigment measurements. This decomposition also dispenses with the need to make assumptions of the fractional contributions of the absorbing components to the total (minus water) absorption coefficient.

The spectral characteristics of the component absorption spectra (Fig. 2.2) are used to construct the basis vectors of the matrix A. Pure water preferentially absorbs longer (red) wavelengths, and has low absorption between 400-500 nm. The magnitude and shape of the pure water spectrum is a known quantity (Pope and Fry, 1997) and is, in practice, removed from the total absorption signal before proceeding with the decomposition. The phytoplankton spectrum is characterized by the two electronic states of the chlorophyll *a* molecule, that cause the absorption peaks at 440 and 676 nm. The gelbstoff and tripton spectra preferentially absorb ultraviolet and short visible wavelengths (200-400 nm), exponentially decreasing in magnitude at longer visible wavelengths. The gelbstoff and tripton absorption spectra are only similar in shape.

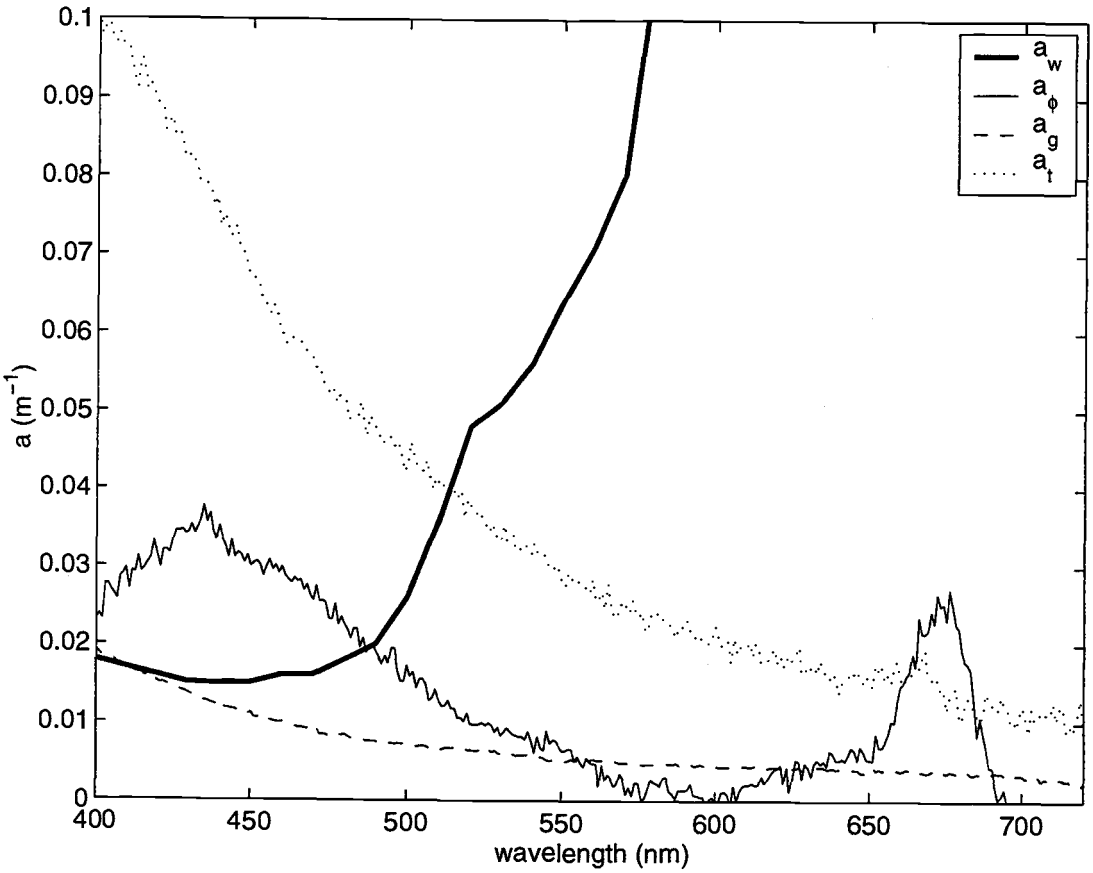

FIGURE 2.2 Major light-absorbing component spectra. The total absorption spectrum is the sum of pure water (a_w), phytoplankton (a_ϕ), gelbstoff (a_g) and tripton (a_t) absorption spectra.

The mathematical expression for the *shape* of a light-absorbing component spectra defines the basis vectors. Roesler et al. (1995) approaches this similar problem where basis vectors of phytoplankton are digitized from laboratory measurements of phytoplankton. The gelbstoff and tripton components have been previously modeled as exponential functions, where the decay rate distinguishes the gelbstoff from a tripton spectra (Carder et al., 1989; Roesler et al., 1989). The decay rates have been estimated from laboratory measurements of gelbstoff and tripton spectra. The basis vectors can then be expressed as,

$$\hat{a}_{\varphi}\ (\lambda) = x_1\ a^n_{\varphi}\ (\lambda) \tag{2.3a}$$

$$\hat{a}_g\ (\lambda) = x_2\ \exp[-S_g(\lambda - \lambda_{ref})] \tag{2.3b}$$

$$\hat{a}_t\ (\lambda) = x_3\ \exp[-S_t(\lambda - \lambda_{ref})]. \tag{2.3c}$$

Although, the shape of the phytoplankton spectrum is dependent upon the taxonomic nature of the phytoplankton, ocean regions have typical phytoplankton assemblages relative to land and as a function of latitude (Round, 1981). The matrix, A, necessarily requires a variety of regionally representative phytoplankton spectral shapes to account for the variations in the phytoplankton community caused by differences in taxonomic compositions. The spectral shapes of pure phytoplankton cultures for construction of the basis vectors is less desirable since the pigment compositions of pure cultures are not representative of the general phytoplankton populations found *in situ* (Roesler and Perry 1995). Representatives of these groups are found within naturally occurring communities *in situ*. The regional phytoplankton spectra used to develop the set of basis vectors are independently published in Roesler and Perry (1995) and are representative of phytoplankton communities dominated by (1) Diatoms, (2) Cyanobac-

teria and Prochlorophytes, (3) Green algae, and (4) Diatoms, Dinoflagellates and Haptophytes. The regionally representative phytoplankton spectra are non-dimensionalized by scaling each element of the spectrum by the sum of the elements of the absorption spectrum. This sets the area under the curve to unity and allows the shapes of different absorption spectra to be comparable.

The non-dimensional gelbstoff and tription absorption spectra, are distinguishable by the extinction coefficient, S_g (nm^{-1}) and S_t (nm^{-1}), respectively. The values of S_g and S_t vary over a range and have been previously determined from laboratory measurements of gelbstoff and tripton absorption spectra (Zepp and Schlotzhauer, 1981; Hayase and Tsubota, 1985; Carder et al. 1989; Roesler et al. 1989). The extinction coefficients for the gelbstoff spectra, S_g, vary between 0.0145 to 0.02. The extinction coefficients for tripton spectra, S_t, vary between 0.009 to 0.011.

In the construction of A, the condition number of A should be kept reasonably small ($< 10^4$) (Candela et al., 1992). In an effort to capture the widest possible ranges of expected absorption component spectra, four phytoplankton, three gelbstoff and three tripton basis vectors were included in A (Fig. 2.3). The sums of the respective component basis vectors are taken as the modeled component absorption spectrum. The manner in which A is constructed gives a condition number for A $O(10^4)$, which is the upper limit for the condition number. The matrix A is underdetermined and of full rank.

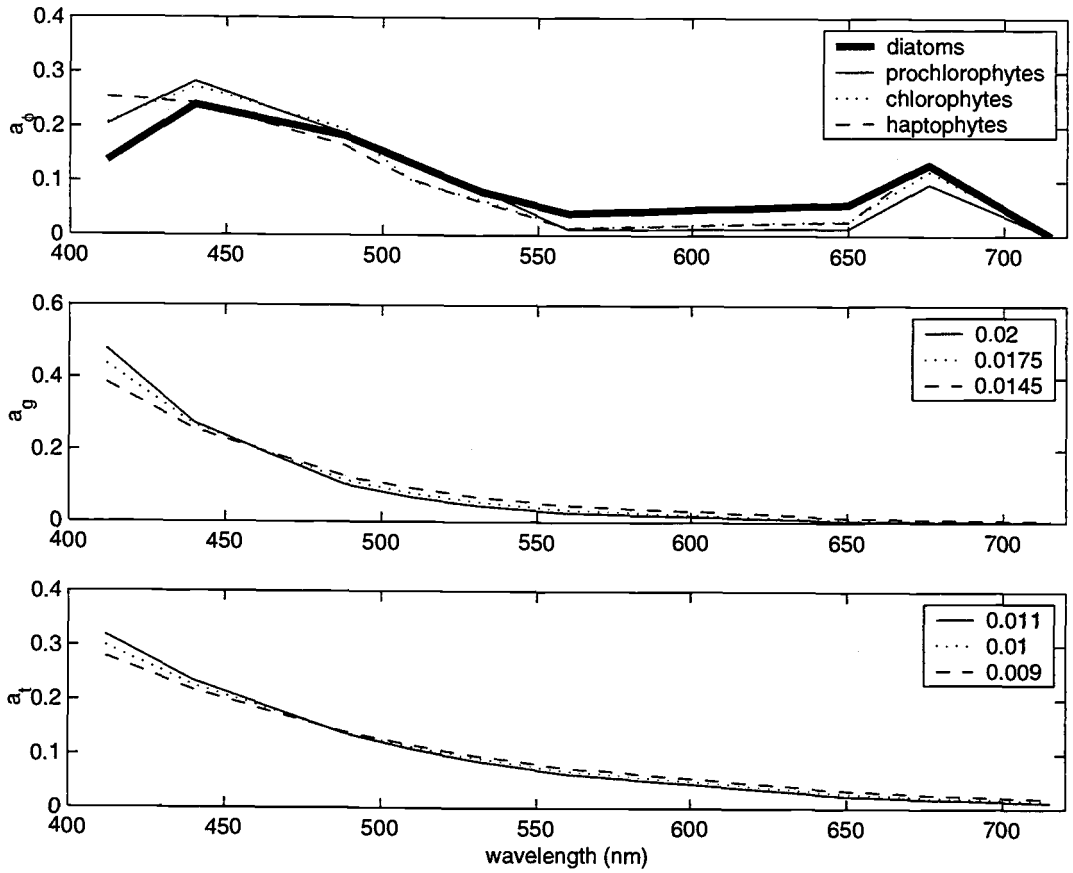

FIGURE 2.3 Non-dimensionalized light-absorbing component spectra. From top to bottom: phytoplankton, gelbstoff and tripton non-dimensional absorption spectra.

Solving an underdetermined least squares problem necessarily yields a range of solutions. In order to obtain the optimal solution, solving the least squares problem requires the minimization of $\| A\,\vec{x} - \vec{y} \|$, subject to $x \geq 0$. The constraint on the solution can potentially enlarge the residuals of the regression, but this constraint remains realistic and physically meaningful. The algorithm for solving non-negative least squares problems is presented by Lawson and Hanson (1974), where a first estimate of a solution is obtained by solving 2.2 using a singular value decomposition. This solution is then examined relative to the imposed criteria. If necessary, editing of the columns of A are performed and the problem is recast until an optimal solution is achieved.

A singular value decomposition (SVD) is used to solve the non-negative least squares problem because it is a numerically more stable method. The inversion of A is prone to large round-off errors so that the use of SVD's is more desirable.

The SVD factorization of A has the form,

$$A = U\,\Sigma\,V^T \tag{2.4}$$

where, U (mxm) and V (nxn) are orthogonal matrices of the eigenvectors of A and Σ (mxn) is a diagonal matrix containing the singular values which are the positive square roots of the eigenvalues of the product A^TA. The singular values of Σ were not edited. Then the least squares approximation of $\mathbf{x}$, $\hat{\mathbf{x}}$, is

$$\hat{\mathbf{x}} = V\,\Sigma^{-1}\,U^{\,T}\,\mathbf{y} \tag{2.5}$$

where Σ^{-1} is the pseudoinverse, a diagonal matrix of the singular values to the -1 power. The residuals of the model estimate are then $\varepsilon = \mathbf{y} - \hat{\mathbf{y}}$. The reader is referred to Lawson and Hanson (1974) for further details of the singular value decomposition and solving least squares problems that are underdetermined and of full rank.

2.4 MODEL VALIDATION

In coastal waters, the fractional contributions of absorbing components can be highly variable (Højerslev, 1979; Jerlov, 1976; Bricaud et al., 1981). In this type of water, the three absorbing components all strongly contribute to the total absorption property. During the Coastal Mixing and Optics Experiment SeaSoar IOP surveys, concurrent measurements were taken by the Oregon State University Optical Oceanography group at a nearby, fixed station (40.5 °N, 70.5°W), where vertical profiles of both a_{T-w} (λ) and a_g (λ) were recorded by deploying two WET Labs ac-9's mounted on a Slow Descent Rate Optical Platform (SlowDROP).

The two SlowDROP ac-9's were used in both unfiltered and filtered (< 0.2 μm) configurations. A processing step, where the measured a_g (λ) is subtracted from the a_{T-w} (λ), permits the retrieval of the particulate absorption, $a_p(\lambda) = a_\varphi(\lambda) + a_t(\lambda)$. Preliminary validation of the decomposition method was conducted using a SlowDROP profile recorded on 20 August 1996. The decomposition method was applied to the observed SlowDROP $a_{T-w}(\lambda)$ (Fig. 2.4) and the observed SlowDROP $a_p(\lambda)$ and $a_g(\lambda)$ are compared with the modeled components from the decomposed SlowDROP $a_{T-w}(\lambda)$ (Fig. 2.5).

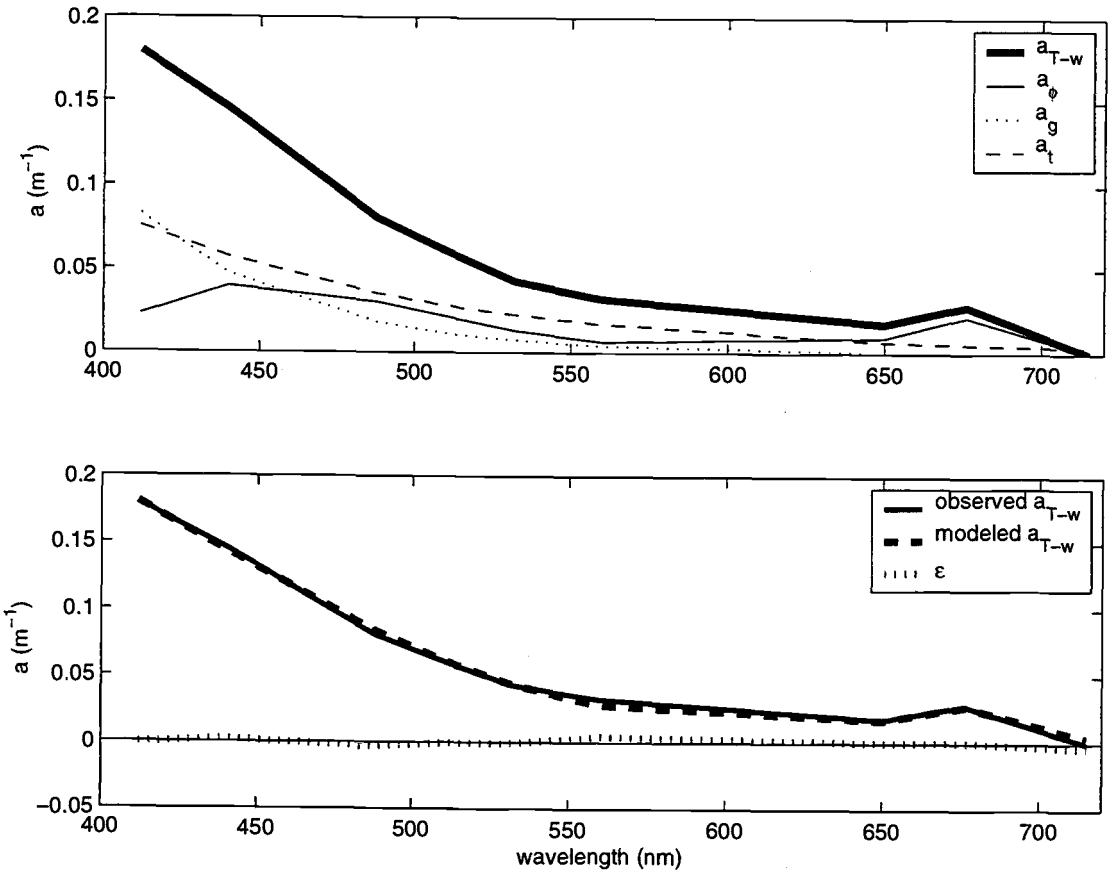

FIGURE 2.4 Decomposed SlowDROP total (minus water) absorption spectrum, $a_{T-w}(\lambda)$. Top panel: Observed a_{T-w} (λ) at 20 meters and modeled component spectra. The modeled phytoplankton spectra is characteristic of diatoms. Extinction coefficients of modeled $a_g(\lambda)$ and $a_t(\lambda)$ are 0.02 nm^{-1} and 0.01 nm^{-1}. Lower panel: Observation and model (sum of modeled component spectra) comparison of a_{T-w} (λ). Residuals are also shown.

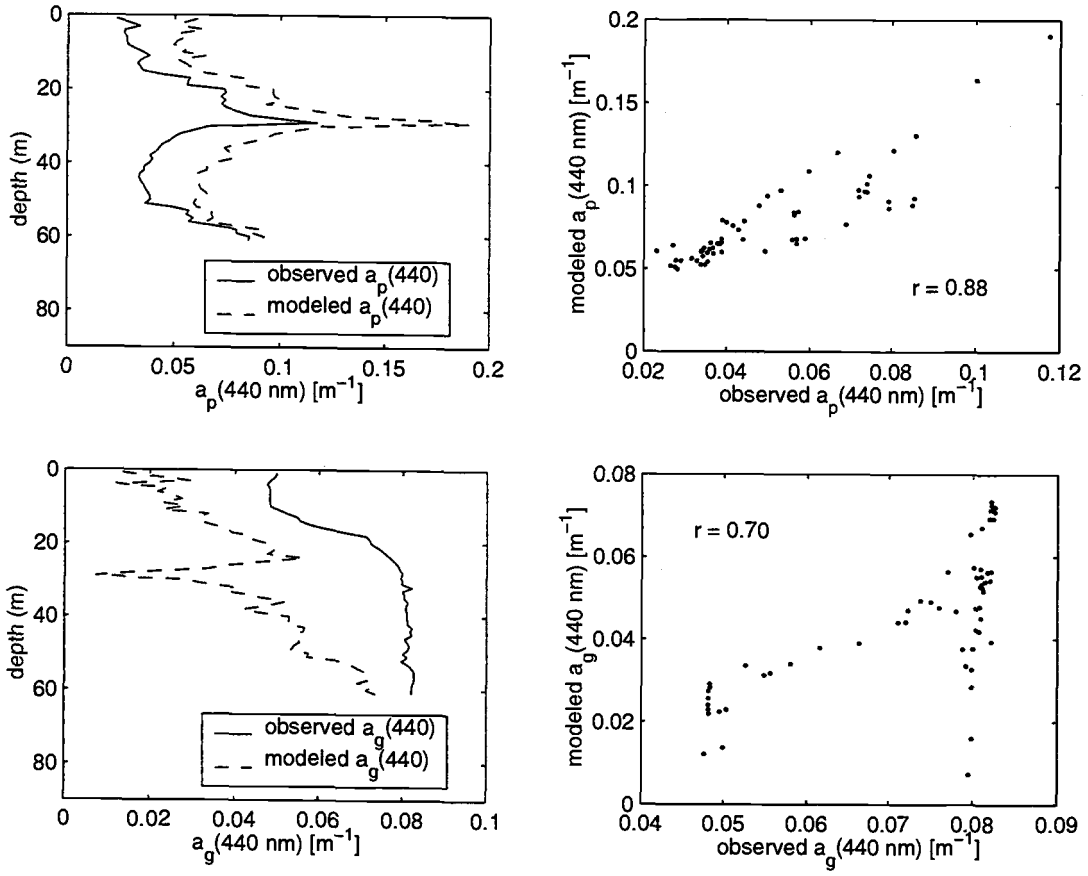

FIGURE 2.5 SlowDROP observed and modeled profile comparison and regression. Left panels: Observed and modeled particulate absorption, $a_p(440\text{ nm})$ [m^{-1}], (top) and gelbstoff absorption, $a_g(440\text{ nm})$ [m^{-1}], (bottom). Right panels: Modeled $a_p(440\text{ nm})$ [m^{-1}] regressed onto observed $a_p(440\text{ nm})$ [m^{-1}] (top), modeled $a_g(440\text{ nm})$ [m^{-1}] regressed onto observed $a_g(440\text{ nm})$ [m^{-1}] (bottom)

The a_{T-w} spectrum measured at a depth of 20 meters decomposed into its component absorption spectra (Fig. 2.4) shows tripton absorption at 440 nm is the dominant contributor to the total absorption in this particular example. Phytoplankton spectra are characteristic of diatoms (Bacillariophytes), which agrees with the identified phytoplanktonic genera (eg. *Cosinodiscus sp.*, Sosik [per. comm.]). Modeled gelbstoff and tripton spectra have extinction coefficients of 0.02 nm^{-1} and 0.01 nm^{-1}, respectively. The hindcast skill of the regression model is good ($\hat{S} = 0.99$) and significant ($\hat{S}_{crit} = 0.43$) at the 95% confidence level. The confidence intervals on the regression coefficients, $\hat{\mathbf{x}}$, are of $O(10^{-4})$. The regressions of the modeled component absorption onto the observed $a_p(440)$ and $a_g(440)$ demonstrate fairly high positive correlations, $r = 0.88$ and $r = 0.70$, respectively. Upon examination of the profiles (Fig. 2.5) of the light-absorbing components, it becomes clear that the model overestimates the contribution by the tripton component and underestimates the contribution by the gelbstoff component.

2.5 RESULTS

The summer 1996 and spring 1997 spatial distributions of the component absorption in three-dimensional physical space are presented in this section. The spatial distributions of temperature (°C), salinity (PSU), scattering coefficient at 440 nm ($b(440)$), total (minus water) absorption coefficient at 440 nm ($a_{T-w}(440)$) and component absorption at 440 nm are presented as sections (y, z) and horizontal maps (x, y). Horizontal maps of hydrographic and inherent optical properties are presented at fixed depths of 5 and 45 meters and at a varying depth of 10 meters above the bottom (mab).

2.5.1 Summer 1996

The summer season in the Middle Atlantic Bight south of Cape Cod, Massachusetts, is characterized by a strongly stratified water column and a strong seasonal pycnocline that is evident in the cross-shelf sections of temperature, salinity and density (Fig 2.6). This stratified structure has been found previous to the CMO Experiment (Aikman, 1984). Surface waters tended to be warm (T $\approx$ 16°C) and fresh (S $\approx$ 32 PSU). Cold (T $<$ 9°C) and fresh (S $\approx$ 32.25 PSU) deeper shelf waters, remnants of winter mixing and known as the "cold pool", were found on the outer shelf (h_b = 80-100 m) at depth and extending into the interior over the slope (h_b $>$ 100 m). Slope waters were warmer (T $\approx$ 10°C) and more saline (S $\approx$ 34 PSU). The density structure demonstrates the strong seasonal stratification and that the temperature and salinity are density compensating. The prominent features of the density structure are the pycnocline and the presence of the shelfbreak front. The base of the pycnocline is delineated by the σ_t = 24.6 kg m^{-3} isopycnal. The shelfbreak front is identifiable by the σ_t = 25.8 kg m^{-3} isopycnal. The foot of the shelfbreak front is located along the 90-m isobath at 40.26°N.

The distributions of IOPs at 440 nm consists of higher magnitudes on the shelf and optically clearer slope waters (Fig. 2.6). The distribution of the scattering coefficient at 440 nm demonstrates large magnitude scattering coefficients (b(440) $\approx$ 0.4 m^{-1}) associated with the pycnocline and the bottom boundary layer. Large magnitude scattering coefficients at 440 nm is also found throughout the water column on the inshore edge of the section ($h_b \leq$ 55 m).

As shown by Barth et al. (1998), the scattering coefficients illustrate the separation of the bottom boundary layer into the interior at the shelfbreak front. The largest magnitudes of the total (minus water) absorption coefficient ($a_{T-w}(440) \approx 0.16\ \mathrm{m}^{-1}$) are found in patches following the base of the pycnocline (delineated by the 24.6 kg m^{-3} isopycnal on Fig. 2.6).

The distributions of the modeled component absorption coefficients at 440 nm (Fig. 2.7) reveals the large magnitude absorption (and scattering) coefficients distributed along the base of the pycnocline, are due to the presence of phytoplankton. The heterogeneity of the phytoplankton layer could be due to the active grazing by gelatinous zooplankton that were found to be abundant during the summer cruise (Simeon et al., 2000). The algal material shown close to the bottom is an artifact of the interpolation method (note data locations). The distribution of gelbstoff absorption at 440 nm tended to have the largest magnitudes ($a_g(440) = 0.06$) close to the bottom, on the shelf. Larger magnitude gelbstoff absorption coefficients are generally found below the pycnocline. The distribution of tripton absorption coefficient at 440 nm shows the largest magnitudes are associated with the subsurface phytoplankton layer following the $\sigma_t = 24.6$ kg m^{-1} isopycnal. The tripton absorption distribution at 440 nm also traces the bottom boundary layer on the shelf and its separation near the foot of shelfbreak front.

Horizontal maps of temperature, salinity, $a_{T-w}(440)\ \mathrm{m}^{-1}$ and $b(440)$ at 5 m, 45 m and 10 m above the bottom are shown in Fig. 2.8. At 5 m, the layer of water is density compensated as seen in the temperature and salinity distributions. Towards the western edge of the survey region, a warm and saline water mass is evident on the shelf. Along 45 m and 10 m above the bottom, the cold pool is observable and is more saline than the overlying shelf waters, which makes

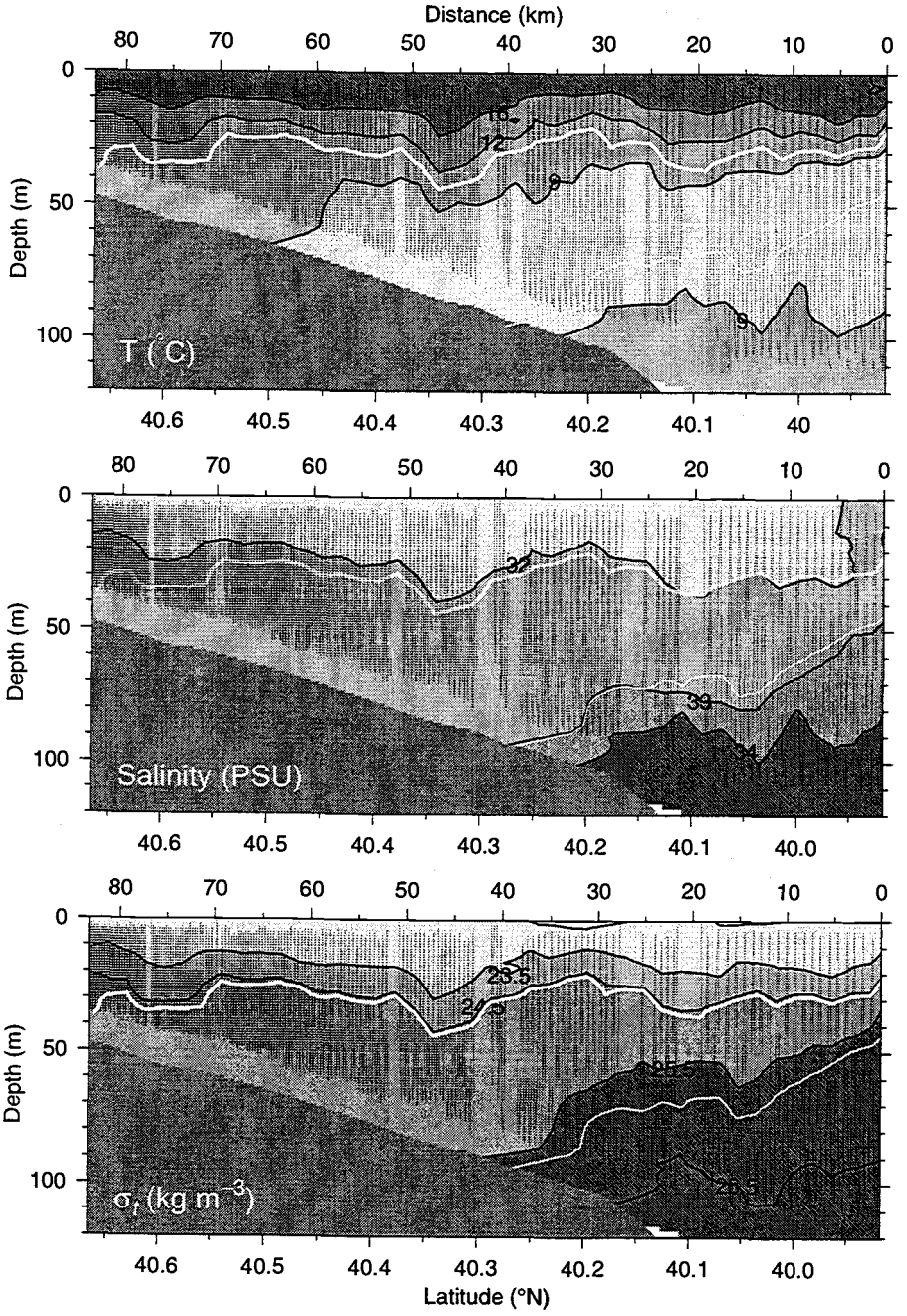

FIGURE 2.6 Cross-shelf spatial distributions of (top) temperature (middle) salinity and (bottom) σ_t during 17 Aug 1996 along 70.2°W. The base of the pycnocline is delineated by the $\sigma_t = 24.6$ kg m^{-3} isopycnal (thick white curve). The thin white curve indicates the presence of the shelfbreak front ($\sigma_t = 25.8$ kg m^{-3}). Variables were contoured onto a 2-km by 2-m grid using a LaPlace interpolation. Data locations are specified by black bullets.

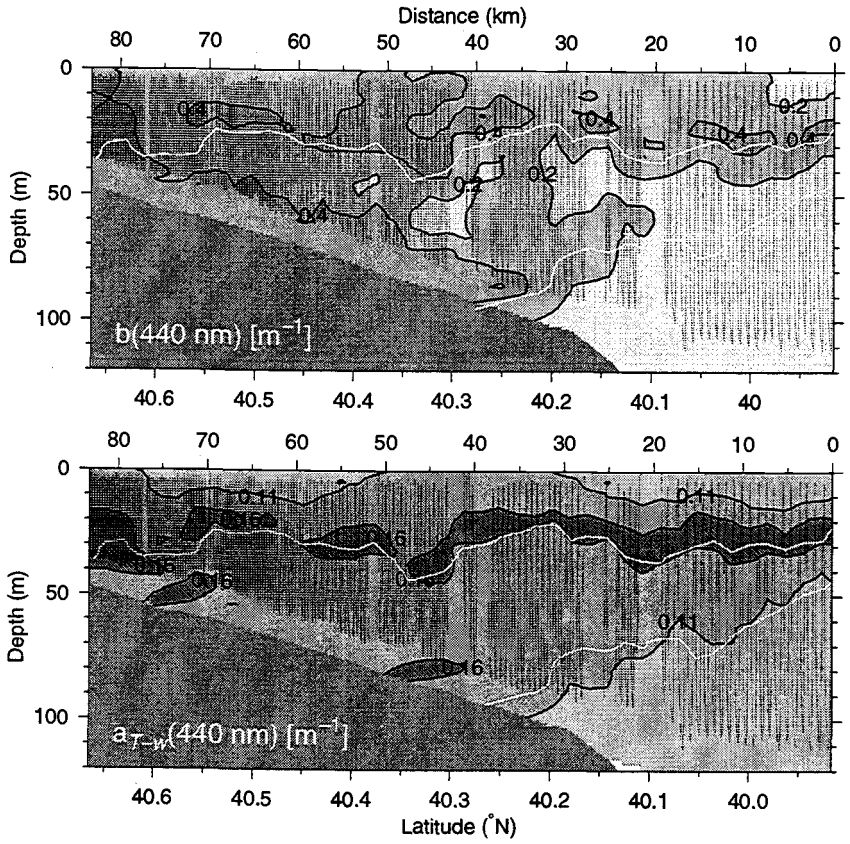

FIGURE 2.6 (Continued) Cross-shelf spatial distributions of (top) $b(440)$ and (bottom) $a_{T-w}(440)$ during 17 Aug 1996 along 70.2°W. Units are m^{-1}. The base of the pycnocline is delineated by the $\sigma_t = 24.6$ kg m^{-3} isopycnal (white curve). The thin white curve indicates the presence of the shelfbreak front ($\sigma_t = 25.8$ kg m^{-3}). Variables were contoured onto a 2-km by 2-m grid using a LaPlace interpolation. Data locations are specified by black bullets.

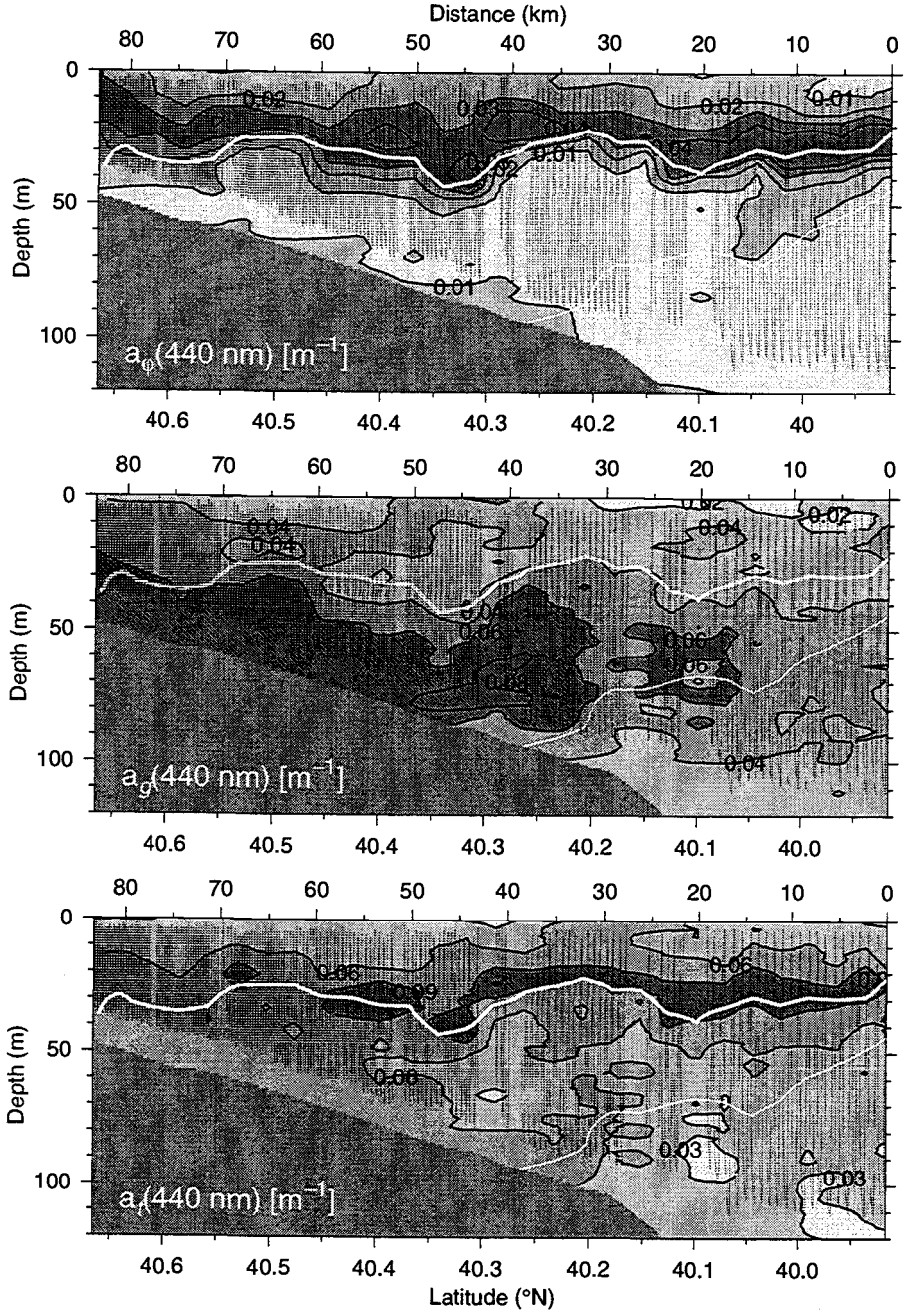

FIGURE 2.7 Cross-shelf spatial distributions of (top to bottom) $a_\varphi(440\text{ nm})$, $a_g(440\text{ nm})$, $a_t(440\text{ nm})$. Units are m^{-1}. Component absorption are obtained by decomposing the $a_{T-w}(\lambda)$ measured during 17 Aug 1996 along 70.2°W. The base of the pycnocline is delineated by the $\sigma_t = 24.6$ kg m^{-3} isopycnal (thick white curve). The thin white curve indicates the presence of the shelfbreak front ($\sigma_t = 25.8$ kg m^{-3}). Variables were contoured onto a 3-km by 3-m grid using a LaPlace interpolation. Data locations are specified by black bullets.

this feature very stable. The distribution of the IOPs at 5 m exhibits a pattern similar to the temperature at 5 m, where warm waters are relatively clearer than the colder waters. At 45 m, the mid-shelf (h_b = 50-80 m) shows distinctively higher IOPs than the optically clearer outer shelf and slope waters. At 10 m above the bottom, the clearer western part of the survey region is contrasted by the relatively higher IOPs of the shelf to the east.

The maps of the distributions of the component absorption at 440 nm are presented in Fig. 2.9. The phytoplankton and gelbstoff absorption at 5 m proportionally reflects the temperature distributions. Tripton absorption at 5 m shows higher values are concentrated over the outer shelf. At 45 m, the $a_{T-w}(440)$ and $b(440)$ on the mid-shelf at 70.5°W is due to $a_{\varphi}(440)$. At 10 m above the bottom, the high $a_{T-w}(440)$ and $b(440)$ on the mid-shelf appears to be largely due to the presence of strongly absorbing tripton and on the outer shelf, $a_g(440)$ m^{-1} becomes the major contributor to the total absorption.

The residuals at 440 nm of the regression model (Fig. 2.10) show are within the instrumental error ($a_{T-w}(\lambda) = 0.005$ m^{-1}). The largest residuals are found to be associated with the bottom boundary layer on the shelf, perhaps indicating the model's difficulty in distinguishing the tripton and gelbstoff components. The residuals are also consistently positive throughout most of the section, suggesting that there is some bias at this wavelength that could be due to a calibration offset.

The model parameters that optimized the least squares regression yields further information about the composition of the particulate and dissolved materials suspended in the water column (Fig. 2.10). The four phytoplankton basis vectors were assigned a number (1 = Diatoms, 2 = Cyanobacteria and Prochlorophytes, 3 = Chlorophytes and 4 = Diatoms, Dinoflagellates and Haptophytes). Diatomaceous phytoplankton were most typical, though some

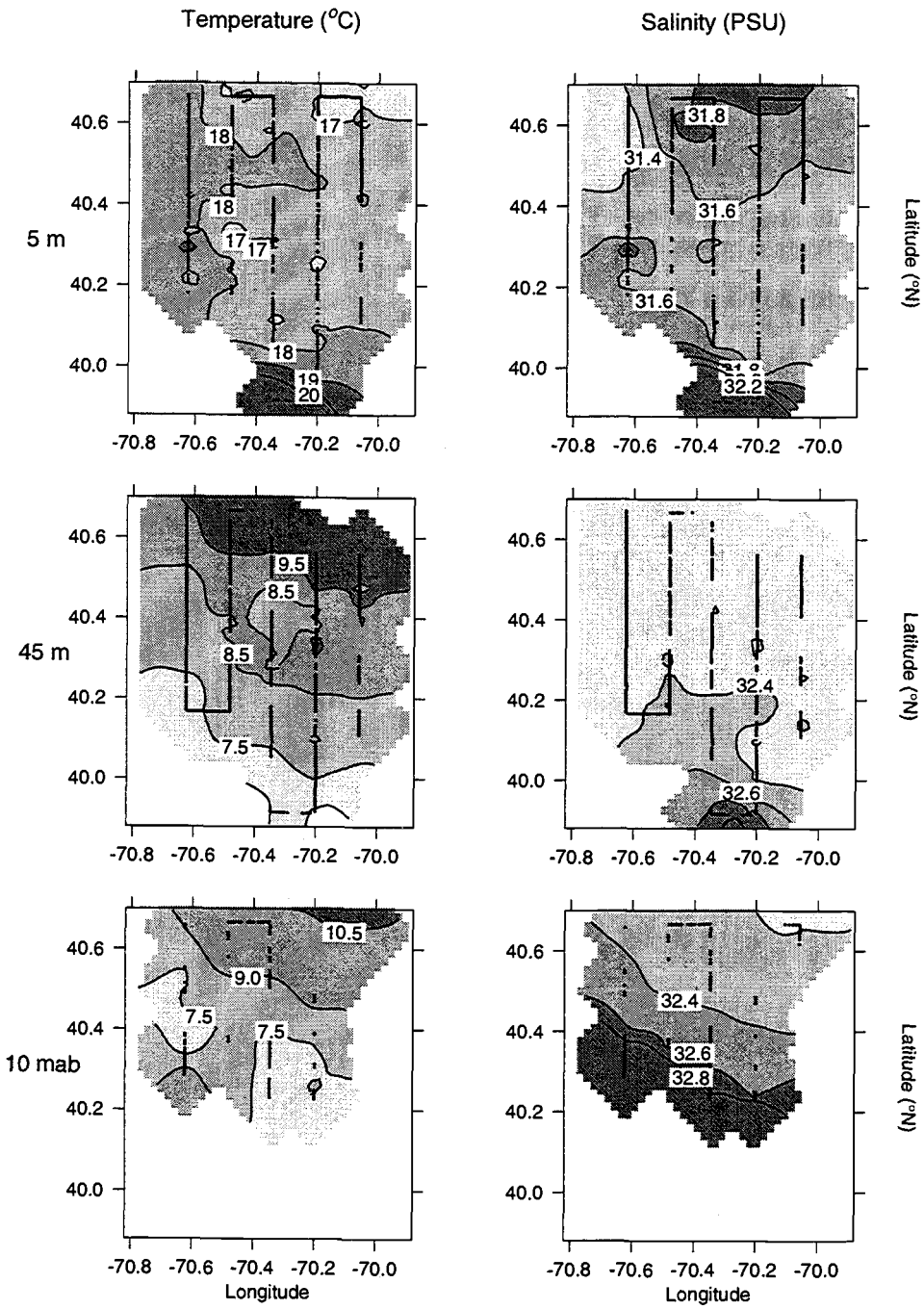

FIGURE 2.8 Maps of horizontal spatial distributions of temperature (left) and salinity (right) at (top to bottom) 5 m, 45 m and 10 m above the bottom during 17-18 Aug 1996. Variables were contoured onto a 2-km by 2-km grid using a LaPlace interpolation. Data locations are specified by black bullets.

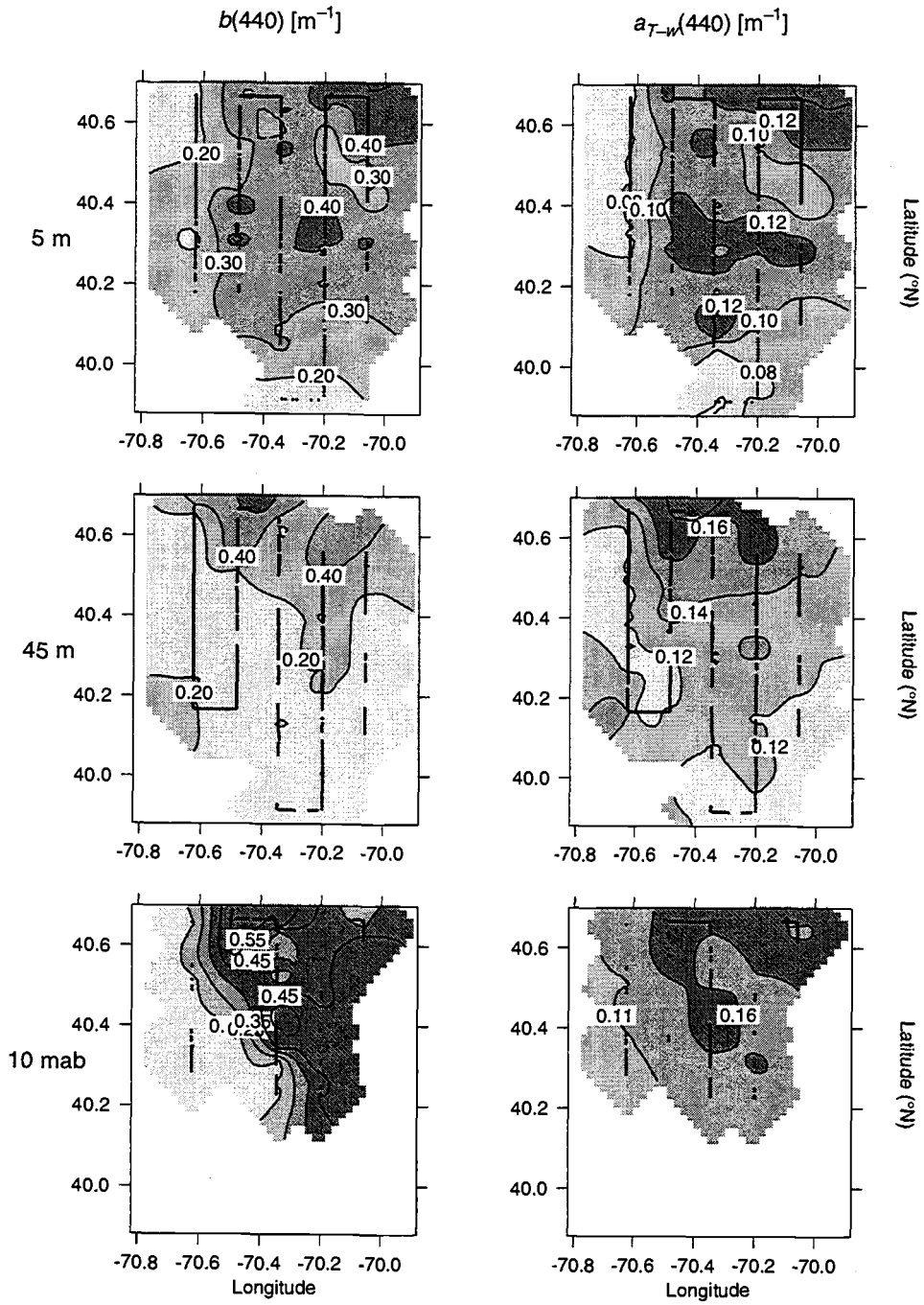

FIGURE 2.8 (Continued) Maps of horizontal spatial distributions of $b(440$ nm) (left) and $a_{T-w}(440$ nm) (right) at (top to bottom) 5 m, 45 m and 10 m above the bottom during 17-18 Aug 1996. Units are m^{-1}. Variables were contoured onto a 2-km by 2-km grid using a LaPlace interpolation. Data locations are specified by black bullets.

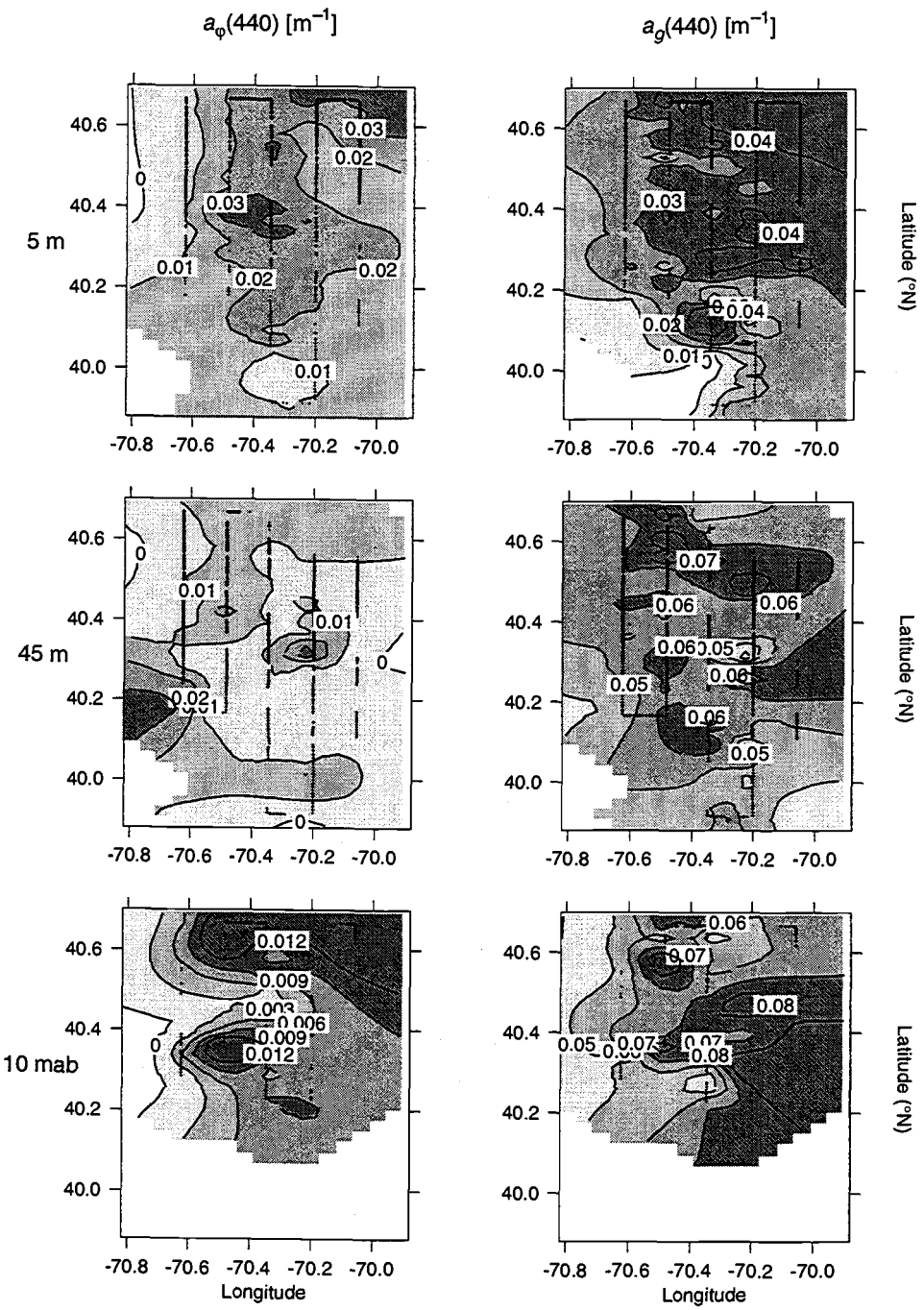

FIGURE 2.9 Maps of horizontal spatial distributions of $a_\varphi(440$ nm) (left) and $a_g(440$ nm) (right) at (top to bottom) 5 m, 45 m and 10 m above the bottom during 17-18 Aug 1996. Units are m^{-1}. Variables were contoured onto a 2-km by 2-km grid using a LaPlace interpolation. Data locations are specified by black bullets.

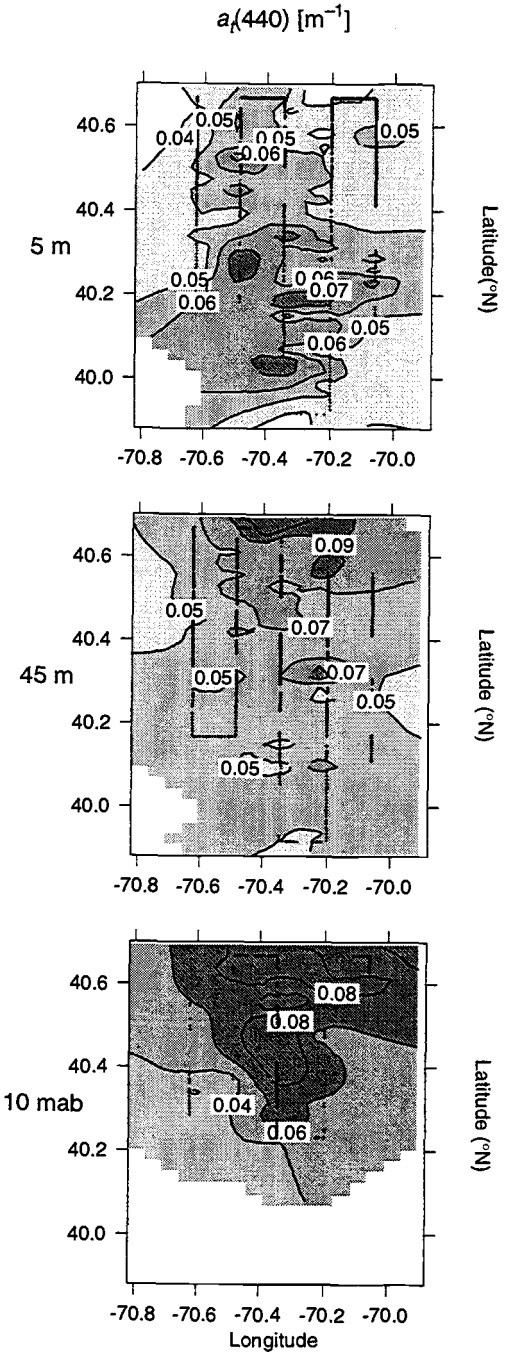

FIGURE 2.9 (Continued) Maps of horizontal spatial distributions of a_t(440 nm) at (top to bottom) 5 m, 45 m and 10 m above the bottom during 17-18 Aug 1996. Units are m^{-1}. Variables were contoured onto a 2-km by 2-km grid using a LaPlace interpolation. Data locations are specified by black bullets.

Cyanobacteria/Prochlorophytes were found at the base of the pycnocline. Offshore, close to the bottom, the regression model tended to select the fourth phytoplankton basis vector. The gelbstoff extinction coefficient indicates the nature of the chromophoric "dissolved" organic materials ($S_g = 0.014$ nm^{-1} are semi-labile humic acids or ($S_g = 0.02$ nm^{-1}) refractory fulvic acids, Carder et al. (1989)).

The distribution of the gelbstoff extinction coefficient shows semi-labile dissolved materials are associated with the phytoplankton in the near surface and within the cold pool and the separating bottom boundary layer. In a similar fashion, the tripton extinction coefficient is indicative of the composition of the particulate matter, but in this case, the inorganic particulates are associated with larger extinction coefficients, while organic particulates are associated with smaller extinction coefficients.

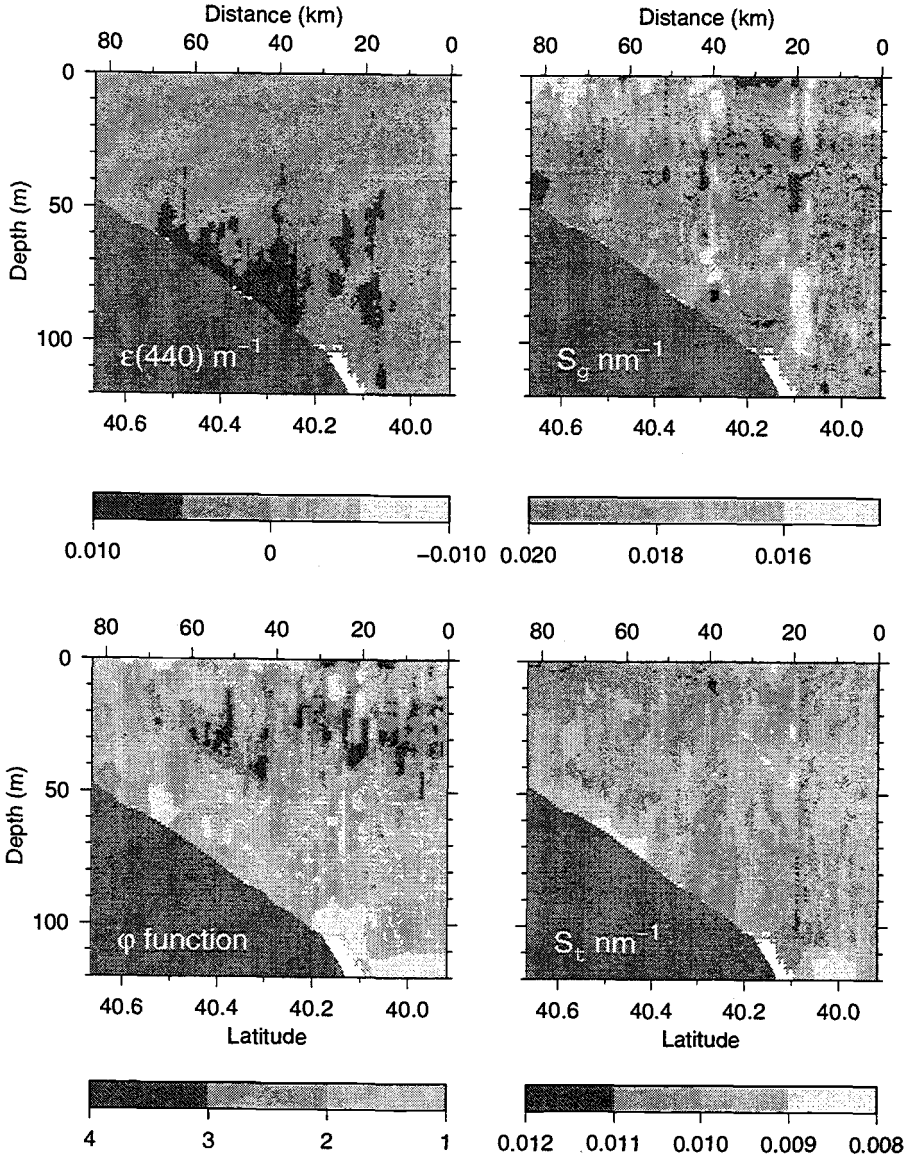

FIGURE 2.10 Cross-shelf spatial distribution of (clockwise) residuals at 440 nm and model parameters: S_g, S_t and φ type during 17-18 Aug 1996. Variables were contoured onto a 1-km by 2-m grid using a LaPlace interpolation.

2.5.2 Spring 1997

In spring 1997, passing storms kept the surface layer fairly deep and well-mixed during this period of re-stratification as shown by the temperature and density structures (Fig. 2.11). The strength of the stratification increased with time (Chang et al., submitted) during the CMO Experiment. Evident in the temperature structure is the onset of stratification, where a 5-m thick warm layer caps the surface. The actual depth of the mixed layer is shown to extend down to 40 meters on the shelf. The cold pool is also evident and is enclosed at is offshore boundary by the onshore advection of warmer deep slope waters that almost reach the mid-shelf ($h_b < 80$ m). The salinity structure also indicates the upslope advection of saline deep slope waters up to the mid-shelf (Fig. 2.11).

The inherent optical properties during the spring provide further evidence of the depth of the surface mixed layer (Fig. 2.11). The region of relatively stronger absorption and scattering (m^{-1}) is above the 25.4 kg m^{-3} isopycnal. The presence of the bottom mixed layer is also made more prominent by its relatively higher scattering coefficients. The optically clearer slope waters contrasts with the more turbid shelf waters.

The decomposition of $a_{T-w}(440)$ m^{-1} into the phytoplankton, gelbstoff and tripton components (Fig. 2.12) shows the large magnitudes associated with the surface mixed layer is due to particulate components. Large magnitude light absorption coefficients below the pycnocline is due to a combination of the gelbstoff and tripton components. Gelbstoff absorption coefficients are largest below the pycnocline and on the mid-outer shelf. The tripton component is the dominant contributor to the total absorption at 440 nm. The model parameters chosen by the regression were constant for this particular section (φ type $= 4$; $S_g = 0.02$ nm^{-1}; $S_t = 0.009$ nm^{-1}). The consistent choice of the fourth phytoplank-

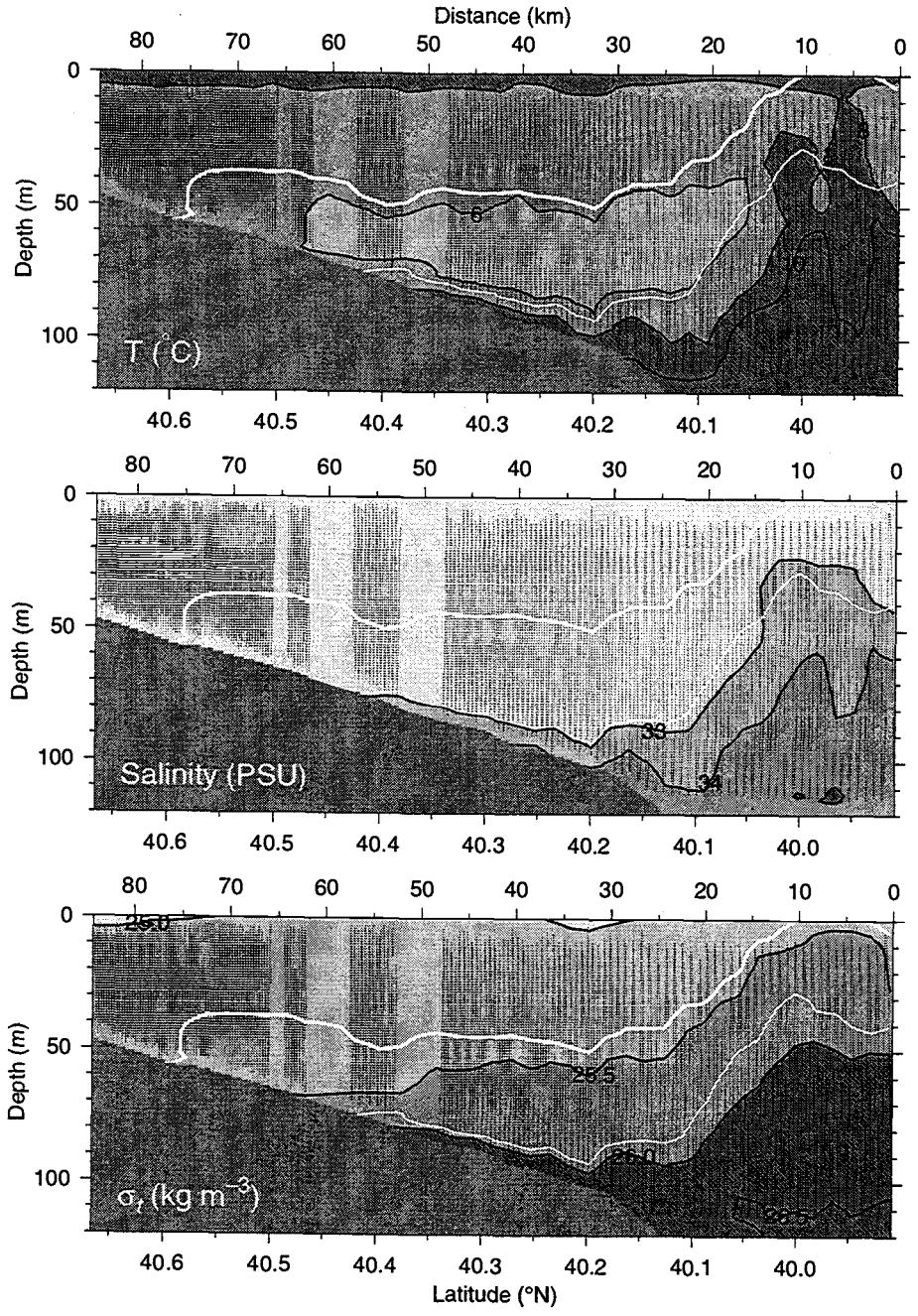

FIGURE 2.11 Cross-shelf spatial distributions of (top) temperature (middle) salinity and (bottom) σ_t during 4 May 1997 along 70.2°W. The base of the pycnocline is delineated by the $\sigma_t = 25.4$ kg m^{-3} isopycnal (thick white curve). The thin white curve indicates the presence of the shelfbreak front ($\sigma_t = 25.8$ kg m^{-3}). Variables were contoured onto a 2-km by 2-m grid using a LaPlace interpolation. Data locations are specified by black bullets.

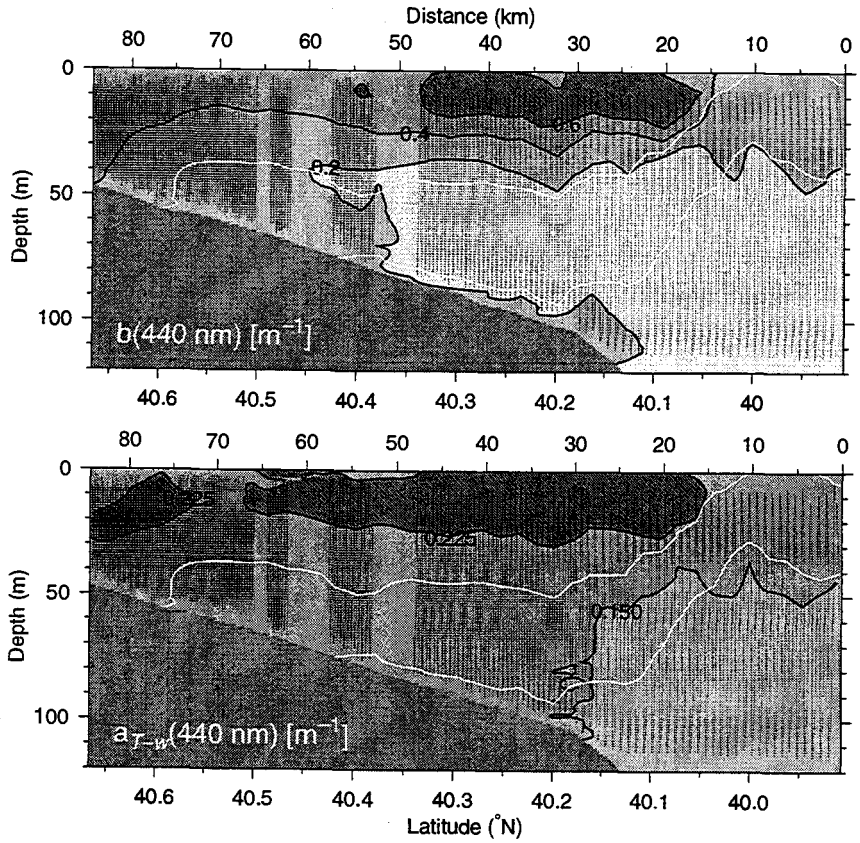

FIGURE 2.11 (Continued) Cross-shelf spatial distributions of (top) $b(440)$ and (bottom) $a_{T-w}(440)$ during 4 May 1997 along 70.2°W. Units are m^{-1}. The base of the pycnocline is delineated by the $\sigma_t = 25.4$ kg m^{-3} isopycnal (white curve). The thin white curve indicates the presence of the shelfbreak front ($\sigma_t = 25.8$ kg m^{-3}). Variables were contoured onto a 2-km by 2-m grid using a LaPlace interpolation. Data locations are specified by black bullets.

ton basis vector is reasonable, considering diatoms and dinoflagellates were the predominant species found during the spring cruise (Roesler, pers. comm.). The residuals are larger than those obtained from the decomposition of the summer data and are consistently negative (Fig. 2.13). This is perhaps indicative of the poorer fitting capabilities of the chosen basis vectors.

The springtime horizontal distributions of the hydrographic and inherent optical properties at 5 m, 45 m and 10 m above the bottom (Fig. 2.14) show at 5 m, the surface temperatures and salinities are fairly uniform. The shelfbreak front is relaxed. At 45 m and 10 m above the bottom, hydrographic properties exhibit the archetypal structure: cool, fresh shelf waters and warmer, saline slope waters that compensate density.

Horizontal distributions of the component absorption coefficients (Fig. 2.15) show that the strong $a_{T-w}(440)$ and $b(440)$ m^{-1} signals at 5 m are equivalently due to the phytoplankton and tripton component. Gelbstoff absorption at 440 nm is strongest over the mid-shelf at 5 m. The distribution of phytoplankton is fairly patchy at 45 m then concentrates over the shelf at 10 m above the bottom. The tripton distribution at 45 m and 10 m above the bottom appears to be horizontally uniform, excepting the northeast corner to the survey region, where tripton absorption m^{-1} is the strongest. At 45 m and 10 m above the bottom, the magnitude of $a_g(440)$ m^{-1} increases by 0.01 m^{-1} on the mid-shelf and remains distinct from the low gelbstoff outer shelf and slope waters.

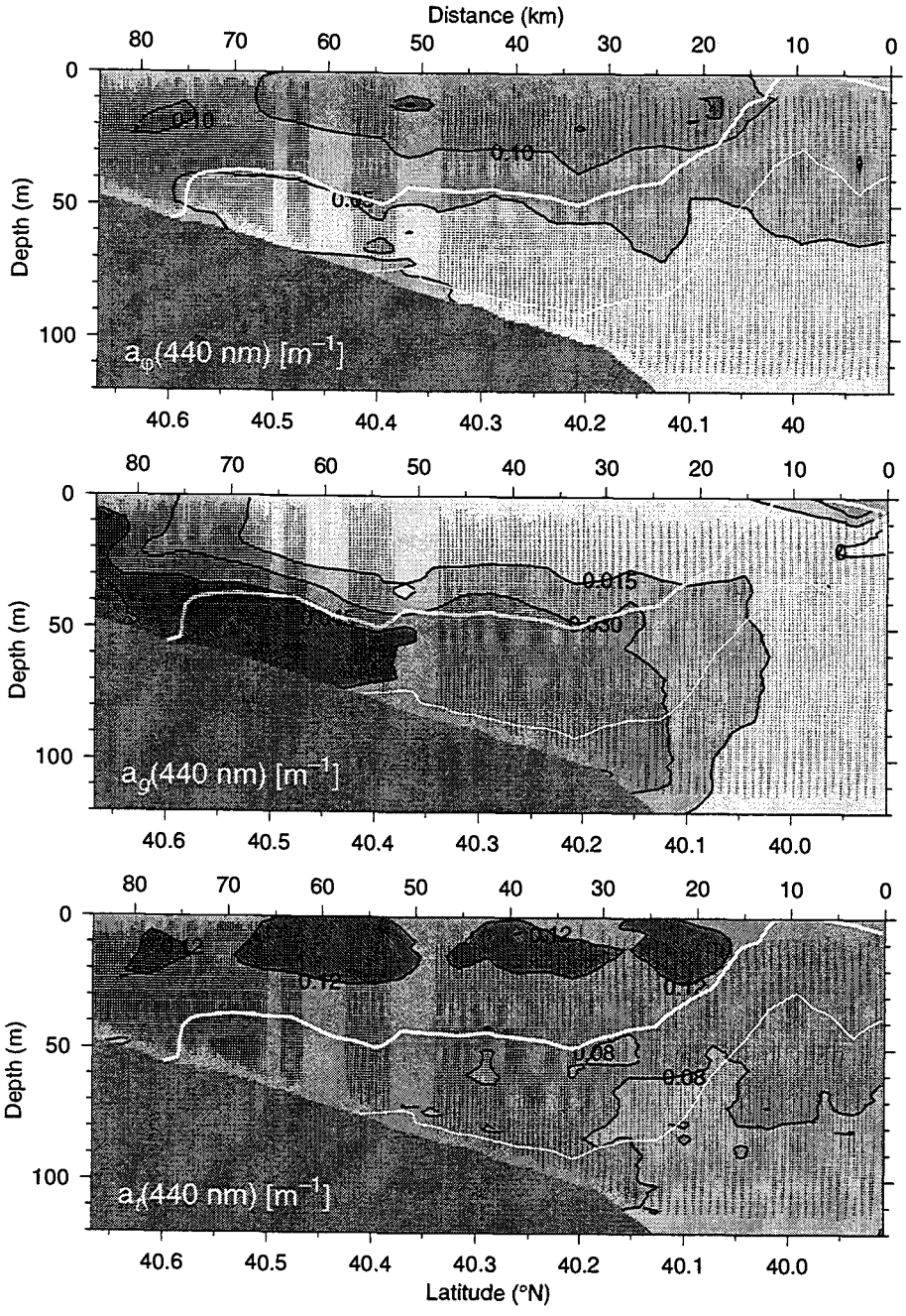

FIGURE 2.12 Cross-shelf spatial distributions of (top to bottom) $a_\varphi(440)$, $a_g(440)$ and $a_t(440)$ during 4 May 1997 along 70.2°W. The base of the pycnocline is delineated by the $\sigma_t = 25.4$ kg m^{-3} isopycnal (white curve). Variables were contoured onto a 2-km by 2-m grid using a LaPlace interpolation. Resolution of measurements is highest on the shelf and decreases over the slope.

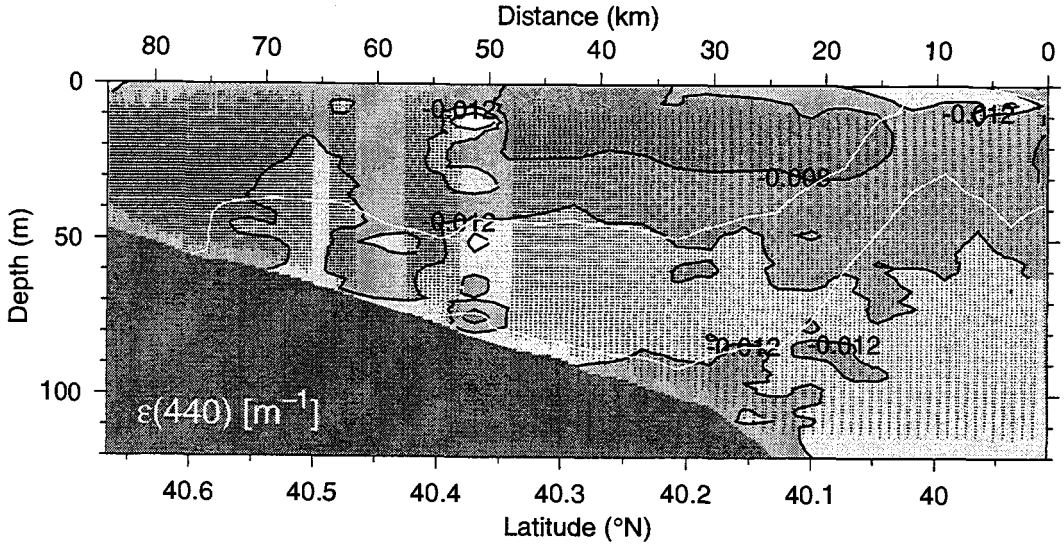

FIGURE 2.13 Cross-shelf spatial distributions of the residuals of the decomposition $\varepsilon(440)$ during 4 May 1997 along 70.2°W. Units are m^{-1}. The base of the pycnocline is delineated by the σ_t = 25.4 kg m^{-3} isopycnal (white curve). Variables were contoured onto a 3-km by 3-m grid using a LaPlace interpolation. Data locations are indicated by black bullets.

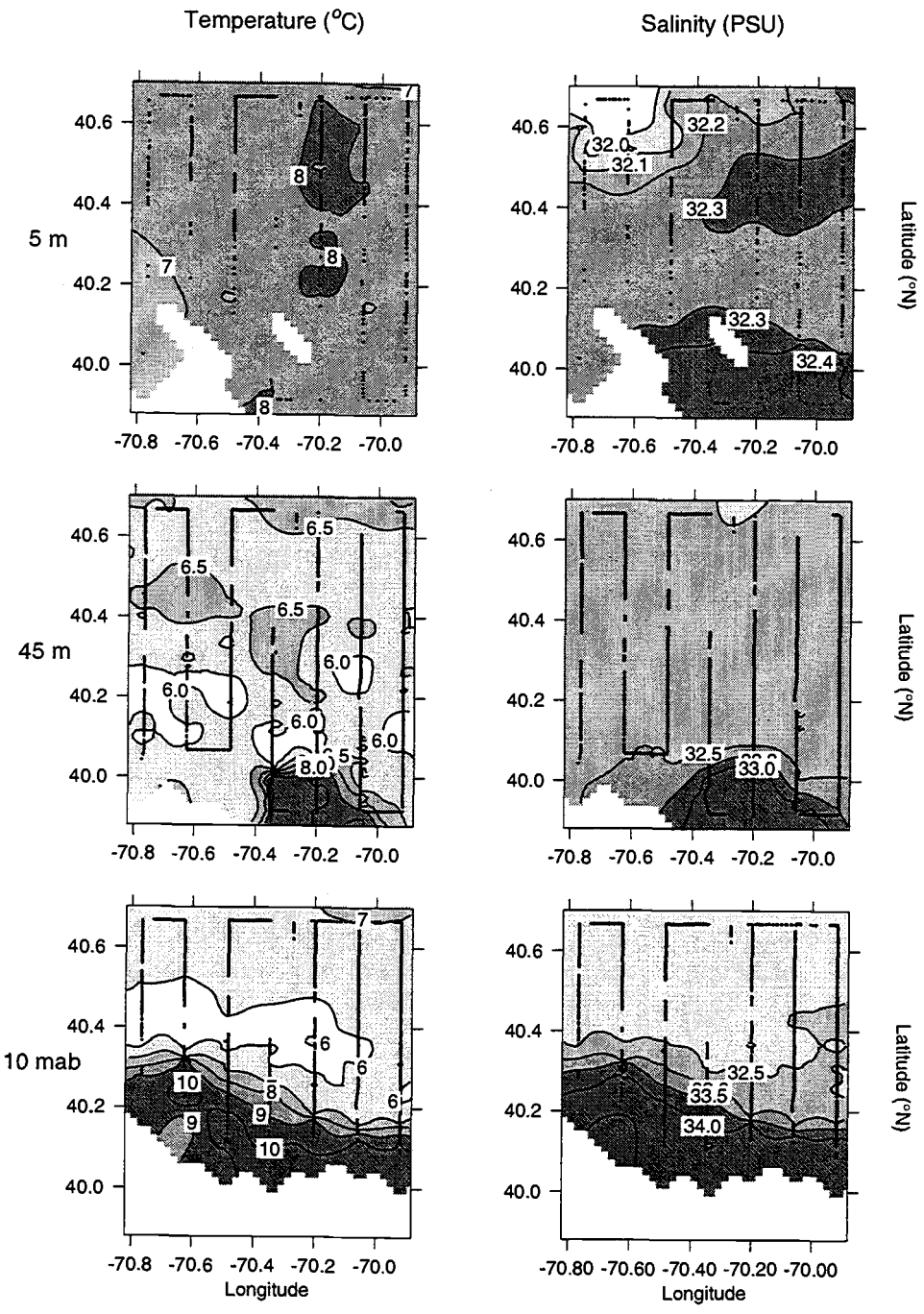

FIGURE 2.14 Maps of horizontal spatial distributions of temperature (left) and salinity (right) at (top to bottom) 5 m, 45 m and 10 m above the bottom during 4-6 May 1997. Variables were contoured onto a 2-km by 2-km grid using a LaPlace interpolation. Data locations are indicated by black bullets.

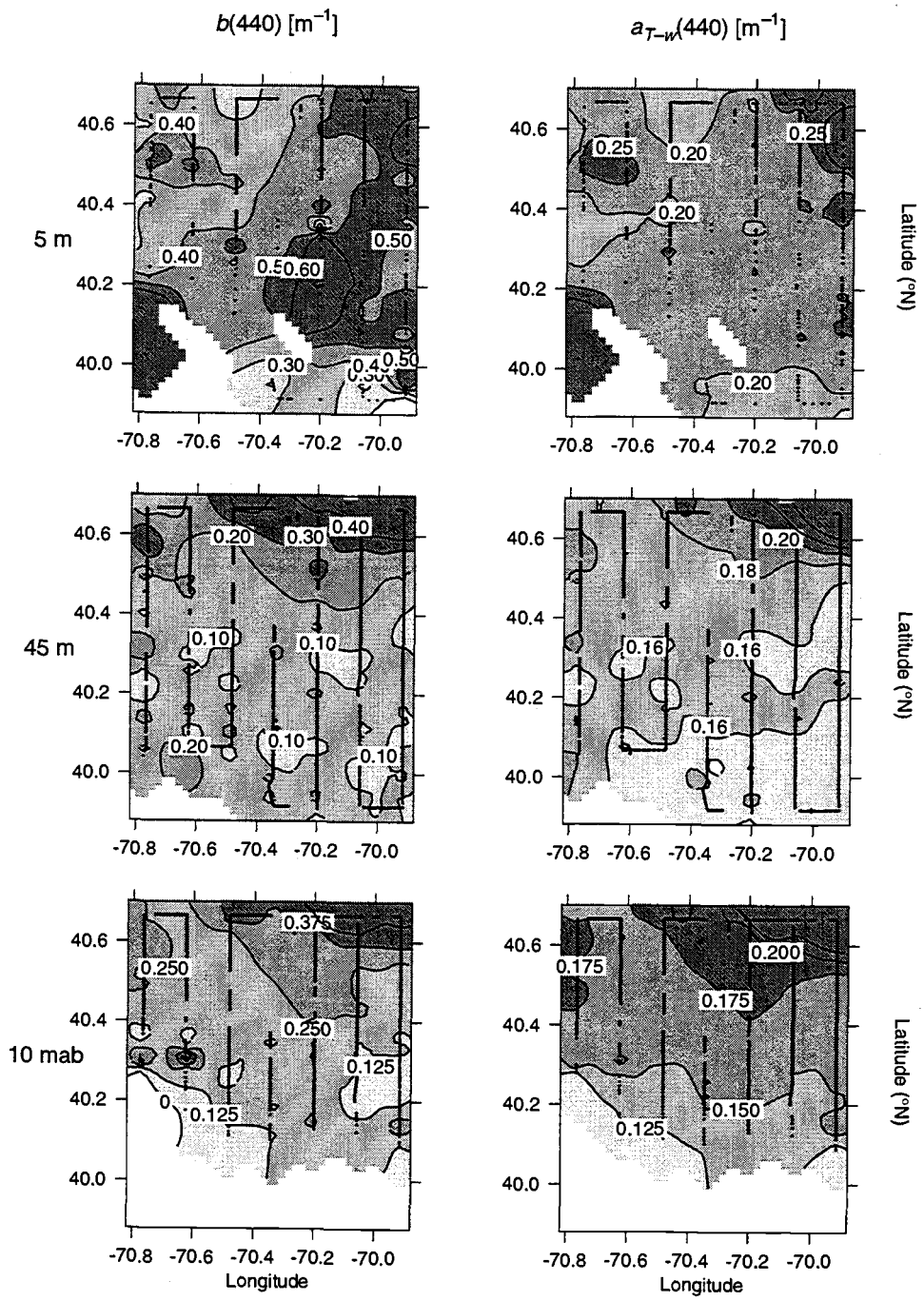

FIGURE 2.14 (Continued) Maps of horizontal spatial distributions of a_{T-w}(440 nm) (left) and b(440 nm) (right) at (top to bottom) 5 m, 45 m and 10 m above the bottom during 4-6 May 1997. Units are m^{-1}. Variables were contoured onto a 2-km by 2-km grid using a LaPlace interpolation. Data locations are indicated by black bullets.

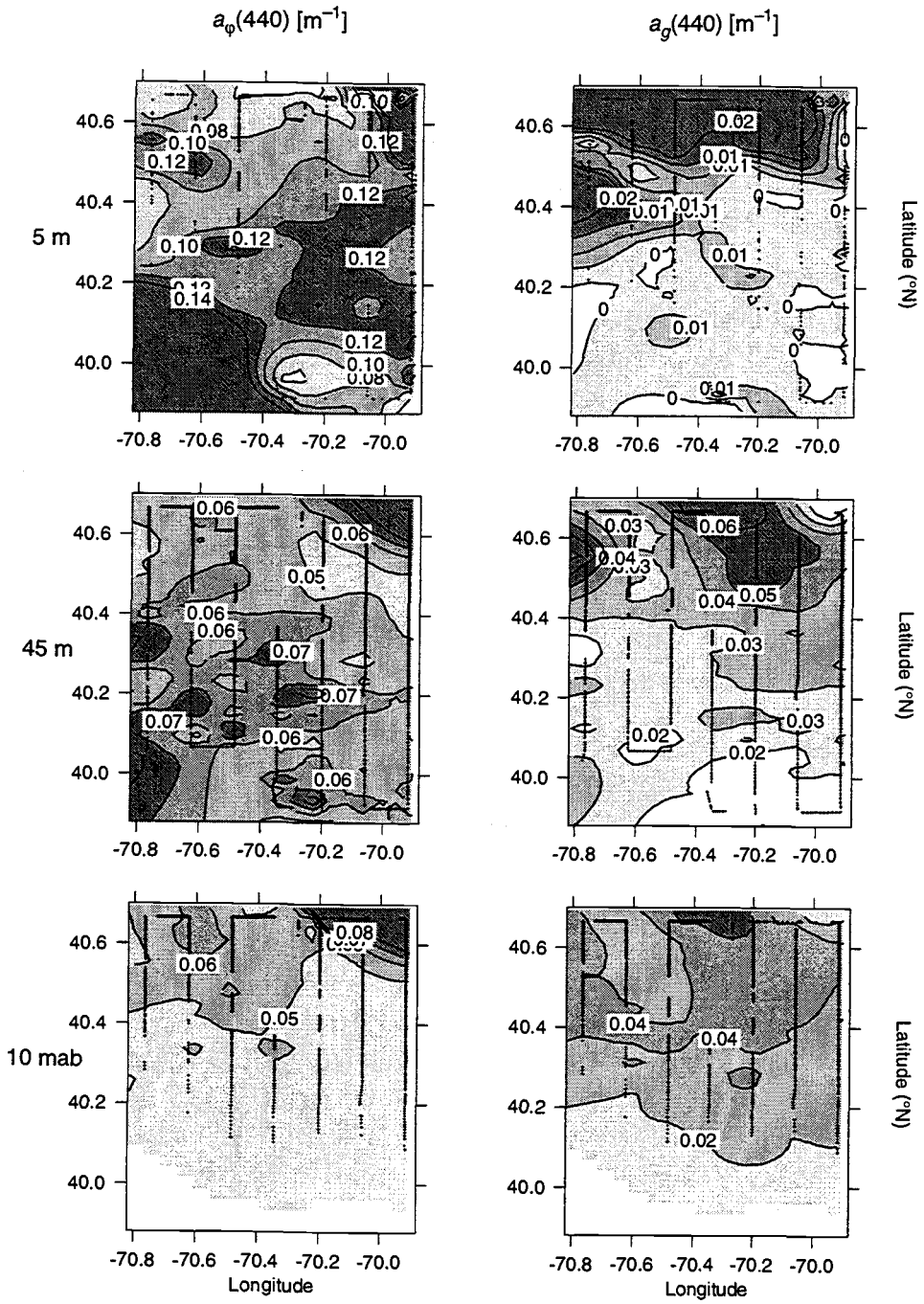

FIGURE 2.15 Maps of horizontal spatial distributions of $a_\varphi(440$ nm) (left) and $a_g(440$ nm) (right) at (top to bottom) 5 m, 45 m and 10 m above the bottom during 4-6 May 1997. Units are m^{-1}. Variables were contoured onto a 3-km by 3-km grid using a LaPlace interpolation. Data locations are indicated by black bullets.

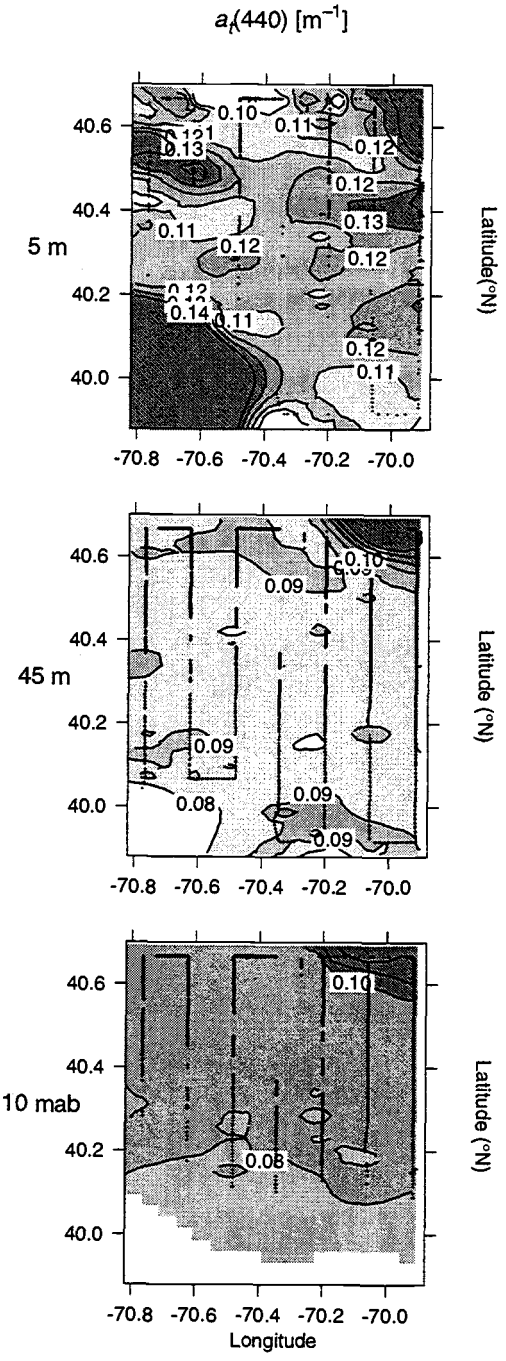

FIGURE 2.15 (Continued) Maps of horizontal spatial distributions of a_t(440 nm) at (top to bottom) 5 m, 45 m and 10 m above the bottom during 4-6 May 1997. Units are m^{-1}. Variables were contoured onto a 3-km by 3-km grid using a LaPlace interpolation.Data locations are indicated by black bullets.

2.6 DISCUSSION AND CONCLUSIONS

The goals for this study are to (1) present a three-dimensional structure of hydrographic and optical properties, (2) present a method for the decomposition of $a_{T-w}(\lambda)$ into $a_\phi(\lambda)$, $a_g(\lambda)$ and $a_t(\lambda)$, (3) to present the three dimensional structure of major light absorbing components, and (4) to provide a brief interpretation of the IOPs in the Middle Atlantic Bight, relevant to the coastal circulation.

The survey region exhibits features found in historical observations, where the presence of the shelf/slope front persists in summer and spring, separating the cooler, fresher, more turbid shelf waters from the warmer, saltier and clearer slope waters, as shown by the vertical sections and horizontal maps of the variables. The mean springtime temperatures are about 4 degrees cooler than in the summertime. The mean spring salinities are about 0.3 PSU more saline than the mean summer salinities.

During the summer, the structure of the hydrographic and optical properties allow the identification of basic water masses, shown in the T-S diagrams (Fig. 2.16). The water masses present during the summer are (1) the relatively clear warm, surface layer, (2) the relative clear water of the cold pool and (3) the very clear deep slope water. The mid-shelf waters are tagged in T-S space by the high absorption, while the absorptive bottom boundary layer can be seen in T-S space (yellow) within the "elbow" of the cold pool. The spring T-S diagram shows some evidence of the surface mixed layer, but the dominant water masses on the shelf takes on the characteristics of the summertime cold pool and the offshore deep slope water. The two spring water masses are contrasted by high absorption on the shelf and the clearer slope waters.

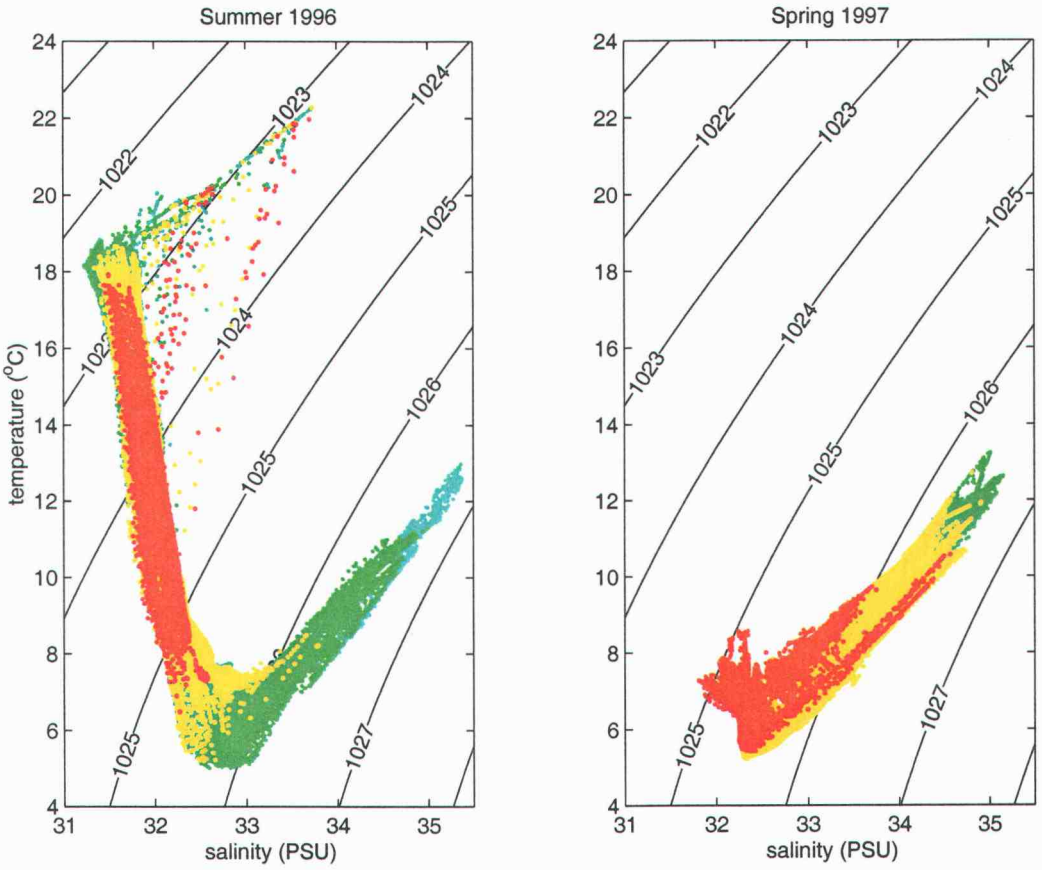

FIGURE 2.16 Temperature-Salinity diagrams for 17-18 Aug (left) and 4-6 May 1997 (right). Background contours of density in [kg m^{-3}. Superimposed in color are the values of $a_{T-w}(440)$ m^{-1}: violet, 0-0.04 m^{-1}; blue, 0.04-0.08 m^{-1}; green, 0.08-0.12 m^{-1}; yellow, 0.12-0.16 m^{-1}; red, 0.16-0.2 m^{-1}.

Based on preliminary validation of the decomposition method, the decomposition retrieves the phytoplankton component with very good precision, but the retrieval of the gelbstoff and tripton components is much less robust and, at best, yields fair results. Directly measured gelbstoff absorption in this region (Boss et al. (submitted)) are extremely similar in magnitude and spatial distribution to the output modeled gelbstoff absorption presented here. The extinction coefficients of the tripton and gelbstoff absorption spectra, though different, are still of the same magnitude, making the least squares distinction of the two spectra difficult.

To improve the separation of the two components, the matrix A, which contains the basis vectors of the component absorption spectra should be augmented with the scattering coefficients. Then A should necessarily be weighted with a variance-covariance matrix, where the diagonals of the weighting matix are the variances of the basis vectors and the off-diagonals are the covariances between the components used to construct the basis vectors. Unfortunately, good data bases of component absorption, in this region, do not exist, and the variance-covariance matrices will vary between oceanic regions.

During the summer, the distribution of phytoplankton closely follow the pycnocline. This distribution of $a_\phi(440)$ is likely a compromise between light and nutrients (Ryan et al., 1999). The algal material found close to the bottom are likely phytoplankton that have been mixed downward on the mid-shelf, then suspended/resuspended and transported offshore by the bottom boundary layer.

The simultaneous examination of the distributions of the scattering coefficient as well as the tripton and gelbstoff absorption coefficients at 440 nm indicate that the high scattering found near the bottom, on the mid-shelf, is likely more inorganic in nature.

Unpublished results of laboratory experiments performed by Roesler et al. showed that the organic particulates tend to be very weakly absorbing. The inorganic fraction of the tripton largely influences the total tripton absorption. The scattering near the bottom, on the outer shelf, is then likely due to resuspended organic particulate matter.

During the spring, the distribution of phytoplankton is concentrated at the surface. The winter mixing of the water column vertically transports nutrients to the well-lit surface waters. The patchy distribution of the tripton component could indicate the presence of established and senescent phytoplankton blooms, where increased tripton absorption would be indicative of a scenescent bloom. The gelbstoff absorption is highest near the bottom, below the pycnocline, suggesting that most of the gelbstoff present is of a refractory nature, as evidenced by the $S_g = 0.02$ nm^{-1}, and is resuspended from the bottom, as speculated by Boss et al. (submitted). Horizontal distributions of $a_g(440)$ m^{-1} at 5 m appears to be correlated to the relatively fresher salinity signature found in the northwest survey region. This water mass was likely advected from a riverine/estuarine inflow within the last several days given that the gelbstoff did appear to have time to photo-oxidize (loss of 10-15 % in absorbance/8 h of mid-day sun, Miller and Moran (1997)) to the lower values found over the outer shelf and slope.

The optical properties presented in this study provide evidence of the relative insulation of the shelf waters, and that offshore flux of shelf waters is more likely to occur at the surface during times when the shelfbreak front is weakened. Evidence of alongshore advection on the shelf is observable with the gelbstoff parameter, S_g nm^{-1}. Summer S_g nm^{-1} are indicative of younger, somewhat recently produced materials, while the spring S_g nm^{-1} are indicative of aged, refractory materials. Also, spring deep slope waters were shown to be virtually

devoid of gelbstoff absorption. The differences between the summer and spring gelbstoff compositions within the cold pool suggest that the cold pool waters are advected alongshore and originate from a recently biologically productive area. Optical properties also provided evidence of the structure of cross-shelf secondary circulation, as previously described by Barth et al. (1998). The horizontal maps of optical properties provided evidence of the alongshore and seasonal structure of the shelfbreak front, where enhanced resuspension of bottom sediments, as indicated by stronger IOPs, can be indicative of regions of increased bottom stress caused by the primary and secondary circulations.

The ratios of the individual absorbing components to the total absorption during the summer (Fig. 2.17) show that the basic water masses in physical space are characterized by particulate components on the shelf and at the surface, while the deep slope water is characterized by dissolved components. The ratios of component to total absorption during the spring show the overall dominance of the tripton component, while the phytoplankton and gelbstoff components are generally associated with waters above and below the pycnocline, respectively.

The ratios of the individual absorbing components to the total absorption during the spring (Fig. 2.17) show that the phytoplankton absorption is largest above the pycnocline, over the slope region. Gelbstoff absorption coefficients again demonstate higher magnitudes below the pycnocline, likely due to photodegradation in the near-surface. Tripton absorption coefficients are fairly uniform, exhibiting the largest magnitudes in the deep slope waters.

The Middle Atlantic Bight has historically been established as a study area for coastal oceanographers because of its proximity to a heavily populated area. The recognition for environmental management of this oceanic region hence prompted the studies for understanding and monitoring the physical oceanography of the

Middle Atlantic Bight. While the hydrographic properties of this region have been very well documented, the IOPs of this region yield more information on the productivity and Lagrangian transport of various types of materials. Although, much information can be inferred from the bulk inherent optical properties, the decomposition of the total absorption is necessary for understanding the compositional nature of the particulate and dissolved materials suspended in the water, given that the composition and source of the materials transported can be inferred from the shape of the the component absorption spectrum (i.e. the model parameters). The high spatial resolution surveys are also useful for developing future small to mesoscale sampling strategies. The contribution of this paper lies in setting the stage for future monitoring of the transport of local inputs of particulate and dissolved materials.

Tracking the presence of local riverine/estuarine inflows can be accomplished from hydrographic and component absorption ($a_g(\lambda)$) observations. Materials on the shelf, in the surface mixed layer, appear stay near the surface and are gradually advected offshore. Alternatively, materials at depth can be advected off shelf in the bottom boundary layer, where the shelfbreak front causes the bottom boundary layer to separate and upwell resuspended bottom materials into the surface. Transport of materials onto the shelf can also occur at depth, when the slope waters intrude onto the shelf.

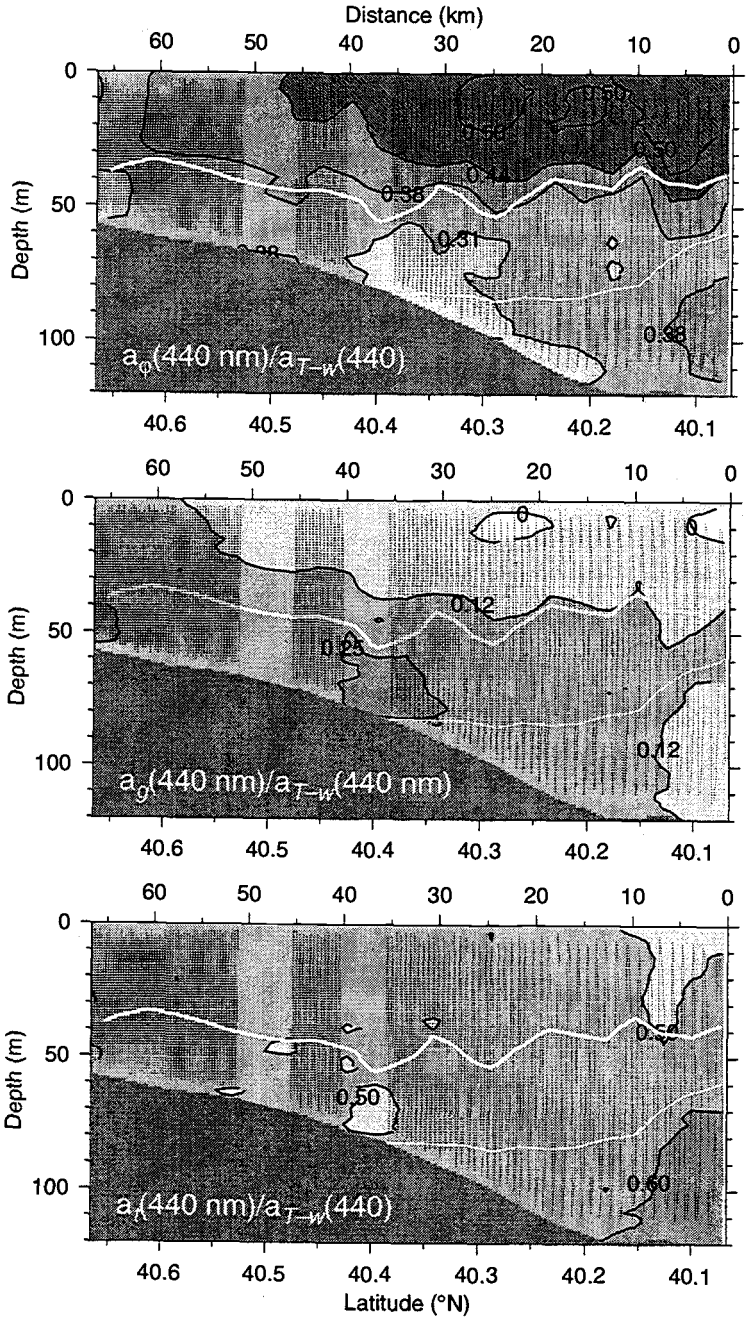

FIGURE 2.17 (Continued) Cross-shelf spatial distributions of ratios of (top to bottom) $a_\varphi(440\ \text{nm})$, $a_g(440\ \text{nm})$ and $a_t(440\ \text{nm})$ to $a_{T-w}(440\ \text{nm})$ during 5-6 May 1997, along 70.5°W. Variables were contoured onto a 3-km by 3-m grid using a LaPlace interpolation. Resolution of measurements is highest on the shelf and decreases over the slope.

2.7 REFERENCES

Aikman, F., III, Pycnocline developement and its consequences in the Middle Atlantic Bight, *J. Geophys. Res.*, **89**, 685-694, 1984.

Barth, J. A., D. Bogucki, S. Pierce and P. M. Kosro, Secondary Circulation Associated with a Shelfbreak Front, *Geophys. Res. Lett.*, **25**, 2761-2764, 1998.

Barth, J. A. and D. Bogucki Spectral light absorption and attenuation measurements from a towed undulating vehicle, *Deep Sea Res. I*, **47**, 323-342, 1999.

Beardsley, R. C. and W. C. Boicourt, On estuarine and continental-shelf circulation in the Middle Atlantic Bight, In *Evolution of Physical Oceanography*, ed. B. Warren and C. Wuncsh, MIT Press, Cambridge, Massachusetts, 1981.

Beardsley, R. C., D. C. Chapman, K. H. Brink, S. Ramp and R. Schlitz, Nantucket Shoals Flux Experiment (NSFE79), Part 1: A basic description of the current and temperature variability, *J. Phys. Oceanogr.*, **15**, 713-748, 1985.

Bigelow, H. B., Studies of the waters on the continental shelf, Cape Cod to Chesapeake Bay. I. The cycle of temperature, *Papers in Physical Oceanography and Meteorology*, **2**, 1-135, 1933.

Boicourt W. C. and P. W. Hacker, Circulation on the Atlantic Continental Shelf of the United States, Cape May to Cape Hatteras, *Mem. Sic, R. Sci. Liege, Ser. 6 10*, 187-200, 1976.

Boss, E., W. S. Pegau, J. R. V. Zaneveld and A. H. Barnard, Spatial and temporal variability of absorption by dissolved material at a continental shelf, *J. Geophys. Res.*, submitted.

Bricaud, A., A. Morel and L. Prieur, Absorption by dissolved organic matter of the sea (yellow substance) in the UV and visible domains, *Limnol. Oceanogr.*, **26**, 43-53, 1981.

Bricaud A. and D. Stramski, Spectral absorption coefficients of living phytoplankton and non-algal biogenous matter: A comparison between the Peru upwelling area and the Sargasso Sea, *Limnol. Oceanogr.*, **35**, 562-582, 1990.

Candela, J., R. C. Beardsley and R. Limeburner, Separation of tidal and subtidal currents in ship-mounted acoustic Doppler current profiler observations, *J. Geophys. Res.*, **97**, 769-788, 1992.

Carder, K. L., R. G. Steward, G. R. Harvey and P. B. Ortner, Marine humic and fulvic acids: their effects on remote sensing of ocean chlorophyll, *Limnol. Oceanogr.*, **34**, 68-81, 1989.

2.7 REFERENCES

Aikman, F., III, Pycnocline developement and its consequences in the Middle Atlantic Bight, *J. Geophys. Res.*, **89**, 685-694, 1984.

Barth, J. A., D. Bogucki, S. Pierce and P. M. Kosro, Secondary Circulation Associated with a Shelfbreak Front, *Geophys. Res. Lett.*, **25**, 2761-2764, 1998.

Barth, J. A. and D. Bogucki Spectral light absorption and attenuation measurements from a towed undulating vehicle, *Deep Sea Res. I*, **47**, 323-342, 1999.

Beardsley, R. C. and W. C. Boicourt, On estuarine and continental-shelf circulation in the Middle Atlantic Bight, In *Evolution of Physical Oceanography*, ed. B. Warren and C. Wuncsh, MIT Press, Cambridge, Massachusetts, 1981.

Beardsley, R. C., D. C. Chapman, K. H. Brink, S. Ramp and R. Schlitz, Nantucket Shoals Flux Experiment (NSFE79), Part 1: A basic description of the current and temperature variability, *J. Phys. Oceanogr.*, **15**, 713-748, 1985.

Bigelow, H. B., Studies of the waters on the continental shelf, Cape Cod to Chesapeake Bay. I. The cycle of temperature, *Papers in Physical Oceanography and Meteorology*, **2**, 1-135, 1933.

Boicourt W. C. and P. W. Hacker, Circulation on the Atlantic Continental Shelf of the United States, Cape May to Cape Hatteras, *Mem. Sic, R. Sci. Liege, Ser. 6 10*, 187-200, 1976.

Boss, E., W. S. Pegau, J. R. V. Zaneveld and A. H. Barnard, Spatial and temporal variability of absorption by dissolved material at a continental shelf, *J. Geophys. Res.*, submitted.

Bricaud, A., A. Morel and L. Prieur, Absorption by dissolved organic matter of the sea (yellow substance) in the UV and visible domains, *Limnol. Oceanogr.*, **26**, 43-53, 1981.

Bricaud A. and D. Stramski, Spectral absorption coefficients of living phytoplankton and non-algal biogenous matter: A comparison between the Peru upwelling area and the Sargasso Sea, *Limnol. Oceanogr.*, **35**, 562-582, 1990.

Candela, J., R. C. Beardsley and R. Limeburner, Separation of tidal and subtidal currents in ship-mounted acoustic Doppler current profiler observations, *J. Geophys. Res.*, **97**, 769-788, 1992.

Carder, K. L., R. G. Steward, G. R. Harvey and P. B. Ortner, Marine humic and fulvic acids: their effects on remote sensing of ocean chlorophyll, *Limnol. Oceanogr.*, **34**, 68-81, 1989.

Chang, G. C. and T. D. Dickey, Optical and physical variability on time-scales from minutes to the seasonal cycle on the New England Shelf: July 1996-June 1997, *J. Geophys. Res.*, submitted.

Chapman, D. C., J. A. Barth, R. C. Beardsley and R. G. Fairbanks, On the continuity of mean flow between the Scotian Shelf and the Middle Atlantic Bight, *J. Phys. Oceanogr.*, **16**, 1986.

Cleveland, J. S., Regional models for phytoplankton absorption as a function of chlorophyll *a* concentration, *J. Geophys. Res.*, **100**, 13,333-13,344, 1995.

Cleveland, J. S. and M. J. Perry, A model for partitioning particulate absorption into phytoplanktonic and detrital components, *Deep-Sea Res. I.*, **41**, 197-221, 1994.

Cresswell, G. H., Quasi-synoptic monthly hydrography of the of the transition region between coastal and slope water south of Cape Cod, Mass., WHOI, Ref. 67-35, Woods Hole Oceanogr. Inst., Woods Hole, Mass., 1967.

Csanady, G. T., Mean circulation in shallow seas, *J. Geophys. Res.*, **81**, 5389-5399, 1976.

DeGranpre, M. D., A. Vodacek, R. K. Nelson, E. J. Bruce and N. V. Blough, Seasonal seawater optical properties of the U.S. Middle Atlantic Bight, *J. Geophys. Res.*, **101**, 22,727-22,736, 1996.

Fairbanks, R. G., The origin of continental shelf and slope water in the New York Bight and Gulf of Maine: Evidence from $H_2^{18}O/H_2^{18}0$ ratio measurements. J. Geophys. Res., **87**, 5796-5808, 1982.

Hayase, K. and H. Tsubota, Sedimentary humic acid and fulvic acid as fluorescent organic materials, *Geochimica et Cosmochimica*, **49**, 159-163, 1985.

Højerslev, N. K., The origin of of yellow substance in the marine environment, In *17th General Assembly of I.A.P.S.O. (Canberra, 1979)*(pp. Abstracts, 71), 1979.

Houghton R. W. and J. Marra, Physical/Biological structure and exchange across the thermohaline shelf/slope front in the New York Bight, *J. Geophys. Res.*, **88**, 4467-4481, 1983.

Jerlov, N. G., *Marine Optics*, Amsterdam, Elsevier, 1976.

Ketchum, B. J. and N. Corwin, The persistence of "winter" water on the continental shelf south of Long Island, New York, *Limnol. Oceanogr.*, **9**, 467-475, 1964.

Kirk, J. T. O., *Light and photosynthesis in aquatic ecosystems, 2nd ed.*, Cambridge, 1994.

Lawson C. L. and R. J. Hanson, *Solving least squares problems*, Prentice-Hall, New Jersey, 1974.

Lee, A. H., The T-S structure, circulation and mixing in the slope water region east of the Scotion shelf, Ph.D. Thesis, Dalhousie University, Halifax, Nova Scotia, 191 pp., 1970.

Loder, J. W., B. Petrie, and G. Gawarkiewicz, The coastal ocean off northeastern North America: A large-scale view, in *The Sea*, vol. 11, *The Global Coastal Ocean: Regional Studies and Syntheses*, edited by A. R. Robinson and K. H. Brink, pp 105-133, John Wiley, New York, 1998.

Mackas, D. L., K. L. Denman and A. F. Bennett, Least squares multiple tracer analysis of water mass composition, *J. Geophys. Res.*, **92**, 2907-2918, 1987.

Miller, W. and Moran, M., Interaction of photochemical and microbial processes in the degradation of refractory dissolved organic matter from a coastal marine environment, *Limnol. Oceanogr.*, **42**, 1317-1324, 1997.

Mooers, C. N., K. R. W. Garvine and W. W. Martin, Summertime synoptic variability of the Middle Atlantic Bight, *J. Geophys. Res.*, **84**, 4837-4854, 1979.

Morrow J. H., W. S. Chamberlin and D. A. Kiefer, A two-component description of spectral absorption by marine particles, *Limnol. Oceanogr.*, **34**, 1500-1509, 1989.

Pope R. M. and E. S. Fry, Absorption spectrum (380-700 nm) of pure water. II. Integrating cavity measurements, Applied Optics, **36**, 8710-8723, 1997.

Roesler, C. S. and M. J. Perry, In situ phytoplankton absorption, fluorescence emission, and particulate backscattering spectra determined from reflectance, *J. Geophys. Res.*, **100**, 13,279-13,295, 1995.

Roesler, C. S., M. J. Perry and K. L. Carder, Modeling in situ phytoplankton absorption from total absorption spectra in productive inland marine waters, *Limnol. Oceanogr.*, **34**, 1510-1523, 1989.

Round, F. E., *The Ecology of Algae*, Cambridge, Univ. Press, 653 pp., 1981.

Ryan, J., J. Yoder, J. A. Barth, P. C. Cornillon, Chlorophyll enhancement and mixing associated with meanders of the shelf break front in the Middle Atlantic Bight, *J. Geophys. Res.*, **104**, 23,479-23,493, 1999.

Shaw, P.-T. and G. T. Csanady, Self-advection of density perturbations on a sloping continental shelf, *J. Phys. Oceanogr.* , **13**, 769-782, 1983.

Simeon, J., J. A. Barth, D. Bogucki, A. Erofeev, R. O'Malley, S. D. Pierce. 2000. SeaSoar spectral light absorption and attenuation observations during the Coastal Mixing and Optics Experiment: R/V Endeavor Cruises from 14-Aug to 1-Sep 1996 and 25-Apr to 15-May 1997. Data Report 179, Ref. 00-3. College of Oceanic and Atmospheric Sciences, Oregon State University.

Simeon J. and J. A. Barth, Decorrelation lengthscales of hydrographic and inherent optical properties and their relationship to circulation on the continental shelf and slope in the Middle Atlantic Bight, in prep.

Sosik, H. M. and B. G. Mitchell, Light absorption by phytoplankton, photosynthetic pigments and detritus in the California Current System, *Deep Sea Res. I.*, **42**, 1717-1748, 1995.

Stommel, H. and A. Leetma, Circulation on the continental shelf, *Proc. Natl. Acad. Sci., U.S.*, **69**, 3380-3384, 1972.

Vodacek, A., N. V. Blough, M. D. DeGranpre, E. T. Peltzer and R. K. Nelson, Seasonal variations of CDOM and DOC in the Middle Atlantic Bight: Terrestrial inputs and photo-oxidation, *Limnol. Oceanogr.*, **42**, 674-686, 1997.

Wright, W. R., Physical oceanography. *Summary of Environmental Inventory on the Continental Slope, Canadian/United States Border to Cape Hatteras, North Carolina*, 4, 4-101, Research Institute of the Gulf of Maine, S. Portland, Maine, 1977.

Zepp, R. G. and P. F. Schlotzhauer, Comparison of photochemical behavior of various humic substances in water. III. Spectroscopic properties of humic substances, *Chemosphere*, **10**, 479-486, 1981.

3 DECORRELATION LENGTHSCALES OF HYDROGRAPHIC AND INHERENT OPTICAL PROPERTIES AND THEIR RELATIONSHIP TO CIRCULATION ON THE CONTINENTAL SHELF AND SLOPE IN THE MIDDLE ATLANTIC BIGHT

3.1 ABSTRACT

The waters on the continental shelf and slope in the Middle Atlantic Bight, south of Cape Cod, Massachusetts contrast by the tidally energetic shelf and the low frequency motion slope waters. Statistical data analyses are utilized to quantitatively define the spatial lengthscale dependence of hydrographic and optical properties over and within these two distinct regimes. The cross-shelf and alongshore decorrelation lengthscales, L (km), of hydrographic and inherent optical properties (IOPs) were calculated for the shelf-slope, shelf only and slope only series at fixed depths and constant isopycnals ($\pm$ 0.025 kg m^{-3}).

At fixed depths, the cross-shelf mean shelf-slope series of hydrographic and optical variables exhibited an L of O(10 km) within the upper 60 meters, below which L linearly decreased. The mean series of hydrographic and optical variables on the shelf only and slope only exhibited L's of O(4 km) and O(5 km), respectively. The L's of mean hydrographic variables within the pycnocline are about 15 km. The L's of the IOPs are shorter within the pycnocline (O(5 km)), but similar to the hydrographic L profiles, in density space, below the pycnocline. Anomaly series of the shelf-slope, shelf only and slope only were similar in magnitude and structure, where L is O(3 km) and fairly uniform with depth.

The decorrelation lengthscales for the shelf-slope mean series of the four variables at fixed depths and isopycnals are generally affected by the shelfbreak front. The L's of the hydrographic variables are susceptible to meanders (horizontal

scale $\approx$ 30 km) and eddy formations (diameter $\approx$ 15 km). The L of optical variables were determined by biological activity above the pycnocline. The L over the individual shelf and slope series is coincident with the observed internal deformation radius (L_R = 5 km). The decrease in L with depth suggests that the foot of the shelfbreak front effectively traps motion, thereby reducing the spatial correlation of the hydrographic and optical properties. The shorter L values (L = 3 km) found in virtually all anomaly series indicate that the internal wave activity is the dominant physical process effecting perturbations from the mean. The statistical results indicate the first order control of physical processes over the mean and anomaly distributions of optical variables.

3.2 INTRODUCTION

The Middle Atlantic Bight (MAB) circulation has been studied as early as 1933 by Bigelow and the general hydrography and currents in the region are well known and documented (Beardsley and Boicourt, 1981; Loder et al., 1998). Earlier efforts have enhanced the dynamical understanding of the large scale properties of the mean circulation in this region (Stommel and Leetma, 1972; Chapman et al. 1986), but the dynamical understanding of the mesoscale circulation is less advanced. High spatial resolution observations were lacking for the validation of previous modeling efforts of the shelfbreak front (Gawarkewicz and Chapman, 1992; Chapman and Lentz, 1994) until the last several years. The development of spatial measurement strategies for future studies of mesoscale circulation requires *a priori* documentation of the correlation dependence of the spatial structure. This study quantifies the small-mesoscale correlation lengthscales to determine the predictablity and reliability of unmeasured estimates, the spatial resolution

required to resolve prominent features, and to provide additional statistical criteria to validate general circulation models for this region. Further, the usefulness of inherent optical properties towards elucidation of physical processes is assessed through these statistical analyses.

The mean coastal circulation in the MAB is driven by an alongshore pressure gradient that is forced by a northern inflow from the Gulf of Maine and Georges Bank, as maintained by the arrested topographic wave dynamics (Csanady, 1978). The continuity of the mean flow in the MAB permits the characteristic alongshore lengthscales to be much longer than cross-shelf lengthscales (Chapman et al. 1986).

The characteristic cross-shelf lengthscales are expected to be strongly a function of the topography of the shelf and slope. The slope itself induces an insulative effect (Chapman et al. 1986). A coastally trapped density front at the shelfbreak starkly delineates the cooler, fresher, more turbid waters of the shelf from the warmer, salty, optically clearer slope waters. The contrasting differences in the hydrographic and optical properties of the shelf and the slope indicate distinct physical processes act within these regions.

Boundary effects between the shelf and slope waters have been previously observed from remotely sensed observations of sea surface temperature. Typical internal deformation radii ($L_R = (g'h)^{1/2}/f$) for observed shelf/slope eddies are of O(5 km) (Csanady and Magnell, 1987) which indicates a meander wavelength of $2\pi\ L_R = 30$ km and an eddy diameter of 15 km. Seaward of the slope, the frontal boundary of the slope waters and Gulf Stream exhibits internal deformation radii for eddies to be O(50-100 km) (Halliwell and Mooers, 1979; Garvine et al. 1988).

The topography also plays a role in the steepening of the internal tide and the formation of tidally forced solitons (Halpern, 1971). Soliton wave packets in the

MAB south of Cape Cod are approximately 5-10 km wide. Distances between packets are approximately 30 km wide, suggesting propagation speeds of 50 cm s^{-1} (using the M_2 tidal period).

In the vertical, solitons also strongly perturb isopycnal surfaces by as much as 5-30 meters (O'Driscoll, 1999). Characteristic vertical lengthscales of physical properties can also be determined by the the surface and bottom boundary effects around a calm, inviscid core.

Developing the use of naturally occurring chromophoric tracers towards enhancing observations of physical processes is of specific interest. Concurrent with hydrographic measurements, observations of the inherent optical properties (IOPs) of water masses potentially provide more information about the state of a water parcel, such as age and degree of mixing, as well as its origins.

A water parcel contains three major light-absorbing groups: (1) phytoplankton, (2) gelbstoff (material $< 2\mu$m), and (3) tripton (includes inorganic sediments, detritus, viruses and bacteria). These chromophoric materials can absorb (annihilate) or scatter (path redirection) a photon propagating through water. The inherent optical properties of water are defined by the absorption, $a(\lambda)$, and scattering, $b(\lambda)$, coefficients for some incident wavelength, λ that are determined by these chromophoric materials suspended in a water parcel.

Before interpretation of optical tracer distributions can be confidently applied towards observations of the physical circulation, the relationship between the physical controls over the IOP distributions requires quantification and analysis. A correlation analysis is utilized. Interpreting the results of the correlation analysis will focus on possible physical factors that can explain the observed statistical result. This investigation does not presume to explain all the observed biological/physiological processes in detail, as this lies beyond the goals of this

analysis and available data. However, general chemical and biological processes related to the variability of the spatial distribution of chromophoric tracers can be inferred. The sources of variablility in the distributions of major-light absorbing components suspended in water differs for each component. The phytoplankton component can exhibit variation due to growth, grazing, photo-acclimation, and taxonomic composition. The gelbstoff component is organic in nature and is subject to photo-oxidation or bacterial remineralization. The tripton component can co-vary with the phytoplankton component. The tripton component has the most variable size range and it's distribution could be variable due to differential sinking rates. The interested reader is referred to Kirk (1994) for further reading on the biological and/or chemical response of chromophoric tracers.

3.3 METHODS

The observations presented in this study are from within a 70 km by 80 km box south of Cape Cod, Massachusetts centered at 40.5^{o}N, 70.5^{o}W (Fig. 3.1). Hydrographic and inherent optical properties were measured with a SeaBird Electronics 9/11+ conductivity-temperature-depth (CTD) instrument and a Western Environmental Technology Laboratories (WET Labs) nine-wavelength light absorption and attenuation instrument (ac-9), respectively. Hydrographic and optical data were collected by towing an undulating vehicle, SeaSoar, in a regular radiator or a butterfly pattern. The observations were recorded during two Office of Naval Research Coastal Mixing and Optics (CMO) Experiment cruises on 14-Aug to 1-Sep 1996 and 25-Apr to 15-May 1997 aboard the *R/V Endeavor*. Details of the data collection, processing and editing have been previously published (O'Malley et al. 1998; Barth and Bogucki, 1999; Simeon et al., 2000).

Brief descriptions of a subset of this data set are presented elsewhere (Barth et al., 1998; Simeon et al., in prep.). Optical data analyzed in this study are the measured absorption coefficients, $a(\lambda)$, which is the sum of the absorption coefficients of major light-absorbing components suspended in water. The scattering coefficient, $b(\lambda)$, is derived from the attenuation, c(λ), directly measured by the ac-9, where the measured $a(\lambda)$ is removed to obtain a measure of the particulate scattering, $b(\lambda)$.

The quantification of the spatial dependence of hydrographic and optical variables is performed by calculating the spatial autocorrelation functions of the variables. Autocorrelation (a.k.a the normalized autocovariance) functions were calculated following a standard procedure (Emery and Thompson, 1997), where the sample covariance between a record and a spatially lagged record, R_{yy}, is normalized by the product of the sample standard deviations of the lead and lag records, $\sigma_x\ \sigma_{x-\tau}$. Hence, the dimensionless value of the autocorrelation function varies between -1 to 1, where positive values indicate a positive correlation and vice versa. Naturally, this statistical method becomes limited by the record length of the data series upon which the autocorrelation is performed as well as the spatial spacing between the elements of the data series.

Although the SeaSoar is capable of making rapid, high-resolution measurements in space, the SeaSoar's path through the water column is saw-toothed and irregularly spaced. This saw-toothed pattern makes the horizontal separation measurements near the surface and bottom about twice that between measurements at mid-depths. Separation between measurements decreases as the water depth decreases, i.e. to the north (Fig. 3.2). The near-zero separation distance at 5 m results from the vehicle turning quickly between an ascending and descending profile. The data coverage in the cross-shelf direction (y) is also variable within

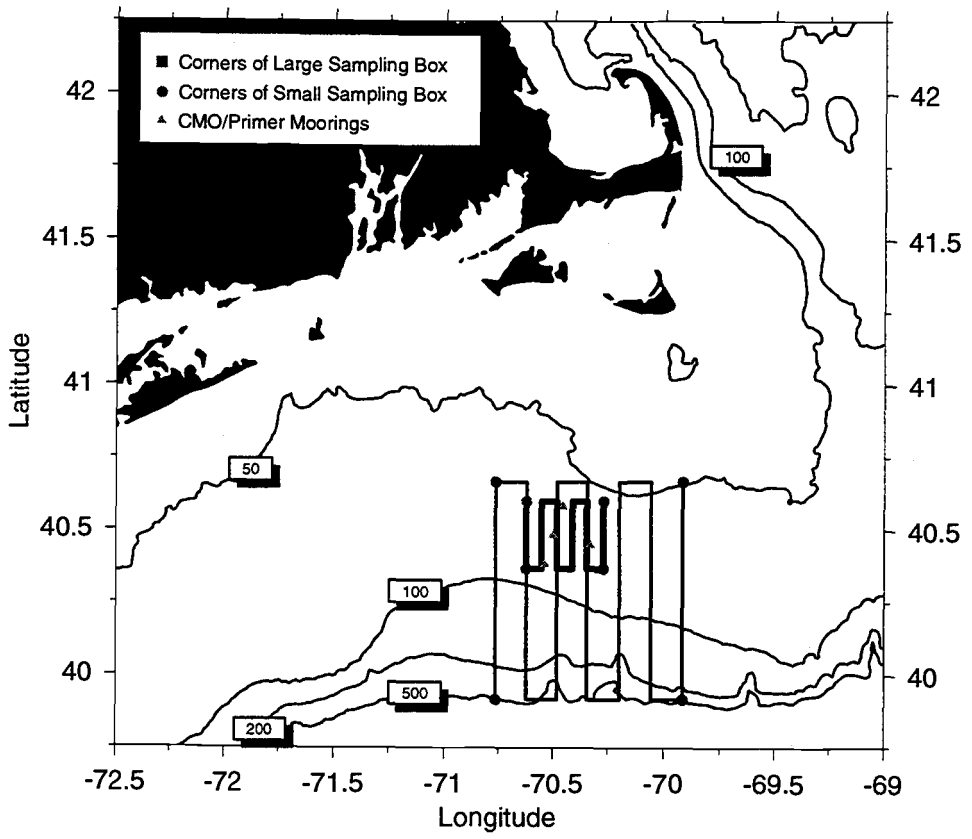

FIGURE 3.1 Map of the Coastal Mixing and Optics study region in the Middle Atlantic Bight south of Cape Cod, Massachusetts. Bottom topography in meters.

the survey region. The mid-shelf (h_b = 50 to 80 m) region was the most frequently visited (Fig. 3.3) and the frequency of measurements reduces by an order of magnitude over the slope. Therefore, prior to calculating the autocorrelation functions, hydrographic and optical observations were bin-averaged in the cross-shelf and vertical directions to produce a regular grid. Different bin-averaging schemes were required for the mean and raw observations.

The following is a description of the construction of the mean of a variable, which is illustrated by Fig. 3.4. The cross-shelf bins were 3-m bottom bathymetry (h_b) intervals on the shelf (h_b <100 m) and 90-m h_b intervals over the slope (h_b >100 m). Bottom bathymetry was obtained from unpublished USGS bottom bathymetry archives compiled by Rich Signell in 1996. The use of the bottom bathymetry for the cross-shelf bin coordinates is an effort to minimize smearing of the cross-shelf structure of the hydrographic and optical variables, while the composite bin intervals preserve the bin sizes over the shelf and slope relative to physical (y) space given the 30-times steeper continental slope. The vertical binning was performed using depth (1-m bins) or σ_t (0.05 kg m^{-3} bins) coordinates. The mean series binned in h_b coordinates were then transposed into physical, y-space via a look-up table composed of a mean shelf-slope profile of the survey region.

The cross-shelf raw data was binned solely in physical space, using 3-km bins in the horizontal, 1-m bins in the vertical. The 3-km bin width was necessary for removing measurement noise due to internal wave motions. The 3-km binned series was then taken as a smoothed representation of the signals of interest, hence was linearly interpolated to 1-km bin intervals to ensure a smooth autocorrelation function. The series was interpolated to reduce noise in the subsequent calculation of the autocorrelation function, though the reader should be aware that the

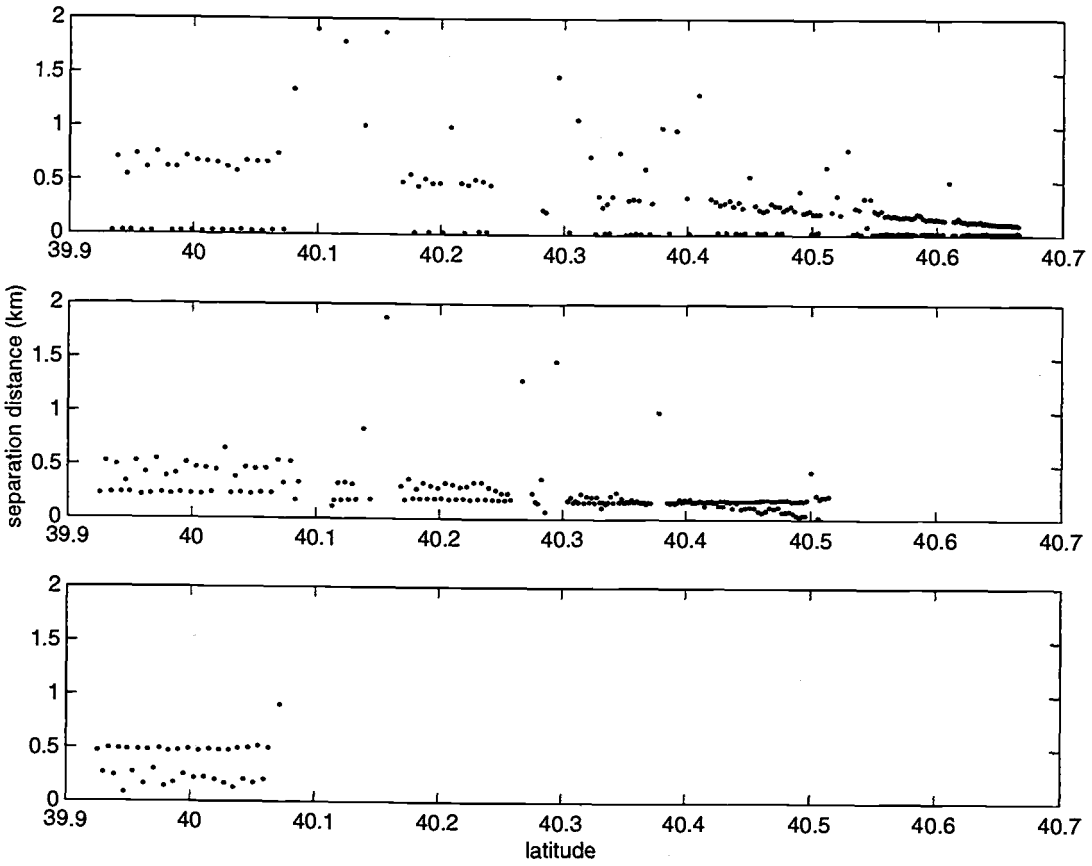

FIGURE 3.2 Example of separation distance between data points at (top) 5 m, (mid) 50 m and (bot) 100 m during a SeaSoar tow. The sawtooth pattern of the tow is expected have the widest separation distances between point near the surface and bottom, while the mid-depths have the smallest separation distances.

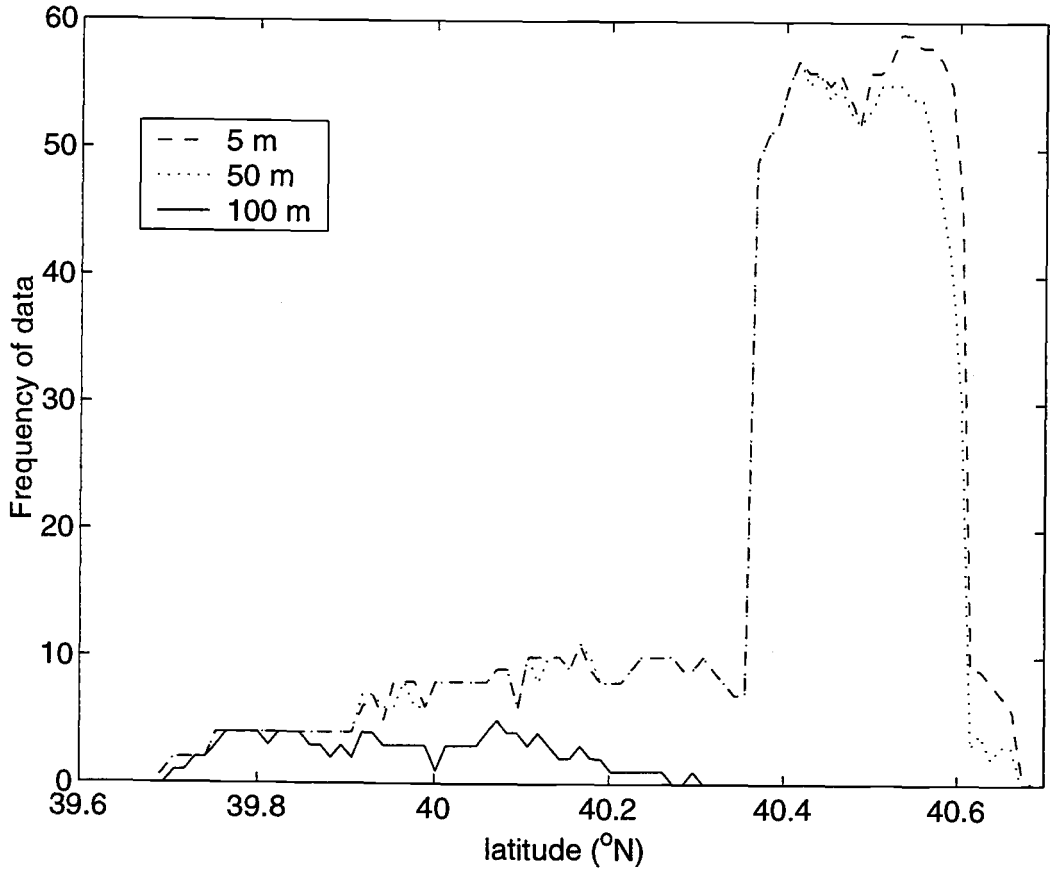

FIGURE 3.3 Frequency of data relative to latitude (cross-shelf distance) used for calculating the autocorrelation functions.

maximum wavenumber resolvable remains $(2\Delta x)^{-1}$ ($\approx$ 6 km), analogous to the Nyquist frequency, which translates to a minimum of 1.5 km for the decorrelation lengthscales of any data series. This process is illustrated in Fig. 3.5. While the majority, by far, of the SeaSoar sections is in the cross-shelf (approximately N-S), a few sections were recorded in the alongshore direction roughly along the 70-m isobath. Alongshore mean and raw data series binned using x and z spatial coordinates (1-km horizontal, 1-m vertical).

The foot of the shelfbreak front, typically found at the 100-m isobath (Linder and Gawarkiewicz, 1998), is used to divide the binned data series accordingly to shelf and slope regions. The autocorrelation functions of variables were then calculated for fixed depths (z=n*5 m, for n = 1,2,3,...,24) and along isopycnals ($\sigma_t \approx 22.6 + n * 0.25$ kg m^{-3}, for n = 1,2,3,...,17). Autocorrelations were performed on mean and anomaly data series. The anomaly series of each radiator pattern were obtained by removing the calculated sample mean from the binned data series. The number of alongshore tows were much fewer. Sample means were calculated using the repetitions of west-east lines of butterfly patterns. All sample mean and anomaly series were detrended by removing a least-squares trend. Once the autocorrelation function was calculated for a particular record, the decorrelation lengthscale of a variable was then defined by the first zero-crossing of the autocorrelation function, which roughly corresponds to the integral lengthscale (Poulain and Niiler, 1989).

Using this one simple statistical analysis, the separation dependence of the hydrographic and optical properties can be quantified. Comparing the decorrelation lengthscales of the optical properties with the hydrographic properties will indicate the similarity between the spatial structures of the variables.

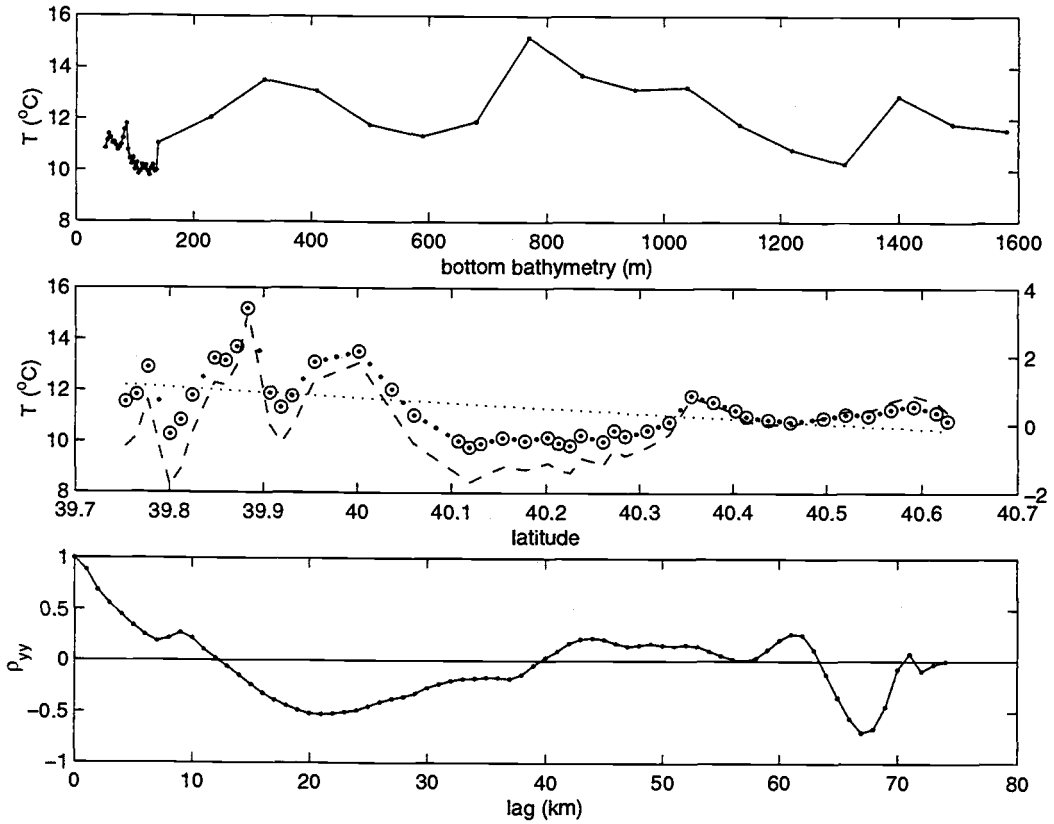

FIGURE 3.4 Illustration of preparation of summer mean of variables prior to calculation of autocorrelation function. From top to bottom: Composite 3-h_b (shelf) and 90-h_b (slope) unit binned mean series at 30 m. The h_b-space mean series converted back into y coordinates (open circles) by using a reference (mean h_b of survey region) and the 1-km linear interpolated mean series (solid circles). A trendline (dotted) is removed and the detrended mean series (solid) is used to calculate the shown autocorrelation function.

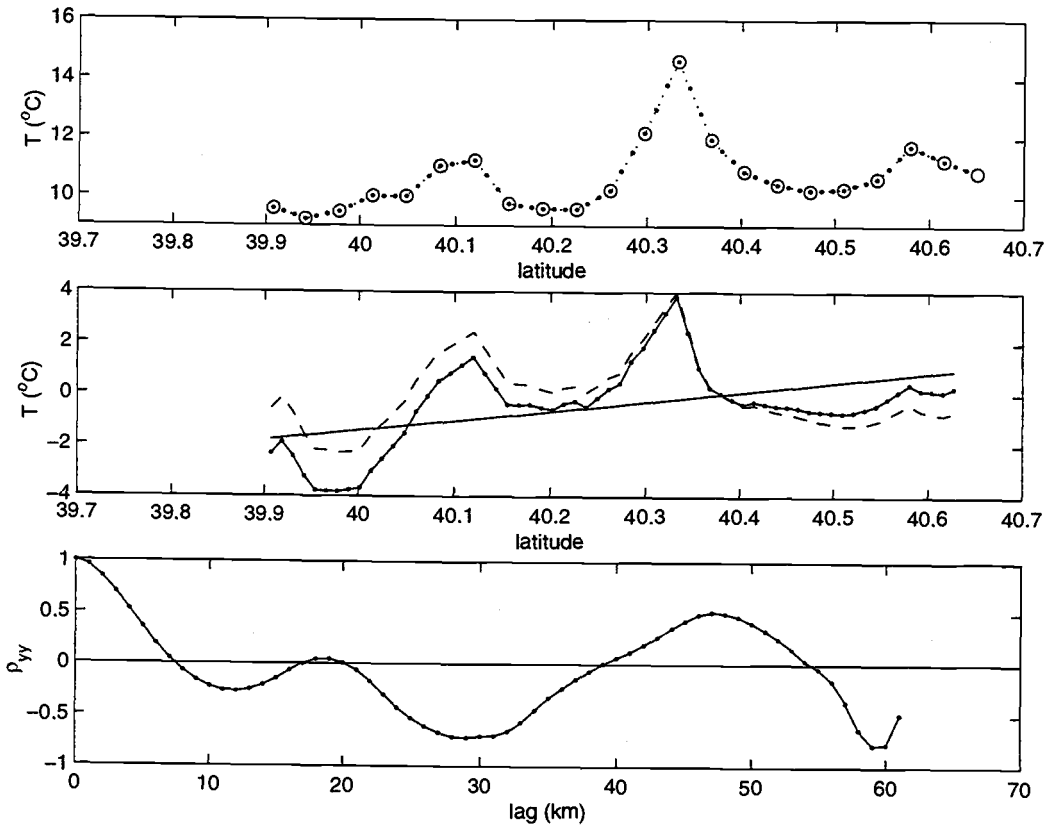

FIGURE 3.5 Illustration of preparation of anomaly series of variables prior to calculation of autocorrelation function. From top to bottom: Three-km binned observations at 30 m, along 70.2 °W (open circles) and the 1-km linear interpolated series (solid circles). The mean (Figure 9) at 30 m is removed from the observations to produce the anomaly series. A trendline (dotted) is removed and the detrended mean series (dashed) is used to calculate the shown autocorrelation function.

3.4 RESULTS

The results presented are regional, synoptic decorrelation lengthscales for the summer of 1996. In a future effort, decorrelation lengthscales for the spring of 1997 will be compared with the decorrelation lengthscales found in the summer surveys. Cross-shelf decorrelation lengthscales are shown for the shelf-slope series (shelf+slope), the shelf ($h_b \leq$100 m), and slope regions ($h_b >$100 m). A total of nine small radiators, three big radiators (as seen in Fig. 3.1) and three alongshore sections (tows along 70 m isobath) were included in the autocorrelation calculations at fixed depths and along isopycnals. The decorrelation lengthscales calculated for mean and anomaly series will be presented as vertical profiles for both cross-shelf and alongshore sections.

The summer CMO cruise was typified by strong seasonal stratification with relatively large horizontal gradients due to the bottom to near-surface shelfbreak front. The sample mean estimated for the summer temperature (^{o}C), salinity (PSU), σ_t (kg m^{-3}), $b(440)$ [m^{-1}] and $a(440)$ [m^{-1}] all demonstrate the stratified state of the water column.

The mean temperature distribution as a function of latitude and depth (Fig. 3.6, top) is fairly typical of the season, where warmer waters cap the surface and the interior is contrasted by the cold pool found on the shelf and the warmer slope waters. The standard deviations of the mean temperature (Fig. 3.6, middle) are largest within the thermocline and associated with the shelfbreak front, indicating the variation in the location of these features. The large standard deviation in mean temperature for depths less than 50 m at 40.4^{o}N, are an aliasing from the presence of anomalous warm slope water intrusions during the small radiator pattern surveys. The standard error of the mean temperature (Fig. 3.6, bottom) reflects the increased uncertainty at the most inshore edge ($h_b <$ 60 m)

and over the outer shelf (h_b = 80-100) and slope due to the reduced data coverage and higher standard deviation within this region.

The mean salinity as a function of latitude and depth (Fig. 3.7, top) shows the density compensation, where cold shelf waters are fresher and the warm slope waters are more saline. The shoreward of the cold pool the mean temperature shows decreased stratification, resulting from more efficient mixing in a shallower water column. The standard deviation of the mean salinity (Fig. 3.7, middle) also shows large deviations around 40.4°N, which is due to aliasing from the many small radiator pattern surveys, during which saline slope water intruded at the offshore edges, and associated with the foot of the shelfbreak front. The standard error of the mean salinity (Fig. 3.7, bottom) again points to the regions of low data coverage and relatively higher standard deviations in the mean salinity over the outer shelf and slope.

The mean density during the summer (Fig. 3.8, top) shows the seasonal stratified condition, where lighter waters rest over denser waters associated with the cold pool and the slope waters. The sloping of the isopycnals at the shelfbreak indicate the presence of the front and a geostrophic current moving westward (out of the page). The standard deviations in the mean density (Fig. 3.8, middle) are associated with the vertical motion of the location of the pycnocline and the lateral motion associated with the shelfbreak front. Note that the density compensating effects of the temperature and salinity do not show the slope water intrusions measured during the small radiator pattern surveys. The standard error of the mean density (Fig. 3.8, bottom) shows the reduced data coverage over the slope, but that the surface waters have small variance, therefore error. The bottom boundary layer over the shelf also shows relatively higher errors.

The mean scattering coefficient at 440 nm, $b(440)$ [m^{-1}], (Fig. 3.9, top) shows a subsurface layer at 20-30 meter depth of larger magnitudes, resulting from scattering by phytoplankton or tripton. Over the mid-shelf, the presence of the bottom boundary layer is distinguished by the scattering of resuspended sediments (Simeon et al., in prep). The slope waters are characterized by a low suspended particulate load, hence, are optically clearer. The largest standard deviations of $b(440)$ [m^{-1}] (Fig. 3.9, middle) are also associated with the subsurface phytoplankton layer and the bottom boundary layer. This indicates, that the phytoplankton layer exhibits some vertical variability either due to the movement of the pycnocline depth or due to biology. The standard error (Fig. 3.9, bottom) shows large values associated with the higher $b(440)$ [m^{-1}] near the bottom on the mid shelf ($h_b < 80$ m) as well as at 25 m over the slope. The error near the bottom could be due to a combination of reduced data points as well as higher standard deviations. The large magnitudes of the standard error over the outer shelf, are due to the relatively higher standard deviations associated with the moving phytoplankton layer (z = 20-30 m) and bottom boundary layer plus the lower number of data points within this region. Offshore, the slope region does not demonstrate larger standard errors due to reduced data coverage, indicating the consistent, low variability in the scattering properties of the deep slope waters.

The mean absorption coefficient, $a(440)$ [m^{-1}], (Fig. 3.10, top) also demonstates larger coefficients associated with the phytoplankton layer and within the fairly mixed region inshore and associated with the bottom boundary layer only on the inshore side of the cold pool. Below the pycnocline, the larger $a(440)$ [m^{-1}] is due to tripton that has likely been resuspended from the bottom. Noted is the absence of the greater offshore extent of the bottom boundary layer signature

found in $b(440)$ [m^{-1}]. This indicates the low organic content of the particulate materials being advected over the outer shelf in the bottom boundary layer. The higher standard deviation of $a(440)$ [m^{-1}] over the shelf, below the pycnocline, relative to the slope, is indicative of the variations due to the diffusion of gelbstoff absorption within the low buoyancy frequency region (Simeon et al., in prep), as seen in the middle panel of Fig. 3.10. Over the shelf, above the base of the pycnocline, the motion and biological variability in the phytoplankton layer is again evidenced by the larger standard deviations. The standard error of the mean $a(440)$ [m^{-1}] (Fig. 3.10, bottom) shows the high error associated with the phytoplankton layer and the variability of the offshore flux of tripton in the bottom boundary layer, as well as the variability of the location of the shelfbreak front. The reduced data coverage and relatively higher standard deviations show the most uncertainty in the data is over the outer shelf. These values are smaller than instrumental error. As seen in the mean $b(440)$ [m^{-1}], the mean $a(440)$ [m^{-1}] also shows the lower error in the clarity of the deep slope waters.

Individual events of offshore surface salinity intrusions were observed along with the previously documented salinity maximum (Houghton and Marra, 1983). Upslope advection of deep, relatively clearer slope water was also observed, which is said to be coupled with winds from the south-southwest, where the cross-shelf flows in the upper Ekman layer is compensated by opposite flows in the lower layer (Boicourt and Hacker, 1976).

The resultant cross-shelf L profiles for the shelf-slope, shelf, then slope series will first be presented, followed by the alongshore L profiles. The cross-shelf decorrelation lengthscale profiles of the mean T (^{o}C), S (PSU), $b(440)$ [m^{-1}] and $a(440)$ [m^{-1}] for the shelf-slope series are shown in Fig. 3.11. The autocorrelations calculated for the shelf-slope temperature series at fixed depths show L values of

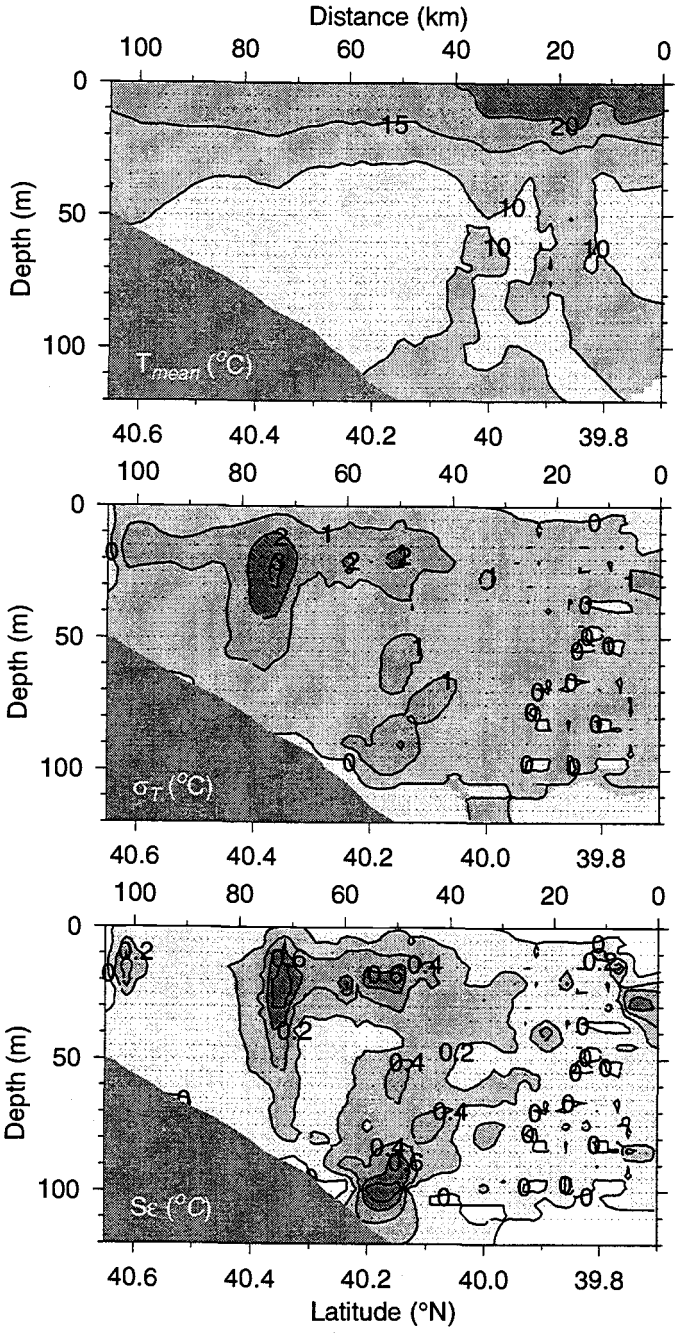

FIGURE 3.6 Mean summer temperature (top), standard deviation from the mean (mid) and standard error of mean estimates (bot). Variables are contoured onto a 2-km, 3-m grid. Bullets indicate data locations.

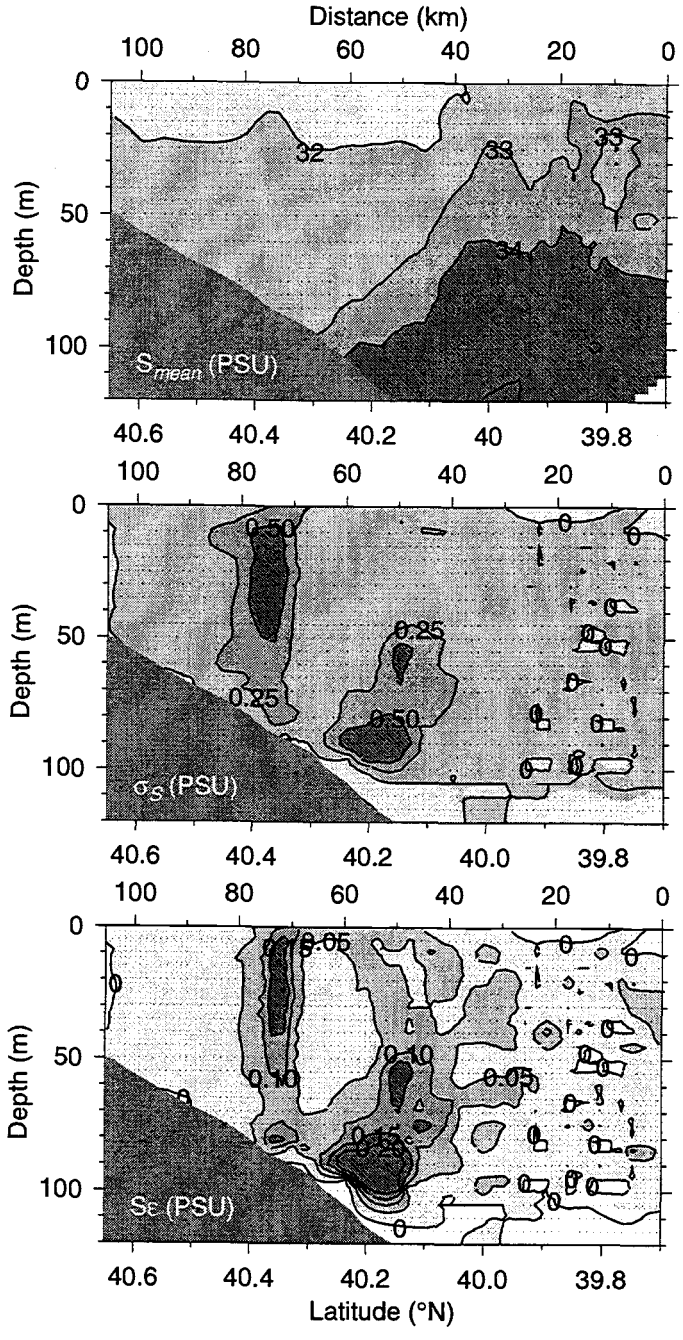

FIGURE 3.7 Mean summer salinity (top), standard deviation from the mean (mid) and standard error of mean estimates (bot). Variables are contoured onto a 1-km, 2-m grid. Bullets indicate data locations.

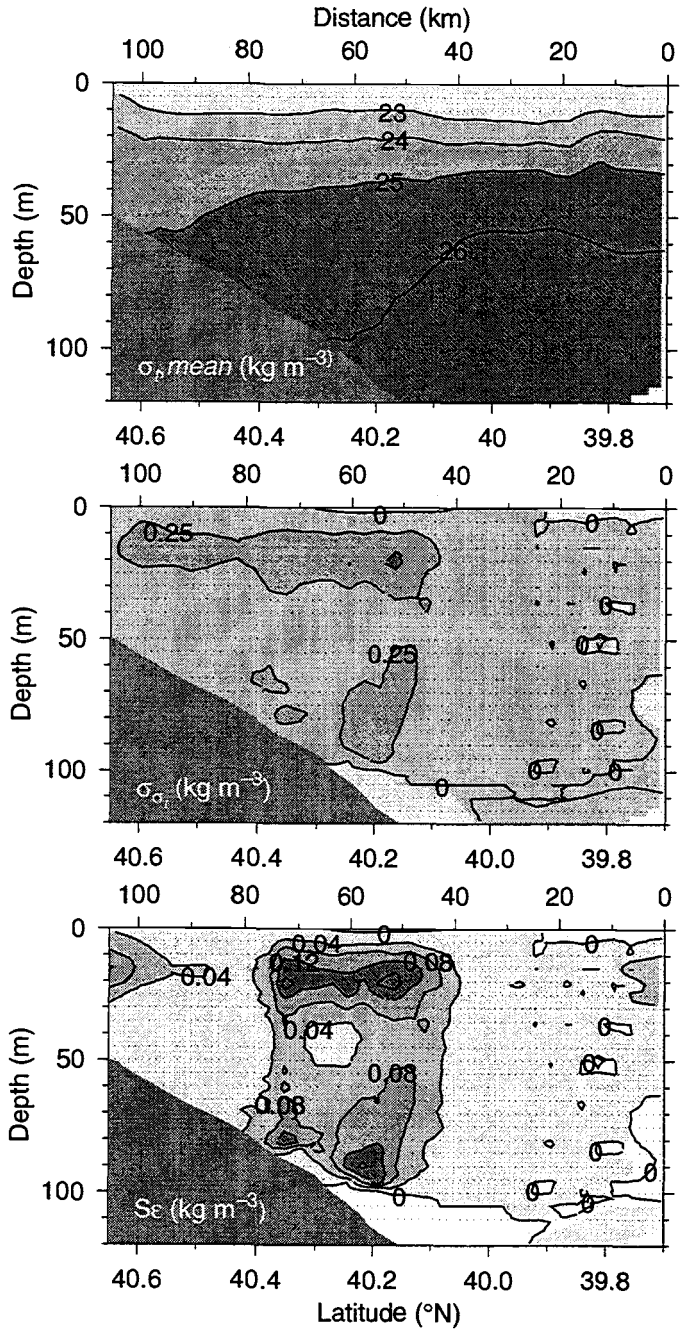

FIGURE 3.8 Mean summer density (top), standard deviation from the mean (mid) and standard error of mean estimates (bot). Variables are contoured onto a 3-km, 3-m grid. Bullets indicate data locations.

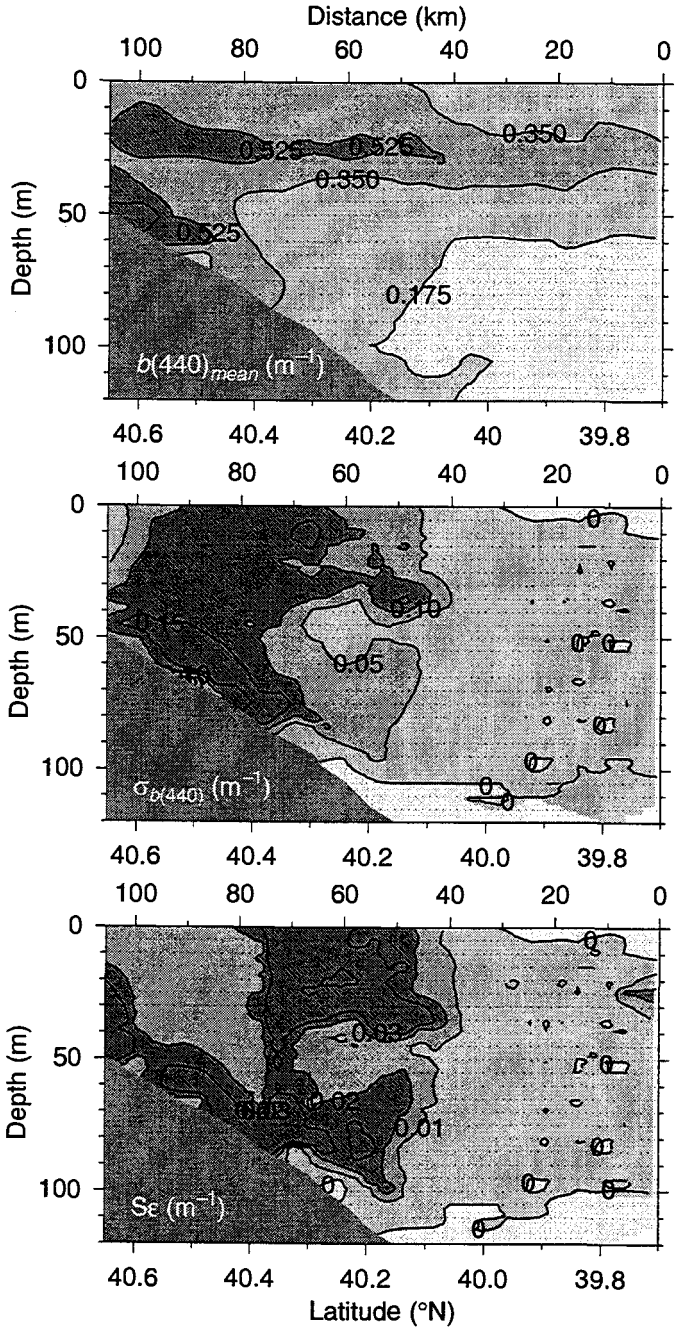

FIGURE 3.9 Mean summer scattering coefficients at 440 nm (top), standard deviation from the mean (mid) and standard error of mean estimates (bot). Variables are contoured onto a 3-km, 3-m grid. Bullets indicate data locations.

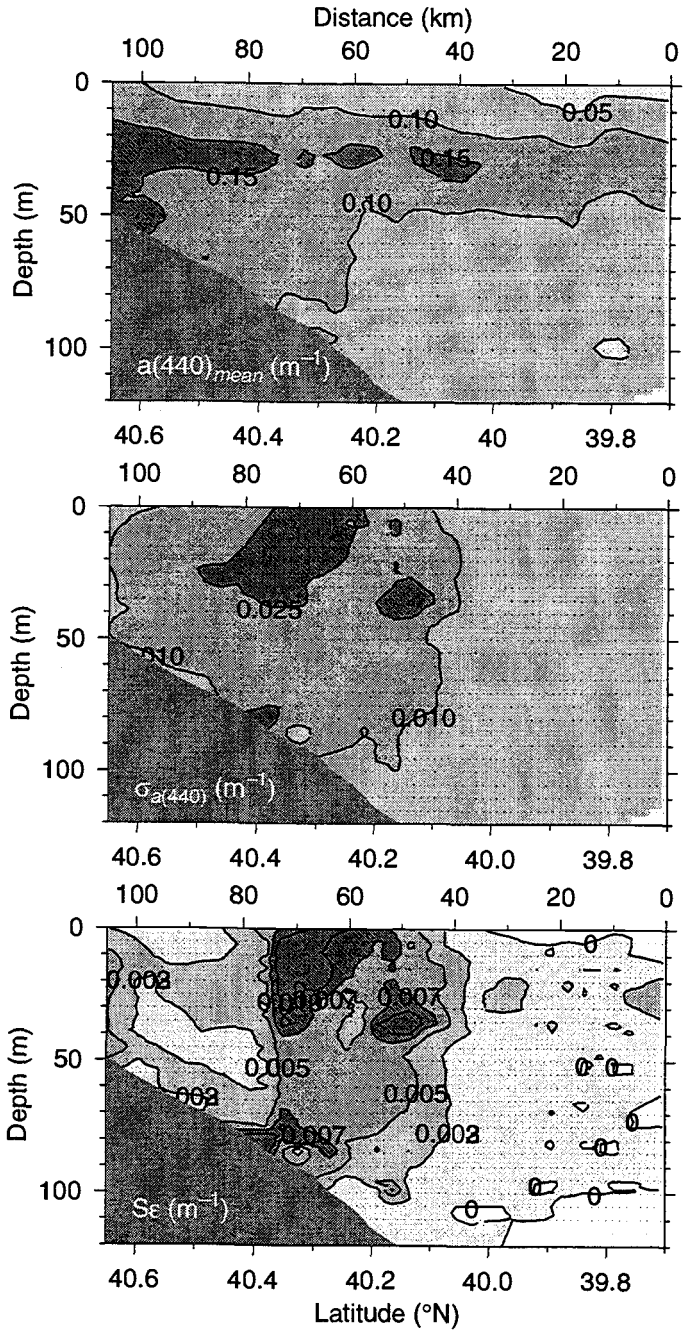

FIGURE 3.10 Mean summer absorption coefficients at 440 nm (top), standard deviation from the mean (mid) and standard error of mean estimates (bot). Variables are contoured onto a 3-km, 3-m grid. Bullets indicate data locations.

13 km above 60 m, below which, L reduces to 5 km. The salinity L values behave similarly, but the reduction in the decorrelation lengthscale begins below 30 m. The optical fields behave inversely with salinity, having lower L values (5-6 km) near the surface, then increasing to 9-10 km below 30 m. In all L profiles, a noticeable decrease of L is evident below 90 m. The cross-shelf decorrelation lengthscale of the mean T (^{o}C), S (PSU), $b(440)$ [m^{-1}] and $a(440)$ [m^{-1}] on the mid-outer shelf all exhibit a fairly uniform L profile above 60 m, below which, a decreasing trend with depth is repeated. The cross-shelf decorrelation lengthscale of the mean T (^{o}C), S (PSU), $b(440)$ [m^{-1}] and $a(440)$ [m^{-1}] over the slope exhibits a fairly uniform L profile for T(^{o}C), while the S, $b(440)$ and $a(440)$ L profiles are longer near the surface ($\leq$ 10 m), then shorten within the pycnocline, lengthen again between 50 and 90 m, before tailing to a value of 2 km. In general, the optical properties appear to more closely mimic the salinity decorrelation lengthscale profiles.

Cross-shelf decorrelation lengthscales for the four mean variables along isopycnals using the shelf-slope series (Fig. 3.12) exhibit similar profile structures with increasing depth as shown by the L profiles in z-coordinates with increasing depth. In this case, the L's of the along isopycnal shelf-slope mean series are up to 5 km longer than in depth coordinates. This indicates that longer scales along isopycnal homogenization of variables are maintained by the stratification, as opposed to the L's in depth coordinates because of the sloping of the isopycnals.

The sample mean hydrographic and optical L profiles calculated for series along isopycnals over the shelf demonstrate a fairly uniform magnitude with increasing density (L = 4 and 3 km, respectively). While L profiles for slope series show fairly uniform hydrographic L values (5 km) with increasing density, while

the L for optical variables are 3-4 km above the pycnocline then lengthen to about 7 km below. Again, the decrease in magnitude near the bottom is evident.

The L profiles for shelf-slope, shelf and slope anomaly series along fixed depths and isopycnals (Fig. 3.13 to 3.18) are all interesting in that they are all fairly uniform with increasing depth and density and are all of O(3-4 km) in a very consistent manner.

The alongshore decorrelation lengthscales are calculated from series that are situated along the 70-m isobath. The decorrelation lengthscales of the sample mean series at fixed depths for T (^{o}C), S (PSU), $b(440)$ and $a(440)$ [m^{-1}] (Fig. 3.19), have L(km) values of 5-6 km and are relatively uniform over depth. In density coordinates, the profiles of L for the mean series of the four variables (Fig. 3.20) exhibit fairly uniform L profiles of O(6 km). The alongshore anomaly series at fixed depths produced L profiles O(5 km) (Fig. 3.21). The L profiles calculated from the alongshelf anomaly series along isopycnals (Fig. 3.22) demonstrated fairly uniform values with increasing density O(5 km) for the hydrographic variables and O(6 km) for the optical variables.

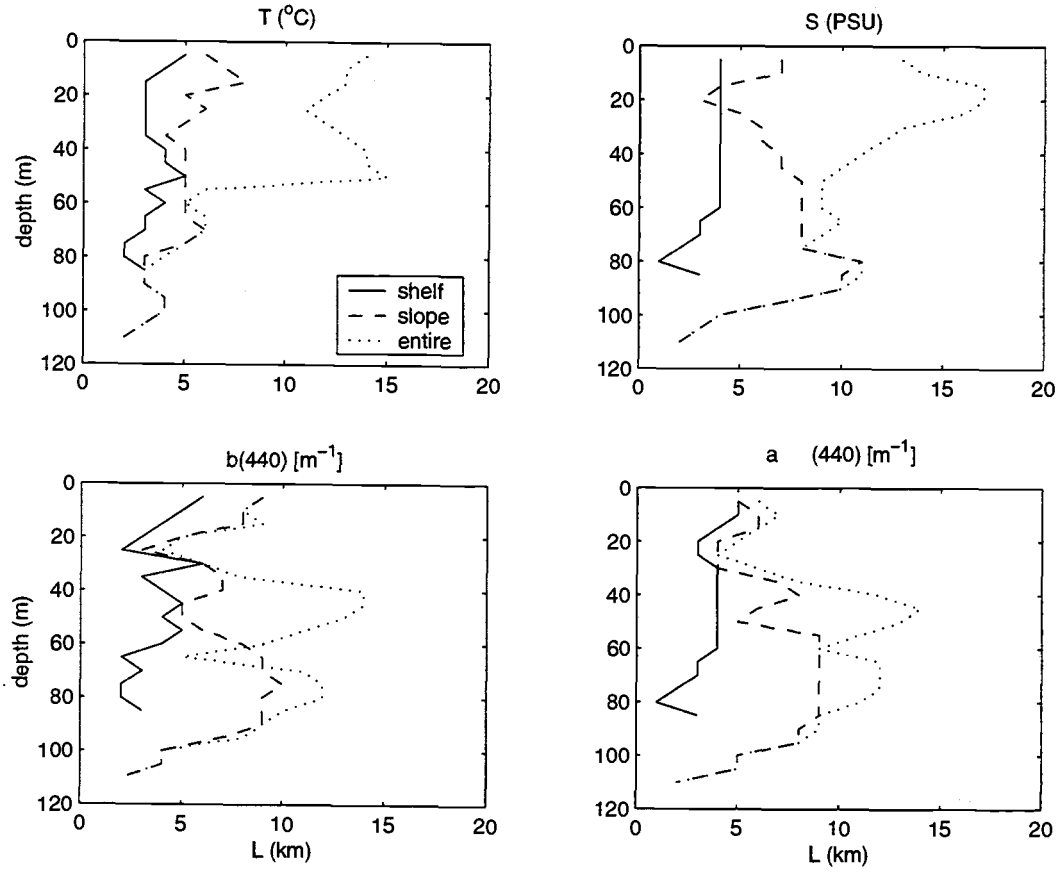

FIGURE 3.11 Decorrelation lengthscale, L, vertical profiles calculated from detrended mean series in cross-shelf and depth coordinates (y,z) for data series encompassing the shelf and slope (dotted), the shelf only (solid) and slope only (dashed), where shelf and slope series are delineated by the 100 m isobath. Clockwise from upper left: T (^oC), S (PSU), $a(440)$ (m^{-1}), $b(440)$ (m^{-1})

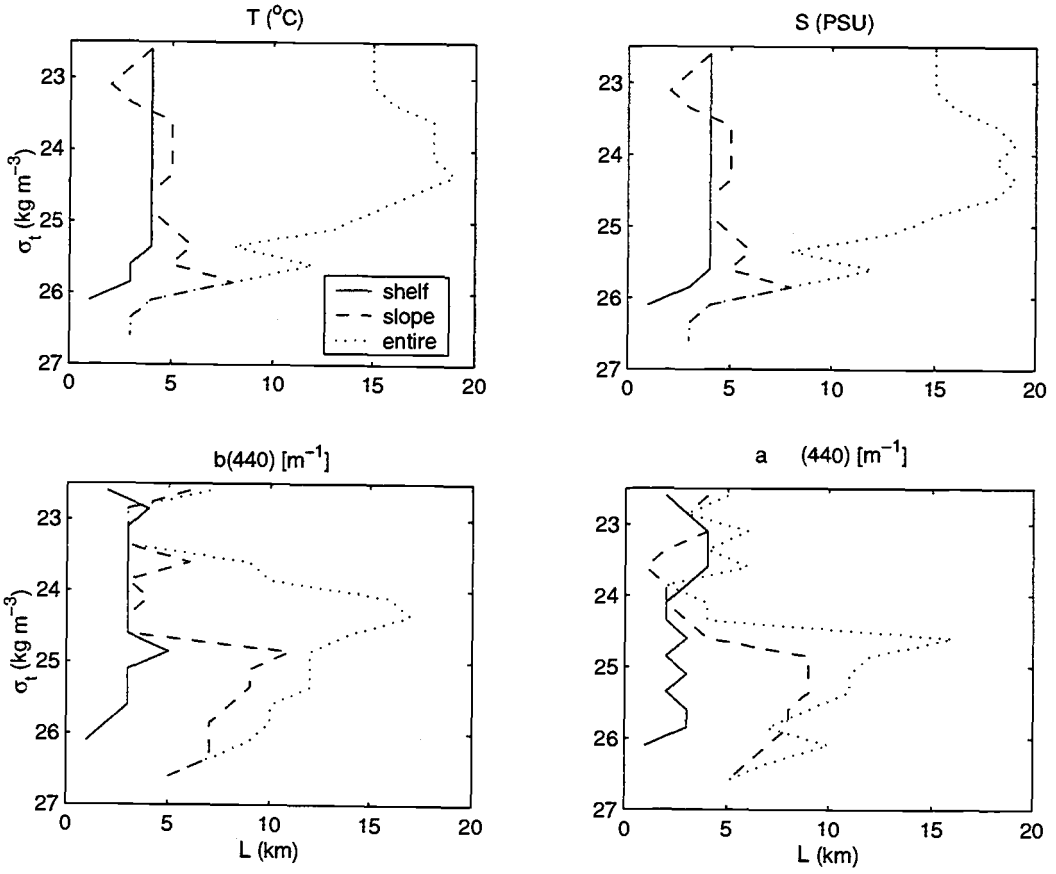

FIGURE 3.12 Decorrelation lengthscale, L, vertical profiles calculated from detrended mean series in cross-shelf and density coordinates (y,σ_t) for data series encompassing the shelf and slope (dotted), the shelf only (solid) and slope only (dashed), where shelf and slope series are delineated by the 100 m isobath. Clockwise from upper left: T (°C), S(PSU), $a(440)$ (m^{-1}), $b(440)$ (m^{-1})

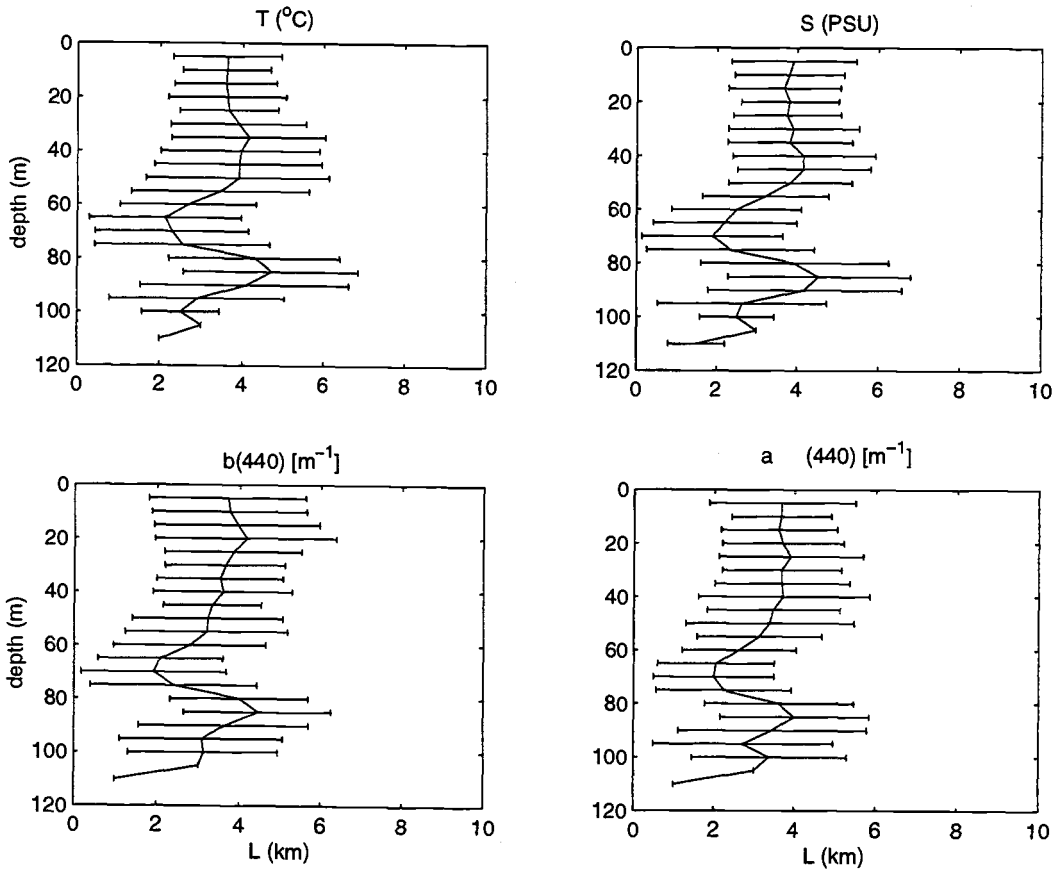

FIGURE 3.13 Ensemble mean decorrelation lengthscale, L, vertical profiles calculated from detrended anomaly series in cross-shelf and depth coordinates (y, z) for data series encompassing the shelf and slope. Superimposed are one standard deviation from the average anomaly profile. Clockwise from upper left: T(^{o}C), S(PSU), $a(440)$ [m^{-1}], $b(440)$ [m^{-1}]

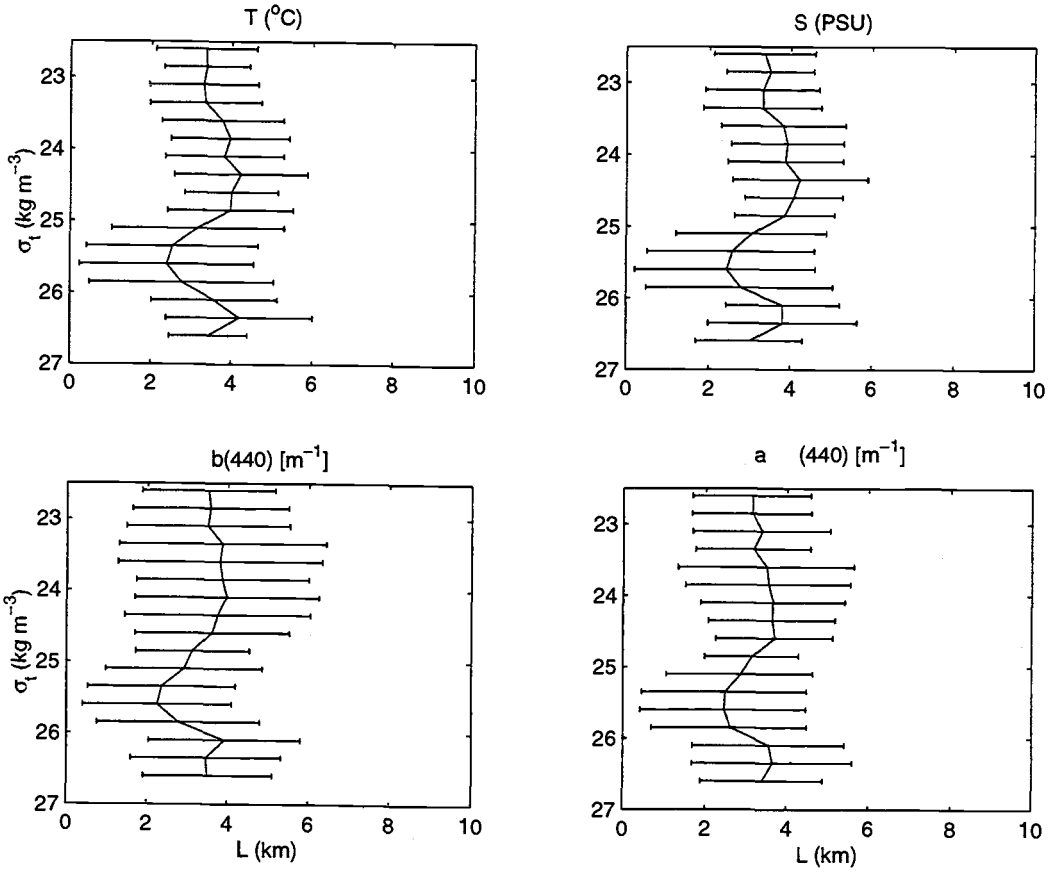

FIGURE 3.14 Ensemble mean decorrelation lengthscale, L, vertical profiles calculated from detrended anomaly series in cross-shelf and density coordinates (y,σ_t) for data series encompassing the shelf and slope. Superimposed are one standard deviation from the average anomaly profile. Clockwise from upper left: T (°C), S(PSU), $a(440)$ [m^{-1}], $b(440)$ [m^{-1}]

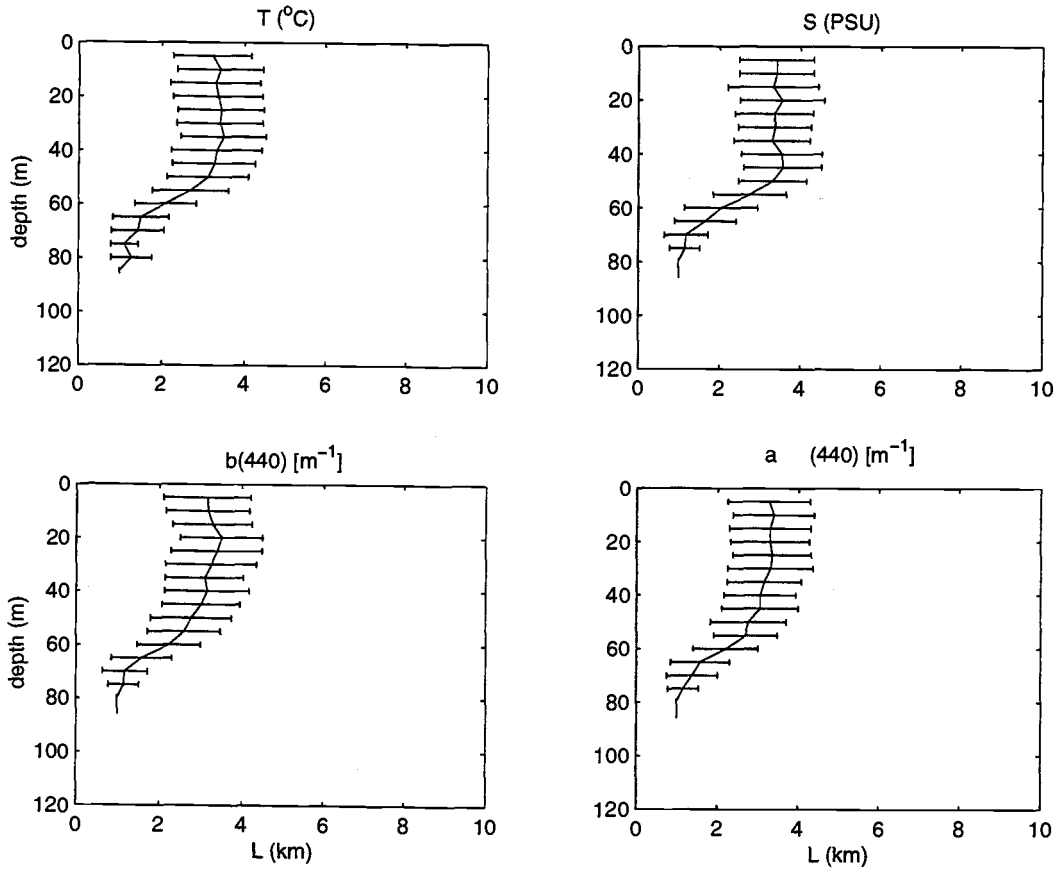

FIGURE 3.15 Ensemble mean decorrelation lengthscale, L, vertical profiles calculated from detrended anomaly series in cross-shelf and depth coordinates (y,z) for data series encompassing the shelf only ($h_b < 100$ m). Superimposed are one standard deviation from the average anomaly profile. Clockwise from upper left: T (°C), S(PSU), $a(440)$ [m^{-1}], $b(440)$ [m^{-1}]

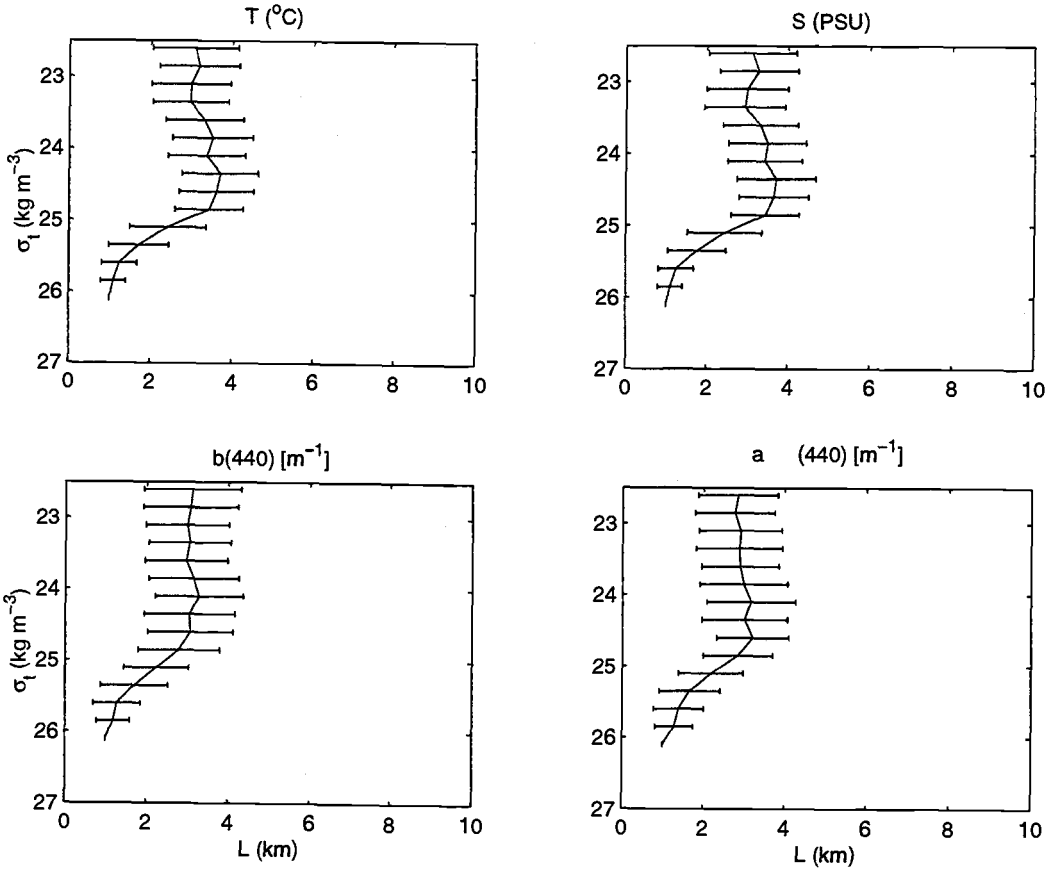

FIGURE 3.16 Ensemble mean decorrelation lengthscale, L, vertical profiles calculated from detrended anomaly series in cross-shelf and density coordinates (y,σ_t) for data series encompassing the shelf only ($h_b < 100$ m). Superimposed are one standard deviation from the average anomaly profile. Clockwise from upper left: T (°C), S(PSU), $a(440)$ [m^{-1}], $b(440)$ [m^{-1}]

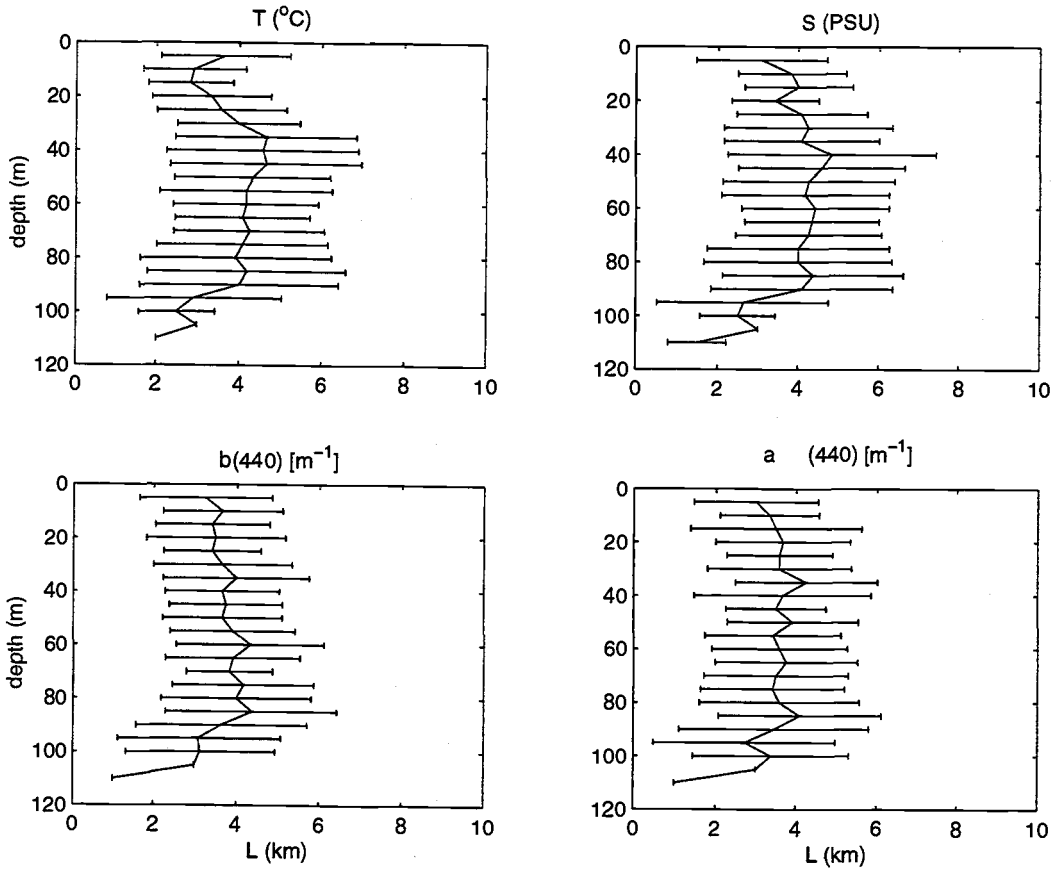

FIGURE 3.17 Ensemble mean decorrelation lengthscale, L, vertical profiles calculated from detrended anomaly series in cross-shelf and depth coordinates (y,z) for data series encompassing the slope only ($h_b > 100$ m). Superimposed are one standard deviation from the average anomaly profile. Clockwise from upper left: T (°C), S(PSU), $a(440)$ [m^{-1}], $b(440)$ [m^{-1}]

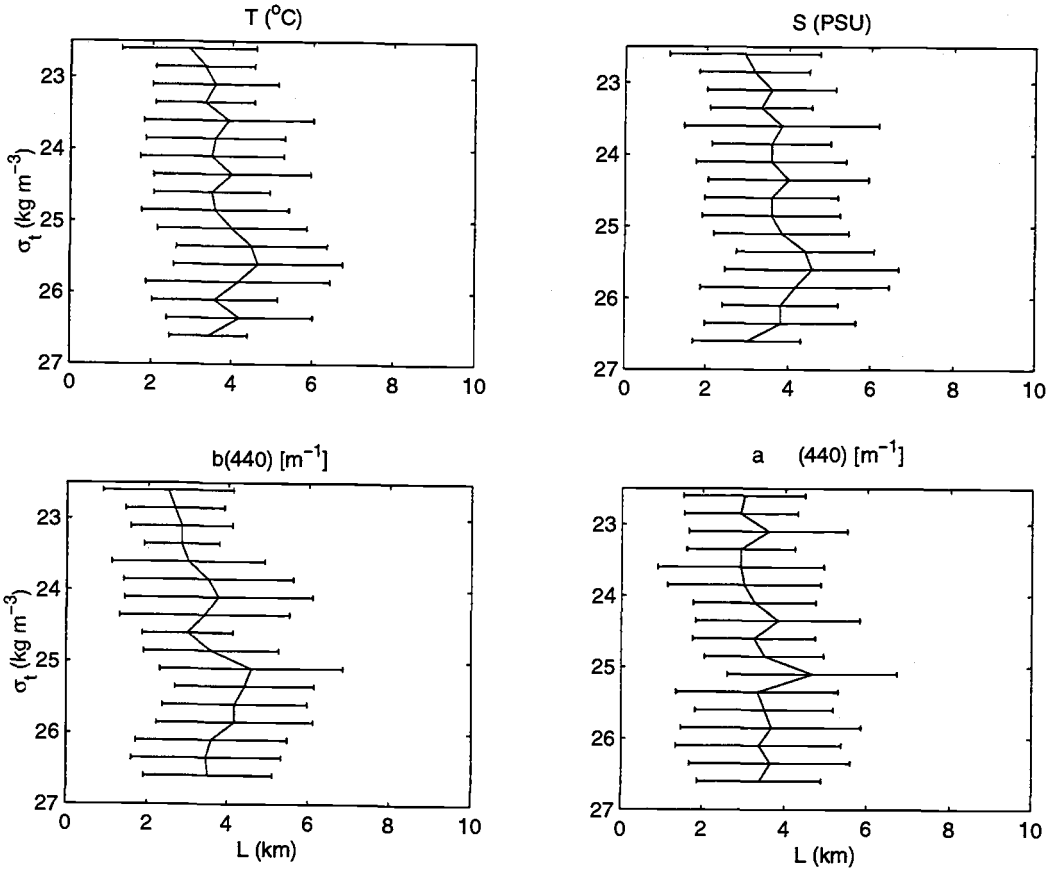

FIGURE 3.18 Ensemble mean decorrelation lengthscale, L, vertical profiles calculated from detrended anomaly series in cross-shelf and density coordinates (y,σ_t) for data series encompassing the slope only ($h_b > 100$ m). Superimposed are one standard deviation from the average anomaly profile. Clockwise from upper left: T (°C), S(PSU), $a(440)$ [m^{-1}], $b(440)$ [m^{-1}]

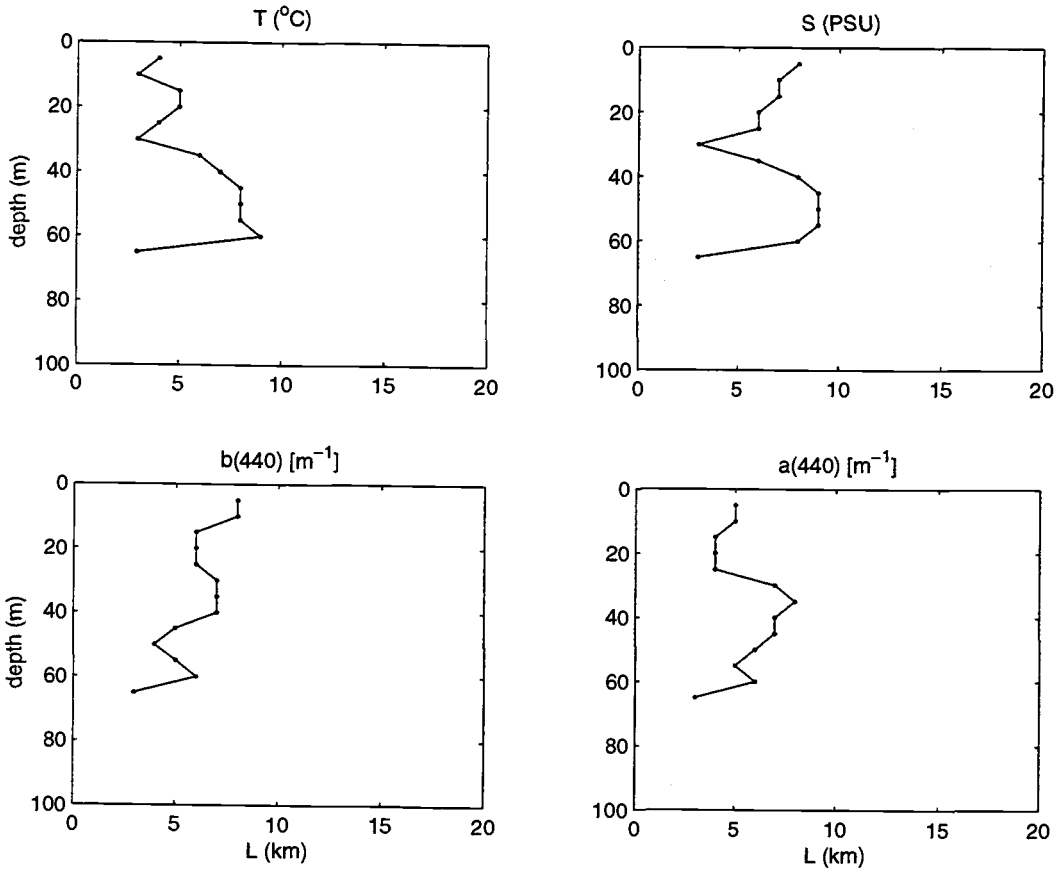

FIGURE 3.19 Decorrelation lengthscale, L, vertical profiles calculated from detrended mean series in alongshore and depth coordinates (x,z) for data series following the 70-m isobath. Clockwise from upper left: T (^{o}C), S(PSU), $a(440)$ [m^{-1}], $b(440)$ [m^{-1}]

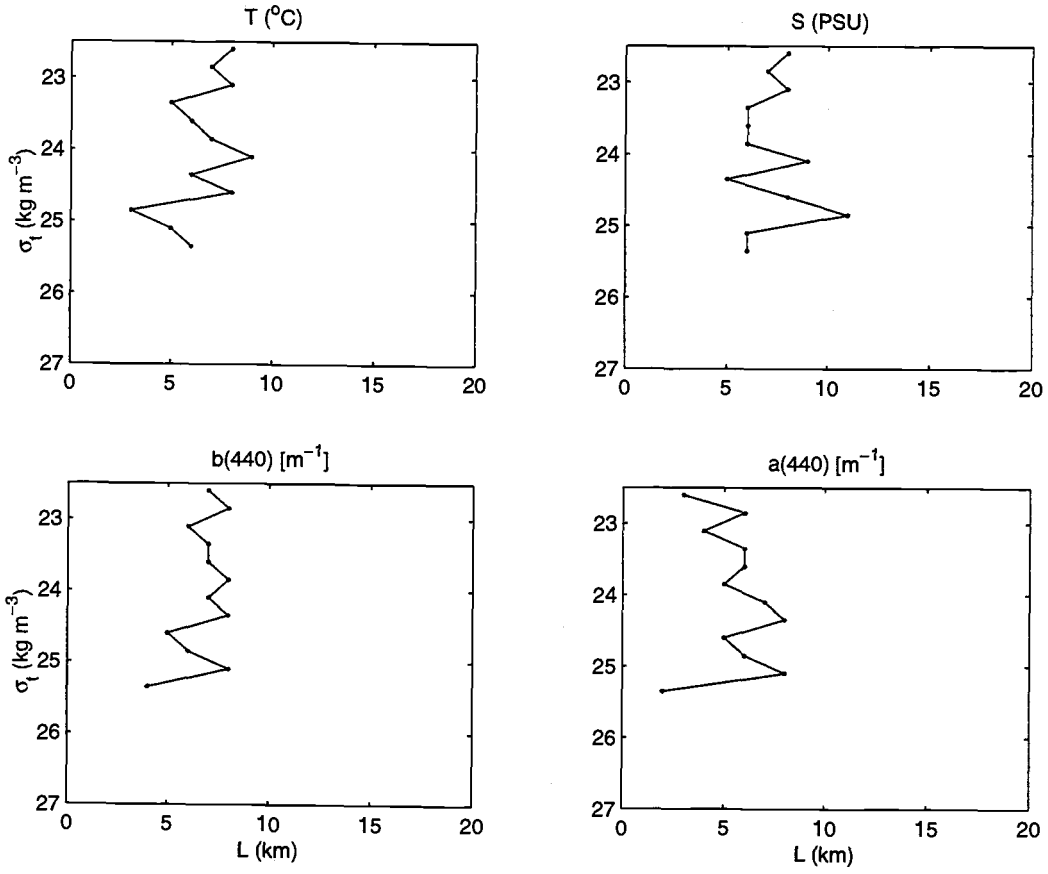

FIGURE 3.20 Decorrelation lengthscale, L, vertical profiles calculated from detrended mean series in alongshore and density coordinates (x,σ_t) for data series following the 70-m isobath. Clockwise from upper left: T (°C), S(PSU), a(440) [m^{-1}], b(440) [m^{-1}]

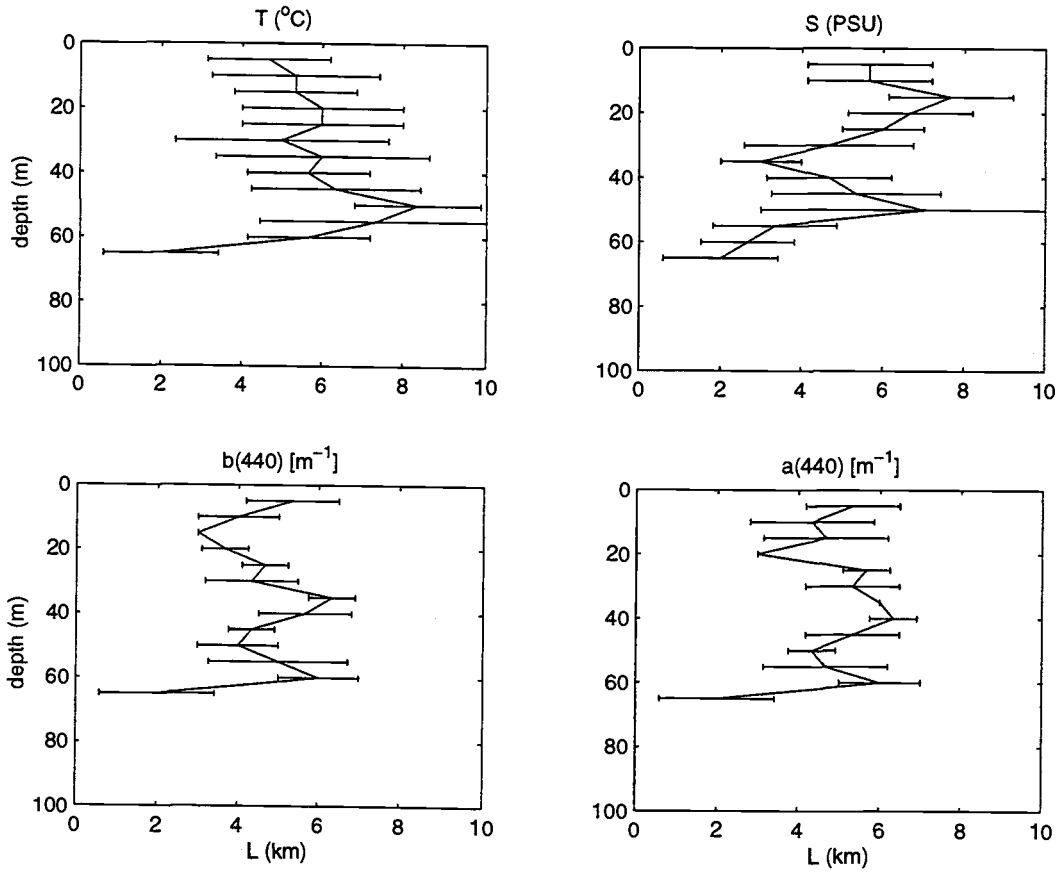

FIGURE 3.21 Ensemble mean decorrelation lengthscale, L, vertical profiles calculated from detrended anomaly series in alongshore and depth coordinates (y,z) for data series following the 70-m isobath. Superimposed are one standard deviation from the average anomaly profile. Clockwise from upper left: T (^{o}C), S(PSU), $a(440)$ [m^{-1}], $b(440)$ [m^{-1}]

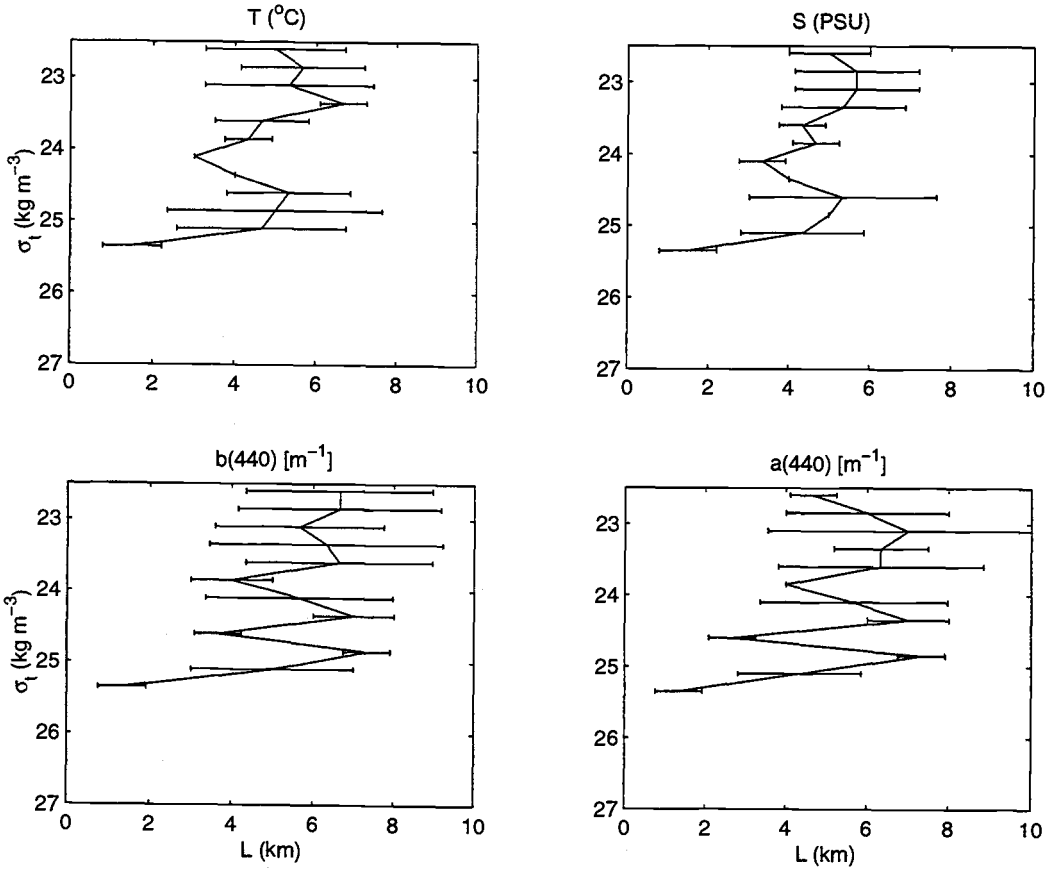

FIGURE 3.22 Ensemble mean decorrelation lengthscale, L, vertical profiles calculated from detrended anomaly series in alongshore and density coordinates (y,σ_t) for data series following the 70-m isobath. Superimposed are one standard deviation from the average anomaly profile. Clockwise from upper left: T (^{o}C), S(PSU), $a(440)$ [m^{-1}], $b(440)$ [m^{-1}]

3.5 DISCUSSION

The dominant features of the summer mean hydrographic and optical properties provide a contrast between the shelf and slope. The temperature was characterized by thermal stratification and a persistent cold pool on the shelf. The warmer slope waters are evident at depth over the slope. The mean salinity was characterized by fresh shelf water and saline slope water. The mean density distribution shows that temperature and salinity are density compensating. The optical variables, demonstrate increased turbidity associated with the shelf waters, while deep slope waters are relatively optically clear. The optical variables also indicate the form and location of the bottom boundary layer separation and its advection into the interior as seen in Barth et al. (1998). The leading cause of deviations from the mean T (^{o}C) and mean S(PSU) appear to be due to the position of the shelfbreak front near the foot. Evident, also, in the sample mean hydrographic variables is some aliasing caused by the measurement of meander variations during the small radiator pattern surveys in the later part of the cruise.

The decorrelation lengthscale profiles for both cross- and alongshore series exhibited varying structure throughout the water column, but one striking characteristic was found in many of the cross-shelf mean series L profiles: the dramatic shortening of L within the bottom boundary layer. The strong stratification during the summer permitted the decorrelation lengthscales along fixed depths to demonstrate an approximately linearly decreasing trend with depth. Here, one could interpret that the motion of the shelfbreak front influences this L profile structure, where one could imagine the surface and interior portions of the front are allowed to move with the ambient circulation, but that the foot of the shelfbreak front remains very stable and is able to reduce the size of the variance ellipses within its vicinity. Also, the bottom boundary layer is characterized

by turbulent mixing, which could cause differential resuspension and settling of chromophoric materials near the bottom. The specific structure of the shelf-slope series at fixed depths and isopycnals are a lengthening of mean T (°C) and S (PSU) L values near the surface and below the pycnocline, a shortening of L. This structure is most sensibly determined by the structure of the shelfbreak front, where the near-surface expression of the front extends further offshore (over the slope) than the foot of the shelfbreak front which is topographically trapped on the outer shelf. The shorter L profiles of the mean series of the hydrographic results from the sloping isopycnals at the shelfbreak.

The structure of the mean series of the optical variables is determined by the biologically active distribution of the phytoplankton that shortens L above the base of the pycnocline ($z \approx 25$ m). Major light-absorbing components such as the phytoplankton component and gelbstoff component can be highly heterogeneous due to *in situ* growth and zooplankton grazing, and photo-degradation, respectively. Shelf waters tend to be more well mixed by tidal influences, hence the short and uniform L profiles of the mean shelf series. The data series over the slope at fixed depths and isopycnals exhibits more structure, showing a shortening L in the upper 50 m in the S (PSU) and optical properties and a lengthening between 60 and 100 m.

Activity of intrusions at the surface over the slope, has also been documented by Houghton and Marra (1983). The presence of the "S_{max}" is fairly common over the summer, but the high temporal resolution of SeaSoar surveys have captured the variability in the persistence of this feature during the summer. The deep slope waters exhibit longer L values as expected for waters characterized by low frequency motion. The mean slope T (°C) deviates from this trend, likely due to the influence of the frontal dynamics, where offshore flux of buoyancy in the bot-

tom boundary layer tends to move lighter water under heavier water, an unstable condition which is quickly rectified by active convective mixing (Gawarkiewicz and Chapman, 1992). It is certainly possible that the mean temperature field is not smoothed enough over the slope region, considering the reduced data coverage over the slope. Near the bottom, the decorrelation lengthscale profile reaches its minimum, demonstrating active mixing, or trapping within the bottom boundary layer.

The cross-shelf anomaly series of all four variables in both depth or density space all exhibit consistently uniform values of O(3-4 km). The identical values exhibited by both hydrographic and optical properties lends strength to the argument that a similar, if not identical, process influences the magnitude of L. Some of the more obvious physical processes which can possibly cause anomalies are increased wind forcing, shelfbreak front meanders appearing as intrusions in the study region, and the passage of internal solitary wave packets. The lengthscale of the perturbing feature that causes a decorrelation lengthscale is probably two to four times the length of the decorrelation lengthscale. Hence, one could guess that the anomalous feature has a lengthscale of 6 to 12 km, which corresponds to the lengthscales of solitary wave packets. It is likely that solitons are the dominant cause of the shorter decorrelation lengthscales observed in the anomaly series. The appearance of the soliton wave packet signals in the along isopycnal series suggests that solitons exert just enough energy for mixing to occur across isopycnals over a range $\pm$ 0.025 kg m^{-3}.

The alongshore L along the 70-m isobath are comparable to the cross-shelf series from the shelf ($h_b < 100$ m). Along fixed depths, the L of the alongshore mean series shows the density compensation in the hydrographic variables. The shorter L's are associated with the pycnocline. The longer L's are associated with the interior. Again, the interpretation of surface mixing and invisid interior is applied. Between 40-60 m a strong westward jet ($\mathbf{u}$ = 5-10 cm s^{-1}) set up by the frontal dynamics was observed (Pierce et al., 1998). The IOPs do not reflect observed hydrography pattern. The L profile of the mean alongshore series of IOPs show lengthening at the base of the pycnocline, likely due to phytoplankton preference for light levels maintaining the correlation over space. Hydrographic and optical properties can diffuse along isopycnals up to 3 km.

The L of alongshore anomaly series at fixed depths suggest much variability in the spatial structure and dependence of hydrographic and optical properties. The alongshore anomaly series at fixed depths are notably of the same magnitude as the L profiles for the alongshore mean at fixed depths. This suggests that the mean does not capture most of the variance observed in the alongshore series.

The shortness of L for alongshore series along isopycnals is largely due to abundant signals introduced by solitons. The L profile structures reflect that both fixed depth and along isopycnal series are perturbed by the passage of solitons.

In sum, the spatial L's on the shelf in depth coordinates can be visualized as a slightly flattened circle, where the wider axis of the flattened circle is oriented along isobaths. In density coordinates the spatial L is more of an ellipse having a semi-major axis, nearly twice the length of the semi-minor axis and being oriented parallel to the isobaths. The semi-minor axis of the spatial L ellipse is oriented normally to isobaths.

3.6 CONCLUSION

Historical descriptions of the distinctiveness between the tidally energetic shelf and the low-frequency motion dominated slope has partially motivated the handling of the data series analyzed for this study.

The strong horizontal gradient introduced by the shelfbreak front is also a persistent characteristic of the Middle Atlantic Bight. The cross-shelf data series were then divided into shelf ($h_b < 100$ m) and slope ($h_b > 100$ m) series. The shelf-slope series (composed of both the shelf and slope data) was examined to determine the regional decorrelation lengthscales. The major results of this study has shown that the lengthscales of the mean cross-shelf (L $O(10$ km$)$) is affected by meander lengthscales. Hence, the meanders found in the surface expression of the shelfbreak front control, to first order, the spatial dependence of hydrographic and optical properties.

The individual mean shelf and mean slope series reflect the inherent differences between the two regions, where tidal influences appear to dominate the shelf (L $O(4$ km$)$), while the deep slope waters are characterized by smaller variances in the hydrographic and optical properties. The vertical structure of the slope series L profiles suggests the presence of a calm, invisid interior at depth (70-100 m, L $O(7$ km$)$.

In density space, the mean hydrographic variables are shown to be density compensating and the L of the optical variables are primarily determined by the underwater light field. The individual mean shelf and mean slope series appear to be close to the magnitude of the observed internal deformation radius ($L_R = 5$ km), suggesting that over shorter distances (and shoreward/seaward of the shelfbreak front), the internal deformation radius exerts a more prominent influence.

The alongshore mean series (along 70-m isobath) also demonstrates a magnitude similar to the deformation radius. The decorrelation lengthscales for the alongshore anomaly series were found to be longer than the cross-shelf anomaly series L's by approximately 1-2 km. The horizontal spatial autocorrelation of the four mean variables on the shelf, in depth coordinates, is nearly circular, while the horizontal spatial autocorrelation in density coordinates takes the form of an ellipse, where the semi-major axis is oriented parallel to the alongshore direction.

A feature common in the cross-shelf mean L profiles was reduction of the magnitude of L near the bottom. This becomes suggestive of the reduction in the size of the velocity ellipses in the highly stable vicinity of the foot of the shelfbreak front.

The decorrelation lengthscales for the anomaly series on the shelf ($h_b < 100$ m) in both the alongshore and cross-shelf directions, as well as in both depth and density coordinates were generally $O(3$ km$)$. This consistently demonstrates the signals of internal wave activity in this survey region.

The link between hydrographic and optical variables becomes evident through this statistical analysis. The physical processes acting on the hydrographic variables appear to play the major role in the determination of the spatial dependence in the optical variables. Although the mean optical variables are biologically and chemically active above the base of the pycnocline, the biological/chemical processes acting beneath the pycnocline influence the properties of the IOPs on timescales longer than the motion of the fluid. In essence, the chromophoric materials predominantly behave as suspended particles, moving according to the dynamics of the coastal circulation in this region. More conclusive results could be provided by cross-correlation analyses which is set aside for future work.

3.7 REFERENCES

Barth, J. A. and D. Bogucki Spectral light absorption and attenuation measurements from a towed undulating vehicle, *Deep Sea Res. I*, **47**, 323-342, 1999.

Barth, J. A., D. Bogucki, S. Pierce and P. M. Kosro, Secondary Circulation Associated with a Shelfbreak Front, *Geophys. Res. Lett.*, **25**, 2761-2764, 1998.

Beardsley, R. C. and W. C. Boicourt, On estuarine and continental-shelf circulation in the Middle Atlantic Bight, In *Evolution of Physical Oceanography*, ed. B. Warren and C. Wuncsh, MIT Press, Cambridge, Massachusetts, 1981.

Bigelow, H. B., Studies of the waters on the continental shelf, Cape Cod to Chesapeake Bay. I. The cycle of temperature, *Papers in Physical Oceanography and Meteorology*, **2**, 1-135, 1933.

Boicourt, W. C. and P. Hacker, Circulation o the Atlantic continental shlef from Cape May to Cape Hatteras. *Mem. Soc. R. Sci. Liege Ser. 6*, **10**, 187-200, 1976.

Chapman, D. C., J. A. Barth, R. C. Beardsley and R. G. Fairbanks, On the continuity of mean flow between the Scotian Shelf and the Middle Atlantic Bight, *J. Phys. Oceanogr.*, **16**, 758-772, 1986.

Chapman, D. C and S. J. Lentz, Trapping of a coastal density front by the bottom boundary layer, *J. Phys. Oceanogr.*, **24**, 1464-1479, 1994.

Csanady, G. T., The arrested topographic wave, *J. Phys. Oceanogr.*, **8**, 47-62, 1978.

Csanady, G. T. and B. A. Magnell, Mixing Processes, in *Georges Bank*, ed. R. H. Backus, MIT Press, Cambridge, 1987.

Emery, W. J. and R. E. Thompson, *Data Analysis Methods in Physical Oceanography*, Pergamon, New York, 1997.

Garvine, R. W., K.-C. Wong, G. G. Gawarkiewicz, R. K. McCarthy, R. W. Houghton and F. Aikman III, THe morphology of shelfbreak eddies, *J. Geophys. Res.*, **93**, 15,593-15,607, 1988.

Gawarkiewicz, G. and D. C. Chapman, The role of stratification in the formation and maintenance of shelfbreak fronts, *J. Phys. Oceanogr.*, **22**, 753-772, 1992.

Halliwell, G. R. and C. N. K. Mooers, The space-time structure and variability of the shelf water-slope water and Gulf Stream surface temperature fronts and associated warm-core eddies, *J. Geophys. Res.*, **84**, 7707-7726, 1979.

Halpern, D., Observations on short-period internal waves in Massachusetts Bay, *J. Mar. Res.*, **29**, 116-132, 1971.

Houghton R. W. and J. Marra, Physical/Biological structure and exchange across the thermohaline shelf/slope front in the New York Bight, *J. Geophys. Res.*, **88**, 4467-4481, 1983.

Kirk, J. T. O., *Light and photosynthesis in aquatic ecosystems, 2nd ed.*, Cambridge, 1994.

Linder C. A. and G. Gawarkiewicz, A climatology of the shelfbreak front in the Middle Atlantic Bight, *J. Geophys. Res.*, **103**, 18,405-18,423, 1998.

Loder, J. W., B. Petrie, and G. Gawarkiewicz, The coastal ocean off northeastern North America: A large-scale view, in *The Sea*, vol. 11, *The Global Coastal Ocean: Regional Studies and Syntheses*, edited by A. R. Robinson and K. H. Brink, pp 105-133, John Wiley, New York, 1998.

O'Driscoll, K., Nonlinear internal waves on the continental shelf: Observations and KdV solutions, M.S. Thesis, Oregon State University, Corvallis, Oregon, 119 pp., 1999.

O'Malley, R., J. A. Barth, A. Y. Erofeev, J. Fleishbein, P. M. Kosro, and S. D. Pierce, SeaSoar CTD observations during the Coastal Mixing and Optics experiment: R/V Endeavor cruises from 14-Aug to 1-Sep 1996 and 25-Apr to 15-May 1997, Data Report 168, Ref. 98-1, College of Oceanic and Atmospheric Sciences, Oregon State University, 1998.

Pierce, S. D., J. A. Barth and P. M. Kosro, Acoustic Doppler current profiler observations during the Coastal Mixing and Optics experiment: R/V Endeavor cruises from 14-Aug to 1-Sep 1996 and 25-Apr to 15-May 1997, Data Report 169, Ref. 98-2, College of Oceanic and Atmospheric Sciences, Oregon State University, 1998.

Poulain, P.-M. and P. Niiler, Statistical analysis of the surface circulation in the California current system using satellite-tracked drifters, *J. Phys. Oceanogr.*, **19**, 1588-1603, 1989.

Simeon, J., J. A. Barth, D. Bogucki, A. Erofeev, R. O'Malley, S. D. Pierce. 2000. SeaSoar spectral light absorption and attenuation observations during the Coastal Mixing and Optics Experiment: R/V Endeavor Cruises from 14-Aug to 1-Sep 1996 and 25-Apr to 15-May 1997. Data Report 179, Ref. 00-3. College of Oceanic and Atmospheric Sciences, Oregon State University.

Simeon, J., J. A. Barth, C. S. Roesler and W. S. Pegau, Distributions of modeled light-absorbing components in the Middle Atlantic Bight, In prep.

Stommel, H. and A. Leetma, Circulation on the continental shelf, *Proc. Natl. Acad. Sci., U.S.*, **69**, 3380-3384, 1972.

4 SUMMARY

The strong horizontal gradient imposed by the shelfbreak front is a persistent characteristic of the Middle Atlantic Bight. This investigation shows that the shelfbreak front plays the key role in determining, to first order, the distribution of hydrographic and optical properties.

Summer distributions of modeled major light-absorbing components demonstrate a subsurface phytoplankton layer following isopycnals at the base of the pycnocline. Large magnitudes of tripton absorption were associated with the subsurface phytoplankton layer and with the bottom boundary layer on the mid-shelf. Large magnitudes of gelbstoff absorption coefficients were found above the bottom, shoreward of the shelfbreak front. Optically clearer slope waters were characterized by weak gelbstoff absorption, suggesting (1) the slope water masses are relatively aged enough to have lost its suspended particulate load and (2) that the water was once exposed to enough sunlight to photo-degrade the gelbstoff component.

Spring distributions of modeled component absorption coefficients were characterized by patchy blooms of phytoplankton in the surface mixed layer. Gelbstoff absorption exhibited larger magnitudes associated with the pore water released by resuspended bottom sediments. Larger magnitudes of tripton absorption were found in the surface mixed layer and above the seafloor.

The distributions of the total (minus water) absorption components demonstrate evidence of the relative insulation of the shelf waters from slope waters and the strong horizontal gradient across the shelfbreak front. The near-surface to bottom structure of the summer shelfbreak front contrasts with the relaxed springtime frontal structure, where the absence of strong stratification minimizes the vertical extent of the front.

The cross-shelf and alongshore data series were examined to determine the vertical structure of the regional horizontal decorrelation lengthscales. The major results of the statistical quantification are that (1) the lengthscales of the mean cross-shelf series (L O(10 km)) are affected by meander lengthscales in the near surface, (2) the foot of the shelfbreak front is a stable feature that is able to reduce the size of the spatial correlation within its vicinity, (3) the decorrelation lengthscale of the anomaly series are inundated with signals from solitary wave activities.

The decorrelation lengthscales of the individual shelf and slope series reflect the inherent differences between the two regions, where tidal influences appear to dominate the shelf (L O(5 km)), while offshore, deep slope waters are of a low-frequency regime. The spatial autocorrelation, in depth coordinates, of the shelf series, could be visualized as nearly circular ellipses near the surface. This is consistent with the nearly circular tidal ellipses found by Pierce et al. (1998) for this region. The flattening of the ellipse becomes more pronounced with depth, with the semi-major axis oriented parallel to the isobaths and the semi-minor axis oriented normal to the isobaths.

The decorrelation lengthscales of the individual shelf and slope series are similar to the magnitude of the observed internal deformation radius ($L_R = 5$ km), suggesting that the internal deformation radius exerts a localized influence.

The alongshore anomaly series (along 70-m isobath) decorrelation lengthscales are slightly longer, by 2 km, than the cross-shelf lengthscales.

The persistent feature common in many of the L profiles was reduction of the magnitude of L near the bottom. This becomes suggestive of the reduction in the size of the variance ellipses in the highly stable vicinity of the foot of the shelfbreak front. The anomaly series both alongshore and cross-shelf as well as both depth

and density space were generally $O(3$ km), which consistently demonstrates the signal of internal wave activity in this survey region.

The link between the hydrographic and optical variables becomes evident through this statistical analysis. The physical processes acting on the hydrographic variables appear to also determine the spatial dependence in the optical variables. The optical variables, in essence, behave as suspended particles, moving according to the dynamics of the coastal circulation in this region. More conclusive results could be provided by cross-correlation analyses which is set aside for future work.

BIBLIOGRAPHY

Aikman, F., III, Pycnocline developement and its consequences in the Middle Atlantic Bight, *J. Geophys. Res.*, **89**, 685-694, 1984.

Barth, J. A., D. Bogucki, S. Pierce and P. M. Kosro, Secondary Circulation Associated with a Shelfbreak Front, *Geophys. Res. Lett.*, **25**, 2761-2764, 1998.

Barth, J. A. and D. Bogucki Spectral light absorption and attenuation measurements from a towed undulating vehicle, *Deep Sea Res. I*, **47**, 323-342, 1999.

Beardsley, R. C. and W. C. Boicourt, On estuarine and continental-shelf circulation in the Middle Atlantic Bight, In *Evolution of Physical Oceanography*, ed. B. Warren and C. Wuncsh, MIT Press, Cambridge, Massachusetts, 1981.

Beardsley, R. C., D. C. Chapman, K. H. Brink, S. Ramp and R. Schlitz, Nantucket Shoals Flux Experiment (NSFE79), Part 1: A basic description of the current and temperature variability, *J. Phys. Oceanogr.*, **15**, 713-748, 1985.

Bigelow, H. B., Studies of the waters on the continental shelf, Cape Cod to Chesapeake Bay. I. The cycle of temperature, *Papers in Physical Oceanography and Meteorology*, **2**, 1-135, 1933.

Boicourt W. C. and P. W. Hacker, Circulation on the Atlantic Continental Shelf of the United States, Cape May to Cape Hatteras, *Mem. Sic, R. Sci. Liege, Ser. 6 10*, 187-200, 1976.

Boss, E., W. S. Pegau, J. R. V. Zaneveld and A. H. Barnard, Spatial and temporal variability of absorption by dissolved material at a continental shelf, *J. Geophys. Res.*, submitted.

Bricaud, A., A. Morel and L. Prieur, Absorption by dissolved organic matter of the sea (yellow substance) in the UV and visible domains, *Limnol. Oceanogr.*, **26**, 43-53, 1981.

Bricaud A. and D. Stramski, Spectral absorption coefficients of living phytoplankton and non-algal biogenous matter: A comparison between the Peru upwelling area and the Sargasso Sea, *Limnol. Oceanogr.*, **35**, 562-582, 1990.

Candela, J., R. C. Beardsley and R. Limeburner, Separation of tidal and subtidal currents in ship-mounted acoustic Doppler current profiler observations, *J. Geophys. Res.*, **97**, 769-788, 1992.

Carder, K. L., R. G. Steward, G. R. Harvey and P. B. Ortner, Marine humic and fulvic acids: their effects on remote sensing of ocean chlorophyll, *Limnol. Oceanogr.*, **34**, 68-81, 1989.

Chang, G. C. and T. D. Dickey, Optical and physical variability on time-scales from minutes to the seasonal cycle on the New England Shelf: July 1996-June 1997, *J. Geophys. Res.*, submitted.

Chapman, D. C., J. A. Barth, R. C. Beardsley and R. G. Fairbanks, On the continuity of mean flow between the Scotian Shelf and the Middle Atlantic Bight, *J. Phys. Oceanogr.*, **16**, 1986.

Chapman, D. C and S. J. Lentz, Trapping of a coastal density front by the bottom boundary layer, *J. Phys. Oceanogr.*, **24**, 1464-1479, 1994.

Cleveland, J. S., Regional models for phytoplankton absorption as a function of chlorophyll *a* concentration, *J. Geophys. Res.*, **100**, 13,333-13,344, 1995.

Cleveland, J. S. and M. J. Perry, A model for partitioning particulate absorption into phytoplanktonic and detrital components, *Deep-Sea Res. I.*, **41**, 197-221, 1994.

Cresswell, G. H., Quasi-synoptic monthly hydrography of the of the transition region between coastal and slope water south of Cape Cod, Mass., WHOI, Ref. 67-35, Woods Hole Oceanogr. Inst., Woods Hole, Mass., 1967.

Csanady, G. T., Mean circulation in shallow seas, *J. Geophys. Res.*, **81**, 5389-5399, 1976.

Csanady, G. T., The arrested topographic wave, *J. Phys. Oceanogr.*, **8**, 47-62, 1978.

Csanady, G. T. and B. A. Magnell, Mixing Processes, in *Georges Bank*, ed. R. H. Backus, MIT Press, Cambridge, 1987.

DeGranpre, M. D., A. Vodacek, R. K. Nelson, E. J. Bruce and N. V. Blough, Seasonal seawater optical properties of the U.S. Middle Atlantic Bight, *J. Geophys. Res.*, **101**, 22,727-22,736, 1996.

Emery, W. J. and R. E. Thompson, *Data Analysis Methods in Physical Oceanography*, Pergamon, New York, 1997.

Fairbanks, R. G., The origin of continental shelf and slope water in the New York Bight and Gulf of Maine: Evidence from $H_2^{18}O/H_2^{18}0$ ratio measurements. J. Geophys. Res., **87**, 5796-5808, 1982.

Garvine, R. W., K.-C. Wong, G. G. Gawarkiewicz, R. K. McCarthy, R. W. Houghton and F. Aikman III, THe morphology of shelfbreak eddies, *J. Geophys. Res.*, **93**, 15,593-15,607, 1988.

Gawarkiewicz, G. and D. C. Chapman, The role of stratification in the formation and maintenance of shelfbreak fronts, *J. Phys. Oceanogr.*, **22**, 753-772, 1992.

Halliwell, G. R. and C. N. K. Mooers, The space-time structure and variability of the shelf water-slope water and Gulf Stream surface temperature fronts and associated warm-core eddies, *J. Geophys. Res.*, **84**, 7707-7726, 1979.

Halpern, D., Observations on short-period internal waves in Massachusetts Bay, *J. Mar. Res.*, **29**, 116-132, 1971.

Hayase, K. and H. Tsubota, Sedimentary humic acid and fulvic acid as fluorescent organic materials, *Geochimica et Cosmochimica*, **49**, 159-163, 1985.

Højerslev, N. K., The origin of of yellow substance in the marine environment, In *17th General Assembly of I.A.P.S.O. (Canberra, 1979)*(pp. Abstracts, 71), 1979.

Houghton R. W. and J. Marra, Physical/Biological structure and exchange across the thermohaline shelf/slope front in the New York Bight, *J. Geophys. Res.*, **88**, 4467-4481, 1983.

Jerlov, N. G., *Marine Optics*, Amsterdam, Elsevier, 1976.

Ketchum, B. J. and N. Corwin, The persistence of "winter" water on the continental shelf south of Long Island, New York, *Limnol. Oceanogr.*, **9**, 467-475, 1964.

Kirk, J. T. O., *Light and photosynthesis in aquatic ecosystems, 2nd ed.*, Cambridge, 1994.

Lawson C. L. and R. J. Hanson, *Solving least squares problems*, Prentice-Hall, New Jersey, 1974.

Lee, A. H., The T-S structure, circulation and mixing in the slope water region east of the Scotion shelf, Ph.D. Thesis, Dalhousie University, Halifax, Nova Scotia, 191 pp., 1970.

Linder C. A. and G. Gawarkiewicz, A climatology of the shelfbreak front in the Middle Atlantic Bight, *J. Geophys. Res.*, **103**, 18,405-18,423, 1998.

Loder, J. W., B. Petrie, and G. Gawarkiewicz, The coastal ocean off northeastern North America: A large-scale view, in *The Sea*, vol. 11, *The Global Coastal Ocean: Regional Studies and Syntheses*, edited by A. R. Robinson and K. H. Brink, pp 105-133, John Wiley, New York, 1998.

Mackas, D. L., K. L. Denman and A. F. Bennett, Least squares multiple tracer analysis of water mass composition, *J. Geophys. Res.*, **92**, 2907-2918, 1987.

Miller, W. and Moran, M., Interaction of photochemical and microbial processes in the degradation of refractory dissolved organic matter from a coastal marine environment, *Limnol. Oceanogr.*, **42**, 1317-1324, 1997.

Mooers, C. N., K. R. W. Garvine and W. W. Martin, Summertime synoptic variability of the Middle Atlantic Bight, *J. Geophys. Res.*, **84**, 4837-4854, 1979.

Morrow J. H., W. S. Chamberlin and D. A. Kiefer, A two-component description of spectral absorption by marine particles, *Limnol. Oceanogr.*, **34**, 1500-1509, 1989.

O'Driscoll, K., Nonlinear internal waves on the continental shelf: Observations and KdV solutions, M.S. Thesis, Oregon State University, Corvallis, Oregon, 119 pp., 1999.

O'Malley, R., J. A. Barth, A. Y. Erofeev, J. Fleishbein, P. M. Kosro, and S. D. Pierce, SeaSoar CTD observations during the Coastal Mixing and Optics experiment: R/V Endeavor cruises from 14-Aug to 1-Sep 1996 and 25-Apr to 15-May 1997, Data Report 168, Ref. 98-1, College of Oceanic and Atmospheric Sciences, Oregon State University, 1998.

Pierce, S. D., J. A. Barth and P. M. Kosro, Acoustic Doppler current profiler observations during the Coastal Mixing and Optics experiment: R/V Endeavor cruises from 14-Aug to 1-Sep 1996 and 25-Apr to 15-May 1997, Data Report 169, Ref. 98-2, College of Oceanic and Atmospheric Sciences, Oregon State University, 1998.

Pope R. M. and E. S. Fry, Absorption spectrum (380-700 nm) of pure water. II. Integrating cavity measurements, Applied Optics, **36**, 8710-8723, 1997.

Poulain, P.-M. and P. Niiler, Statistical analysis of the surface circulation in the California current system using satellite-tracked drifters, *J. Phys. Oceanogr.*, **19**, 1588-1603, 1989.

Roesler, C .S. and M. J. Perry, In situ phytoplankton absorption, fluorescence emission, and particulate backscattering spectra determined from reflectance, *J. Geophys. Res.*, **100**, 13,279-13,295, 1995.

Roesler, C. S., M. J. Perry and K. L. Carder, Modeling in situ phytoplankton absorption from total absorption spectra in productive inland marine waters, *Limnol. Oceanogr.*, **34**, 1510-1523, 1989.

Round, F. E., *The Ecology of Algae*, Cambridge, Univ. Press, 653 pp., 1981.

Ryan, J., J. Yoder, J. A. Barth, P. C. Cornillon, Chlorophyll enhancement and mixing associated with meanders of the shelf break front in the Middle Atlantic Bight, *J. Geophys. Res.*, **104**, 23,479-23,493, 1999.

Shaw, P.-T. and G. T. Csanady, Self-advection of density perturbations on a sloping continental shelf, *J. Phys. Oceanogr.* , **13**, 769-782, 1983.

Simeon, J., J. A. Barth, D. Bogucki, A. Erofeev, R. O'Malley, S. D. Pierce. 2000. SeaSoar spectral light absorption and attenuation observations during the Coastal Mixing and Optics Experiment: R/V Endeavor Cruises from 14-Aug to 1-Sep 1996 and 25-Apr to 15-May 1997. Data Report 179, Ref. 00-3. College of Oceanic and Atmospheric Sciences, Oregon State University.

Simeon J. and J. A. Barth, Decorrelation lengthscales of hydrographic and inherent optical properties and their relationship to circulation on the continental shelf and slope in the Middle Atlantic Bight, in prep.

Simeon, J., J. A. Barth, C. S. Roesler and W. S. Pegau, Distributions of modeled light-absorbing components in the Middle Atlantic Bight, In prep.

Sosik, H. M. and B. G. Mitchell, Light absorption by phytoplankton, photosynthetic pigments and detritus in the California Current System, *Deep Sea Res. I.*, **42**, 1717-1748, 1995.

Stommel, H. and A. Leetma, Circulation on the continental shelf, *Proc. Natl. Acad. Sci., U.S.*, **69**, 3380-3384, 1972.

Vodacek, A., N. V. Blough, M. D. DeGranpre, E. T. Peltzer and R. K. Nelson, Seasonal variations of CDOM and DOC in the Middle Atlantic Bight: Terrestrial inputs and photo-oxidation, *Limnol. Oceanogr.*, **42**, 674-686, 1997.

Wright, W. R., Physical oceanography. *Summary of Environmental Inventory on the Continental Slope, Canadian/United States Border to Cape Hatteras, North Carolina*, **4**, 4-101, Research Institute of the Gulf of Maine, S. Portland, Maine, 1977.

Zepp, R. G. and P. F. Schlotzhauer, Comparison of photochemical behavior of various humic substances in water. III. Spectroscopic properties of humic substances, *Chemosphere*, **10**, 479-486, 1981.